WA School of Mines:
Minerals, Energy and Chemical Engineering

Experimental Study of Impregnated Diamond Bit Wear

Rui Huang
0000-0002-2654-2639

This thesis is presented for the Degree of
Doctor of Philosophy
of
Curtin University

January 2025

To the best of my knowledge and belief this thesis contains no material previously published by any other person except where due acknowledgement has been made. This thesis contains no material which has been accepted for the award of any other degree or diploma in any university.

Rui Huang

20^{th} January 2025

"*Objectives, initiation, self-control, and persistence are key to success.*"

— Wei Huang

Acknowledgements

First and foremost, I would like to express my deepest gratitude to my supervisors, Dr. Thomas Richard and Dr. Masood Mostofi. Thanks for guiding me through this PhD journey and seeing potential in me that I had not yet discovered. Your expertise and meticulous attention to detail have been crucial in shaping this research into what it is today.

A special thanks goes to my colleagues and friends at the Drilling Analytics Research Centre (DARC) at Curtin University. The collaborative environment and valuable insights have been a source of inspiration and motivation. I am particularly grateful to Mr. Hing Hao Chan for his assistance with experimental work and data analysis.

I would also like to acknowledge the financial support provided by MinEx CRC and the Research Training Program (RTP) Scholarship from the Australian Commonwealth.

On a personal note, I am forever indebted to my family for their unwavering love and support. To my parents, Mr. Wei Huang and Ms. Jiaolan Wan, and my parents-in-law, Mr. Guoliang Shen and Ms. Xiaojuan Zhang, your belief in me has been a constant source of strength. To my dear wife, Dr. Qiqing Shen, I cannot thank you enough for inspiring me and being patient all the time. And to the cutest dog in the world, Qi Qi, you have brought me so much joy and I am truly lucky to build such an inseparable bond with you.

Lastly, I extend my gratitude to all those who have contributed to this thesis, directly or indirectly. Your support and encouragement have been invaluable.

Abstract

Impregnated diamond (ID) bits are commonly used for drilling hard and abrasive rocks thanks to their robust structure and self-sharpening nature. Despite the development of various models to predict ID bit performance, many fail to distinguish between effects attributable to rock properties and bit wear. Specifically, researchers relying on specific energy (energy required to remove a unit volume of rock) find that an increase in specific energy simply indicates more energy required to remove rock, without clarifying whether this increase stems from an increased rock hardness or bit polishing. The gap arises from the challenge of assessing the bit wear state (topology of the cutting face) during drilling. Therefore, this research aims to bridge this gap by (i) developing a rigorous and novel experimental methodology to track the evolution of both bit wear state and drilling response; (ii) performing extensive drilling experiments using state-of-the-art lab-scale drilling rigs to establish quantitative relationships between depth of cut, applied forces, and bit wear rate across different bit wear states, rock and fluid properties.

The complex bit topology is reduced to a single equivalent blade characterised by three scaled (nominal) lengths: diamond protrusion ($\bar{p}$), diamond wear flat length (L_d), and matrix wear flat length (L_m). This reduction enables the establishment of quantitative relationships between nominal lengths and drilling response, effectively distinguishing the effect of bit wear state from rock properties. By leveraging these relationships, this research provides a methodology for inferring bit wear state from forces and depth of cut.

A conceptual wear model is also established to quantitatively relate depth of cut, rock and drilling fluid properties to bit wear mechanisms and wear rate. It consists of three wear regimes: polishing dominant, where diamonds polish with minimal material loss; fracturing dominant, characterised by diamonds breakage and an increased wear rate; and pull-out dominant, which involves the detachment of diamonds, resulting in the highest wear rate. The transition from the polishing-dominant to the fracturing-dominant regime is controlled by the Mohs hardness of the rock, shifting from no diamond fracturing to more than 40% of diamonds experiencing fracturing wear at a given depth of cut. The transition from the fracturing-dominant to the pull-out-dominant regime is influenced by fluid viscosity; an increase in fluid viscosity decreases the depth of cut at the transition, leading to a higher wear rate at a given depth of cut. This model provides a comprehensive framework for understanding how various factors contribute to bit wear, offering insights into optimising drilling performance by selecting the optimal depth of cut and predicting wear behaviour under different conditions.

Contents

List of Figures

List of Tables

Chapter 1

Introduction

Metals and rare earth materials are essential for modern technologies and economies, especially as many countries commit to achieve net zero emissions by 2050, a crucial strategy to combat climate change and limit global warming (United Nations (2015)). This transition necessitates an increased supply of materials to transform electricity systems that emit no net CO_2 and promote widespread electrification (Parmesan et al. (2022)). As a result, mineral exploration plays a pivotal role in facilitating the energy transition and advancing the process of decarbonisation.

In mineral exploration, drilling is a critical method for sampling subsurface materials and gaining valuable information on the composition and characteristics of the formation. Common techniques includes reverse circulation (RC) drilling and diamond core drilling. In RC drilling, a pneumatic hammer drives a drill bit into the rock, with cuttings transported to the surface through the drill rods. This method is noted for its speed and cost effectiveness in comparison to diamond core drilling. However, its performance diminishes with depth as maintaining sufficient air pressure to drive the hammer and retrieve cuttings becomes more challenging (Hapugoda and Manuel (2010)). Diamond core drilling, on the other hand, excels in producing high-quality cylindrical core samples that meticulously preserve geological features and structures. These samples offer precise details on rock types, mineralogy, alteration zones, and structural geology. Dia-

mond drilling is particularly indispensable for deeper mineral exploration where accurate geological data is essential. It is worth noting that while large and easily accessible shallow deposits may have been extensively explored using faster methods like RC drilling, diamond core drilling remains indispensable for delving deeper into the earth's subsurface.

Figure 1.1 shows a picture of a truck-mounted diamond core drilling rig, which combines the functionality of a standard rig with the mobility facilitated by a truck chassis. The mast, affixed to the truck, supports the drill head and facilitates the raising and lowering of the drill string. The drill head exerts a downward force (weight) and rotational motion, which are transmitted through

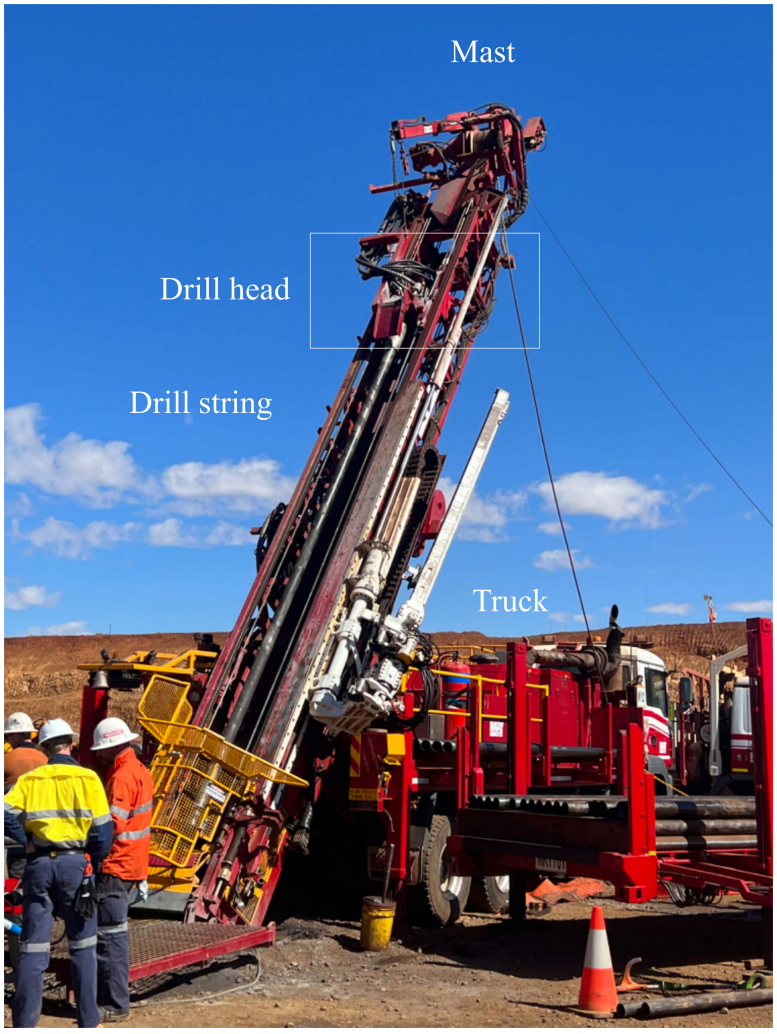

Figure 1.1: Diamond core drilling rig.

the drill string to the bit. The bit then fragments the rock into fine debris (cuttings), forming a borehole. Simultaneously, drilling fluid is pumped through the drill string to carry the cuttings back to the surface through the annulus between the drill pipe and the borehole wall.

The selection of drill bits depends on specific requirements and geological conditions. Figure 1.2 shows three types of commonly used diamond core bits. PDC

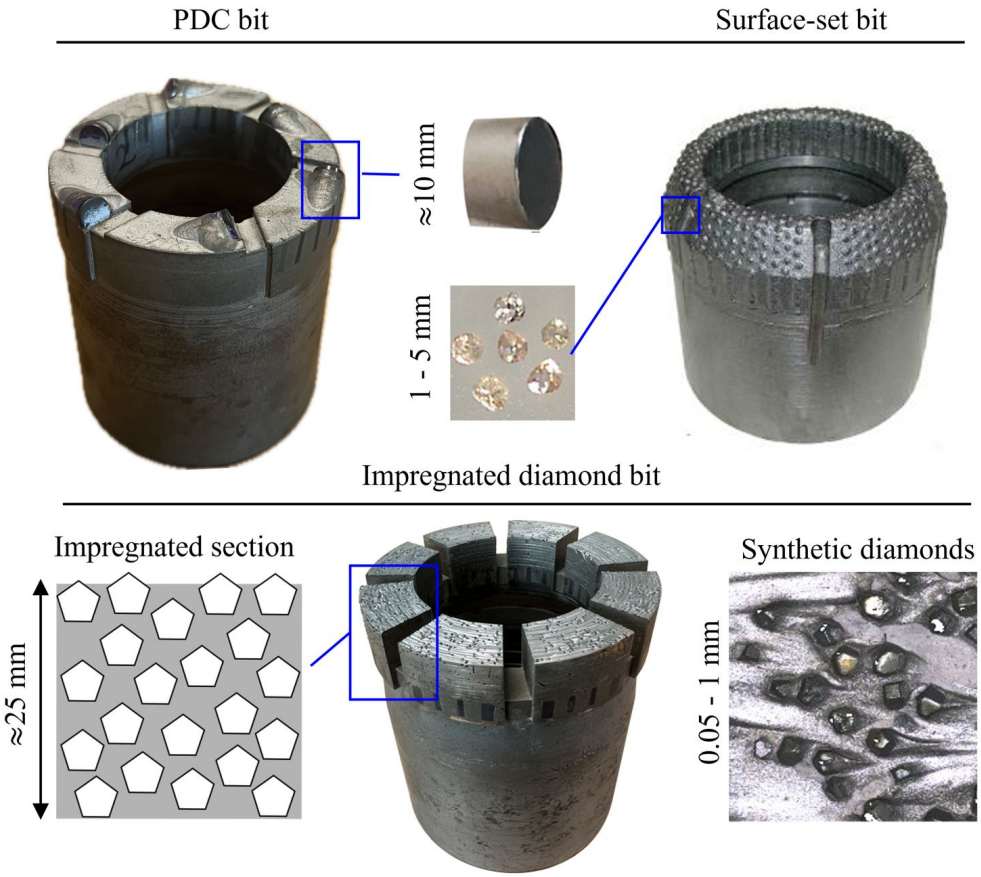

Figure 1.2: Different types of diamond core bits.

(Polycrystalline Diamond Compact) bits use diamond-enhanced cutters, known as PDC cutters, to drill through rocks (Sneddon and Hall (1988); Geoffroy and Minh (1997)). These cutters are made by bonding a layer of synthetic diamonds under high pressure and temperature, creating a hard, wear-resistant cutting face. Surface-set diamond core bits have individual diamonds set on the metal matrix of the bit body (Rowley and Appl (1969)). Both PDC and surface set bits are

known for their ability to achieve high penetration rates due to the large protrusion and hardness of individual cutters. However, they are prone to failure under strong repeated vibrations and mechanical stress, especially in extremely hard and abrasive formations. These conditions can reduce drilling efficiency and shorten the bit life.

Impregnated diamond (ID) bits are specifically designed for drilling in hard and abrasive rock. They are composed of multiple segments attached to a bit shank or steel body. Each segment is made from a mixture of synthetic diamonds and metallic powder, which are cold pressed, and sintered together (Dwan (1998); Kieback and Sauer (2000)). The multiple layers of diamond enable the ID bit to release worn diamonds and expose new sharp ones, and thus maintain performance despite wearing out, i.e. losing material and height.

Despite the extensive use of ID bits in mineral exploration and the substantial investments made by bit manufacturers to optimise bit design, there remains a fundamental gap in understanding the wear processes of these bits and accessing bit wear state, defined as the topology or geometry of the cutting face, and wear rate while drilling. Consequently, the success of the operation heavily relies on the driller's experience. Even when dealing with identical lithological intervals, large discrepancies in operating practices exist among different drillers. Therefore, the overarching goal of this research is to further our understanding of the wear process mobilised at the bit/rock interface through extensive lab-scale drilling experiments and to establish a methodology to estimate bit wear state from surface measurement, such as relationship between forces and penetration rate or depth of cut.

1.1 Merits of laboratory testing

The major advantage of conducting drilling experiments on a lab scale is the ability to halt drilling and examine the bit wear state, which is not feasible in the field. In field operation, removing the bit from the borehole is time-consuming,

logistically challenging and often impractical. Additionally, specialised equipment like high-precision microscope are not available. In contrast, in the lab, it takes less than 1 minute to extract the bit and prepare it for scanning in the lab, with equipment readily available for detailed examinations of bit wear state. This is essential for understanding wear mechanisms and measuring bit wear rate.

Establishing relationships between bit wear state and drilling response requires an extensive amount of drilling and scanning tests. This experimental workflow is time-consuming and impractical to execute in the field. Besides bit wear state, drilling response is also controlled by bit design, rock properties, and drilling fluid properties. It is crucial to isolate and control these variables to ensure that any observed changes in drilling performance are attributable to the parameters being studied. This level of control and precision is feasible only in a controlled lab environment, making the lab setting indispensable for accurate model development and understanding the complex interactions between bit wear and drilling dynamics.

1.2 Objectives and significance

The primary objective of this research is to develop a methodology for capturing the evolution of both the bit wear state and the drilling response. Subsequently, an extensive drilling experiments will be performed to establish relationship between bit wear state (topology of bit cutting face) and drilling response (relationship between forces and depth of cut). The second objective is to investigate bit wear, focusing on the changes in bit wear mechanisms, bit wear state, and bit wear rate under different drilling conditions, including operating parameters, rock properties, and drilling fluid properties.

The outcome of this research offer valuable insights into the wear process of ID tools through a comprehensive quantitative analysis. The model developed in this research can serve as a tool to identify the optimum operating parameters in which a balance between the drilling rate and the life of the bit is achieved.

Additionally, the drilling and scanning data obtained in this research can be used to develop algorithm for automation, enhancing efficiency in drilling operations.

1.3 Organization of thesis

Chapter 2 provides an overview of the existing research on the drilling performance of impregnated diamond bits. The chapter delves into the experimental results from drilling with ID bits, followed by a review of various predictive models developed from these results. At the end, it summarises the shortcomings of the current research, highlighting gaps in quantitative analysis on bit wear.

Chapter 3 provides a detailed description of bit wear state and explores how it affects the drilling response and evolves over time under various drilling conditions. Then it thoroughly describes the experimental workflow, equipment, and materials used in this research.

In Chapter 4, relationships between bit wear state and drilling response are established through a series of drilling and scanning experiments with ID bits at various wear states.

Chapter 5 focuses on evolution of bit wear state and bit wear rate under various drilling conditions. Key variables include depth of the cut, rock type, and drilling fluid properties.

Finally, Chapter 6 outlines the contribution of this thesis and proposes possible future work to overcome the limitations found in this research.

Chapter 2

Literature Review

2.1 Introduction

In this chapter, the literature related to the study of drilling performance of impregnated diamond bits is reviewed. The discussion begins with the drilling response and associated parameters. In this context, the penetration rate (V) is replaced by the depth of cut (d), a length scale corresponding to the thickness of rock removed over one bit rotation. Then I summarise experimental work dedicated to understanding relationship between weight of the bit (W), torque on bit (T), and depth of cut (d), and the controlling parameters that affect drilling performance, including bit design, rock properties and bit wear state. In the end, models available in the literature are listed and their shortcomings are highlighted.

2.2 Drilling response and concept of depth of cut

In drilling with diamond bits, a weight (W) is applied to the bit that is set to rotate at a given angular speed (Ω). As a result, a torque (T) is generated, the rock is fragmented into cuttings (fine derbies) carried out by fluid flow at a given

rate (Q), while the bit penetrates the rock at a certain rate (V), as illustrated in Figure 2.1.

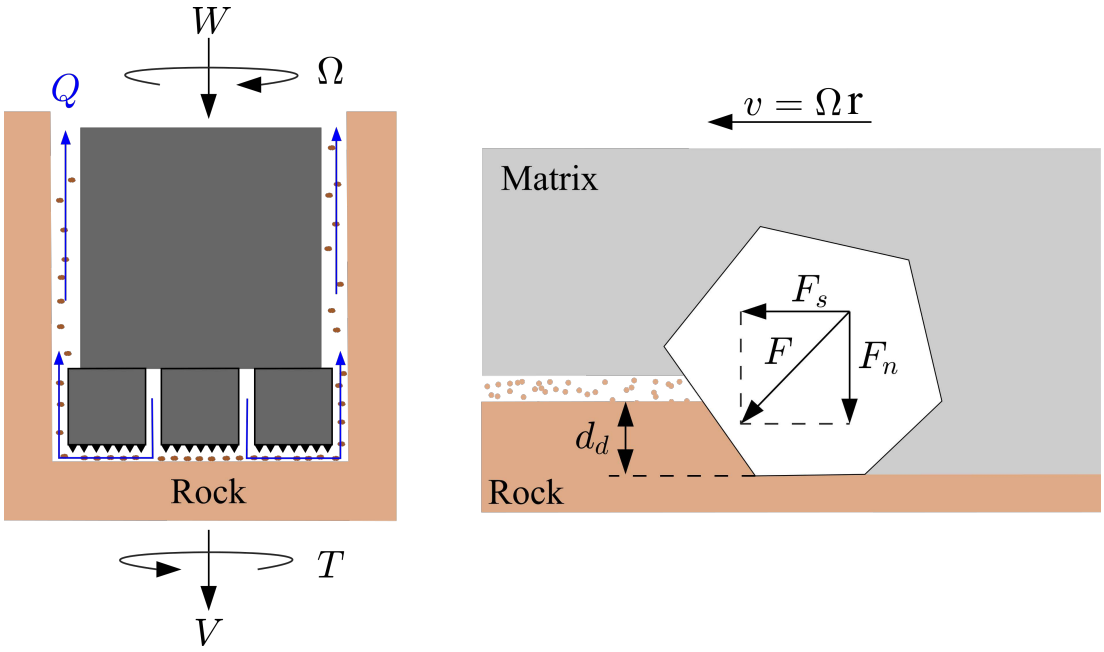

Figure 2.1: State variables acting at an ID bit (left) and the smallest cutting element on the bit (right).

At the diamond scale (the smallest cutting element on the bit), forces acting on the bit are distributed across all diamonds on the bit face, resulting a normal force (F_n) and a tangential force (F_s) acting on each diamond. Each diamond removes a certain thickness of rock (d_d) per bit rotation while travelling at a linear speed (v):

$$v = \Omega r \tag{2.1}$$

where $r = (r_o - r_i)/2$, r_o and r_i are the outer and inner radius of the bit.

The drilling response of the bit is characterised by the relationship between the control parameters (W, Ω, and Q) and the performance variables (T and V), which are affected by the bit, rock and drilling fluid (Detournay and Defourny (1992)). Assuming that these variables are averaged over at least one revolution

of the bit, we establish the following relationship:

$$W(d) = W(\text{bit}, \text{rock}, \text{fluid}) \tag{2.2}$$

$$T(d) = T(\text{bit}, \text{rock}, \text{fluid}) \tag{2.3}$$

where d is the depth of cut corresponding the thickness of rock removed by the bit over one rotation, $d = 2\pi V/\Omega$.

The depth of cut of the bit is shared by all diamonds on the bit face if the diamonds are evenly distributed (Peterson (1976)), and can be read as:

$$d = \sum_{i=1}^{n}(d_d) = nd_d \tag{2.4}$$

where n is the number of diamond on the same perimeter. d_d represents the depth of cut per diamond on that same perimeter.

Compared to the penetration rate (V), depth of cut provides a measure of how much rock is removed per bit rotation. As a length scale, it can be compared with other length scales, such as mean diamond size, diamond wear flat length, and median grain size of the rock. For example, the median grain size of a Bluestone granite is about 0.1 mm. If the depth of cut applied to the bit is less than $n\times$0.1 mm/rev, it is likely that the diamonds cut through the grain rather than breaking the grain boundaries. In addition, the inverse of depth of cut, expressed as revolutions per inch (RPI) or revolution per centimetre (RPC) of advance, is a commonly used criterion in the field to optimise drilling efficiency (Boart Longyear (2009); Atlas Copco Australia (2015); Dimatiec Inc. (2019)).

2.3 Experimental observation

Lab drilling tests are commonly used to obtain drilling responses (Singh (1973)), not only for ID bits (Paone and Madson (1966); Bullen (1982)), but also for all other diamond tools (Rowley and Appl (1969); Warren and Sinor (1986); Franca

(2010)). It involves drilling with full-size bits (Paone and Madson (1966)) or micro-bits (Spink (1972)) under a given weight on bit (Siribumrungsukha (1980)) or depth of cut (Bullen and Bailey (1979)). Although conducting drilling tests with controlled weight on bit can closely simulate the field condition, controlling the depth of cut makes it easier to reproduce the results, which is crucial for validating theoretical models (Di Ilio and Togna (2003)) and comparing different bit designs or operating parameters (Mostofi et al. (2018)).

Regardless of the mode of control, it was found that the weight on bit increases linearly with the depth of cut to a critical depth of cut, beyond which the weight on bit continues to increase but at a much higher rate (Paone and Madson (1966); Siribumrungsukha (1980); Miller and Ball (1990)). Figure 2.2 shows that the weight on bit increases linearly with the depth of cut up to approximately 0.08 mm/rev and then increases at a rate about four times higher. Such response was also observed in other types of bit (Franca (2010)). This observation was later linked to bit cleaning issues due to the excessive accumulation of cuttings between the matrix and the rock surface (Mostofi et al. (2013)).

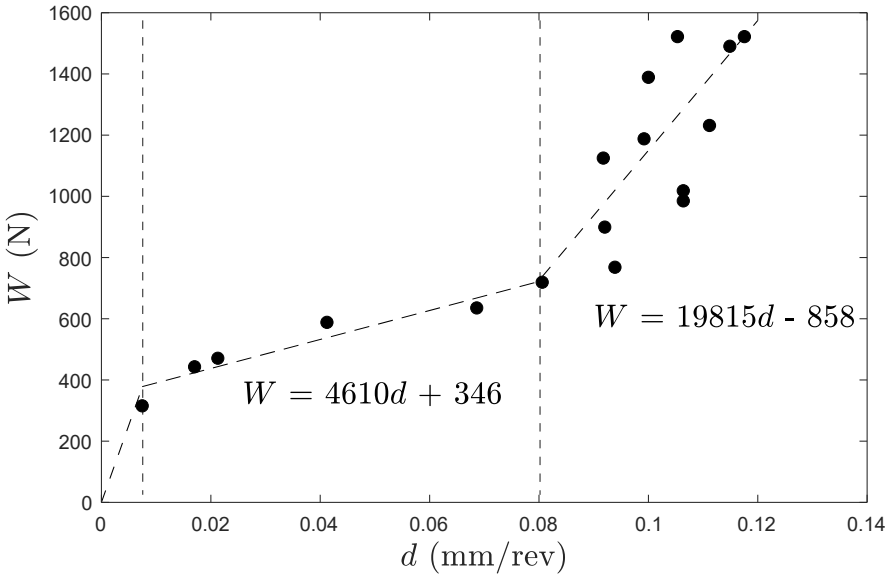

Figure 2.2: The relationship between weight on bit (W) and depth of cut (d). Drilling experiments were carried out using a field-size ID bit in Bushveld norite at a rotational speed of 3500 rpm (redrawn[1] from Miller and Ball (1990)).

Figure 2.3 shows that as the depth of cut increases, the space between matrix and rock is narrowed, more cuttings are produced at the interface, eventually leading to excessive three-body contact between matrix, and rock cuttings that produces extra forces on the bit. It is also observed that the intercept of the

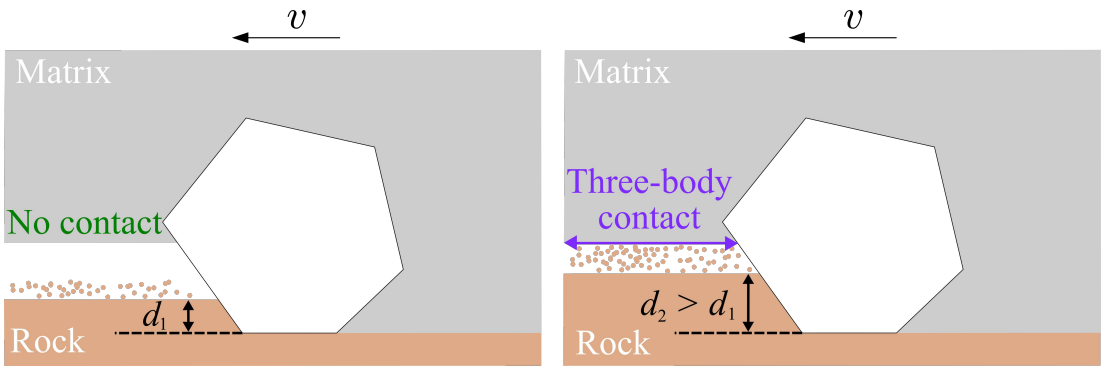

Figure 2.3: Conceptual illustration of three-body contact caused by depth of cut, shallow depth of cut (left) and large depth of cut (right).

first regime is greater than 0, suggesting the presence of an another regime at shallow depth of cut. Therefore, the drilling response can be characterised by three distinct regimes, expressed as follows:

$$W = \begin{cases} = \alpha_{\mathrm{I}} d & d \leq d_* \\ = \alpha_{\mathrm{I}} d_* + \alpha_{\mathrm{II}}(d - d_*) & d_* < d \leq d_{**} \\ = \alpha_{\mathrm{I}} d_* + \alpha_{\mathrm{II}}(d_{**} - d_*) + \alpha_{\mathrm{III}}(d - d_{**}) & d_{**} < d \end{cases} \tag{2.5}$$

where α is the slope of each regime, and subscripts I, II, and III stand for regime I, regime II and regime III, respectively. The critical depths of cut, d_* and d_{**}, are the depth of cut at the onset of regime II and III.

The slope of regime II (α_{II}) is found to be a function of both bit design and rock properties (Chan (2022)). Siribumrungsukha (1980) conducted drilling experiments with an ID bit in three different rocks and found that the slope of regime II increases with rock strength, as shown in Figure 4.17. The slope of

[1]The digitized data from the source are plotted with the formalism and notation used later in the results section. This consistent format helps identify trends and discrepancies between the source data and the new findings.

regime II also increases with matrix hardness (Busch and HILL (1975); Mostofi et al. (2013)). Figure 2.5 shows the slope of regime II by 50% when using a bit with a hard matrix. The slope of regime II also increases with matrix hardness (Busch and HILL (1975); Mostofi et al. (2013)). Figure 2.5 shows the slope of regime II by 50% when using a bit with a hard matrix. Additionally, it was

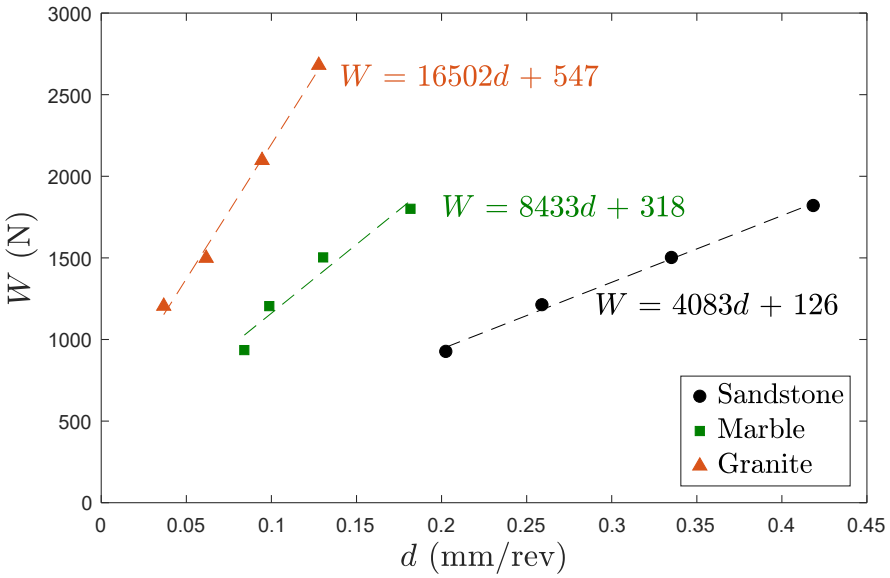

Figure 2.4: Effect of rock on the relationship between weight on bit (W) and depth of cut (d). Tests were conducted at a rotational speed of 385 rpm (redrawn from Siribumrungsukha (1980)).

found that the drilling response is also affected by the bit wear state, specifically size of diamond wear flat area (Malkin and Cook (1971); Bullen (1984); Mostofi et al. (2013)). Figure 2.6 shows that, for a given bit and rock, the weight on bit increases across all depths of cut as with the diamond wear flat area increases. Consequently, it is critical to differentiate the effect attributed to the drilling conditions (bit design, rock properties, etc.) and the bit wear state (diamond wear flat area and matrix wear flat area).To the best of my knowledge, research on the relationship between bit wear state and drilling response is limited, with most studies being qualitative.

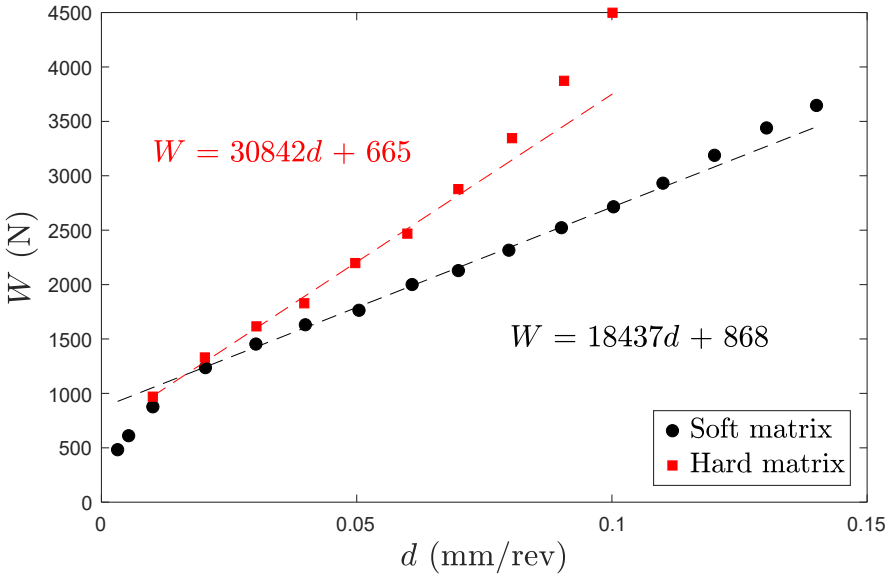

Figure 2.5: Effect of matrix hardness on the drilling response. Tests were conducted using a micro-core bit in American Black granite (redrawn from Mostofi et al. (2013)).

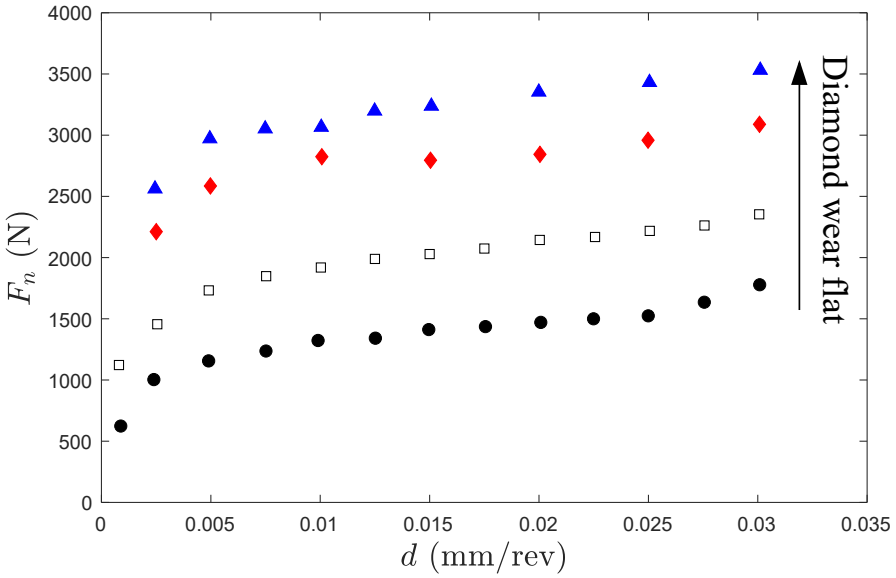

Figure 2.6: Effect of diamond wear flar area on the cutting response of an ID segment in drilling Harcourt granite (redrawn from Mostofi et al. (2013)).

2.4 Bit wear

To better understand the wear process of the bit, researchers conducted drilling (wear) experiments where a rock is drilled at a given weight on bit or depth of cut, and the bit wear state is inspected after the test using scanning equipment (Miller and Ball (1990); Hird and Field (2004); Zacny and Cooper (2004); Mostofi and Franca (2014); Mostofi et al. (2018)).

Figure 2.7 shows that both the weight on bit and the torque on bit increase by threefold when the bit drills at a depth of cut of 0.03 mm/rev for an extended period of time, during which the linear cutting distance (s) covered by the cutting structure reaches about 4000 m. The increases in weight on bit is due to diamond polishing, which creates large wear flats along with most of the work converted to frictional heat (Miller and Ball (1990)). Figure 2.8 shows conceptual drawings and scanned images of a sharp diamond and a polished diamond. It is evident that a polished diamond has a larger wear flat area. Conversely, diamond polishing leads to a decrease in depth of cut when drilling under a controlled weight on bit (Selim et al. (1969); Malkin and Cook (1971); Bullen (1984)).

When drilling at a larger depth of cut, approximately 0.1 mm/rev, the weight on bit remains relatively constant due to fracturing wear (Miller and Ball (1990)). Diamond fracturing causes the diamonds to break into smaller fragments, resulting in surfaces covered with numerous sharp points and, consequently, a reduced wear flat area. Different wear mechanisms and controlling parameters will be discussed in more detail in Chapter 3.

2.5 Different class of model

Different models have been developed to establish predictive equations for drilling with ID bits. These equations are presented here to demonstrate their diverse forms. For comprehensive details on the variables used, please refer to the original publications.

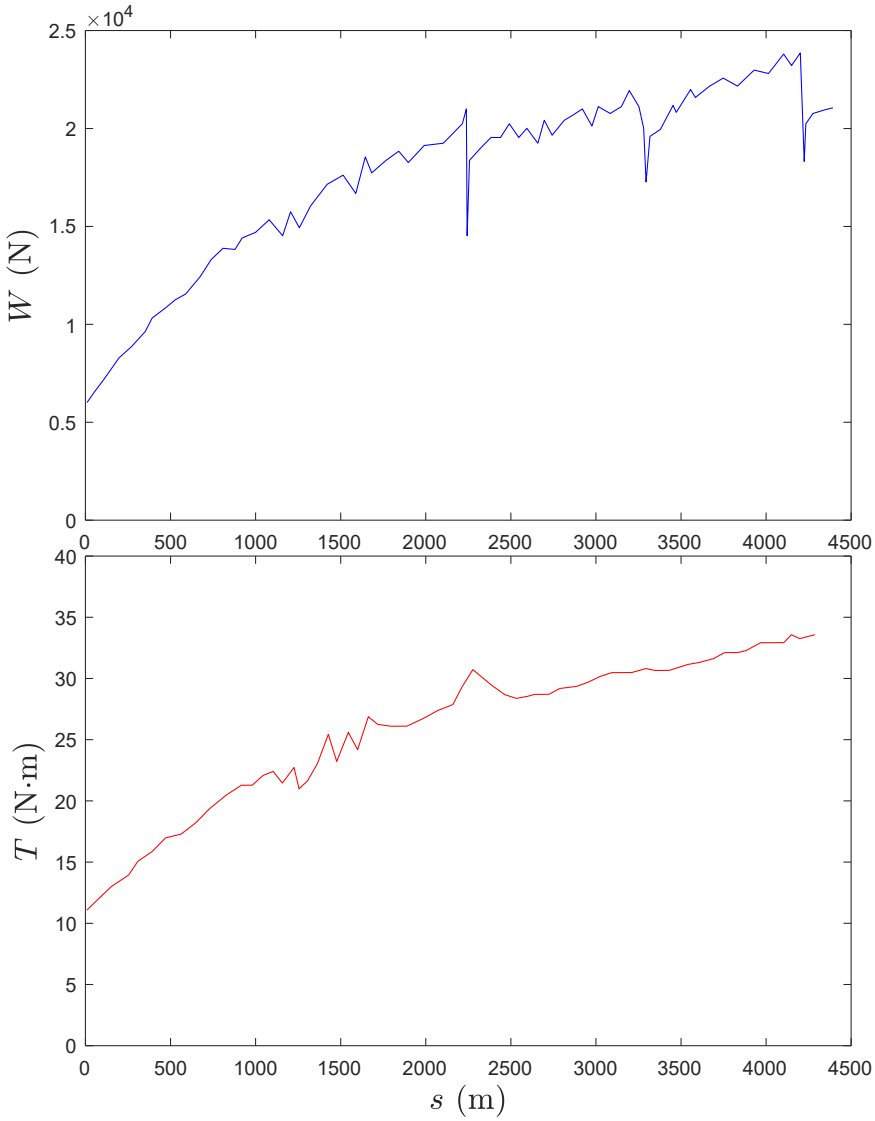

Figure 2.7: The variation of forces (W and T) due to bit wear when drilling at 0.03 mm/rev depth of cut. Drilling experiments were performed using an ID bit in Radiant Red granite (redrawn from Mostofi and Franca (2014)).

2.5.1 Energy approach

Using energy balance, it can be written that the energy required to excavate the rock is equal to the sum of the work done by weight on bit (W) and the work done torque on bit (T). The total work done ($\mathcal{W}$) per bit rotation can be written

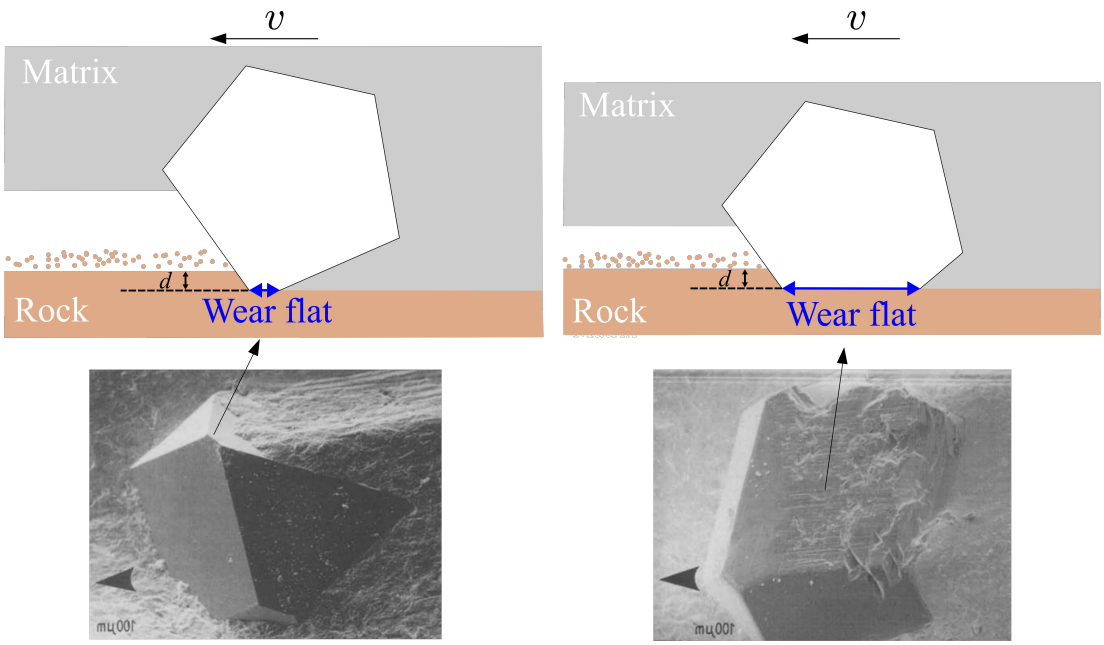

Figure 2.8: Conceptual drawings and real images of a sharp (left) and a polished (right) diamond (Miller and Ball (1991)).

as:

$$\mathcal{W} = Wd + 2\pi T \tag{2.6}$$

Paone and Bruce (1963) considered the work is used to fragment the rock which is proportional to the compressive strength of the rock (q).

$$q\mathcal{A}d = Wd + 2\pi T \tag{2.7}$$

where $\mathcal{A}$ is the bit cross-sectional area .

In addition, the torque on bit is decomposed into the portion used for rock fragmentation and the portion used to overcome friction (μW), where μ is the friction coefficient between bit and rock. Therefore,

$$q\mathcal{A}d = Wd + 2\pi T - 2\pi\mu W r \tag{2.8}$$

solving for d, yields

$$d = \frac{2\pi(T - \mu W r)}{q\mathcal{A} - W} \tag{2.9}$$

Other authors use specific energy (E), defined as the energy required to excavate a unit volume of rock, to evaluate the drilling performance (Teale (1965); Spink (1972); Moller and Spink (1973)). Dividing the work ($\mathcal{W}$) by volume ($\mathcal{V}$) of work removed gives:

$$E = \frac{\mathcal{W}}{\mathcal{V}} = \frac{W}{\mathcal{A}} + \frac{2\pi T}{\mathcal{A}d} \tag{2.10}$$

Miller and Ball (1990) proposed a conceptual model based on the relationship between weight on bit and specific energy. At a low weight on bit, before the transition, only a few diamonds indent the rock and participate in drilling, leading to a predominant wear flat development and a decrease in depth of cut. Up to the transition point, where the specific energy is at the minimum, all exposed diamonds are actively engaged in drilling. This results in a steady weight on bit at a given depth of cut with promoted diamond fracturing. A further increase in weight on bit causes the specific energy to rise again due to cleaning issue, which promotes bit wear. Insufficient clearance between the bit and the rock inhibits effective flushing and cooling with the result of clogging or stalling.

Using the energy approach to evaluate the drilling performance of an ID bit has several limitations. First, the method cannot distinguish between the effects of changing operating conditions and bit wear. While the specific energy increases with issues such as poor cleaning, increased rock strength, or bit polishing, it does not identify the exact cause of the increase. Secondly, the minimum specific energy observed from the study of Teale (1965) often occurs at a relatively low weight on bit and a depth of cut below the maximum rates achievable with a higher weight on bit. Last but not least, since the power supply costs in drilling are usually insignificant in comparison with time costs, simply comparing specific

energy values may not provide a complete picture of operating efficiency (Maurer (1966)).

2.5.2 Empirical correlations

Sasaki et al. (1962) proposed a proportional relationship between weight (W), penetration rate (V) and angular speed (Ω) based on experimental results:

$$V = \Omega(W - W_o)k\frac{d}{W} \tag{2.11}$$

where W_o is an initial weight at zero penetration rate (projected from the linear portion of the weight-penetration rate curve), and k is correction factor.
Paone et al. (1966) conducted statistical regression analysis on the results of drilling tests in a wide range of rock types with a various physical properties. The most successful empirical predictor equation for laboratory diamond drilling with ID bits was as follows:

$$d = 0.0001997 + 0.0006714W - 0.04279q - 0.0001273A_r - 0.03448\mathcal{S} + 0.1135\mathcal{E} \tag{2.12}$$

where q is the rock uniaxial compressive strength, A_r is the relative abrasiveness, $\mathcal{E}$ is the Young's modulus, and $\mathcal{S}$ is the shear modulus.

A similar model was proposed by Ersoy and Waller (1995a) using a multivariate linear regression analysis, but with a wider range of rock properties. Models based on empirical correlation are highly based on data collection under specific drilling conditions. The accuracy and reliability of these models depend on how well the data used to develop the correlations represent the conditions under which the model will be applied.

2.5.3 Models for bit wear

As the drilling process is accompanied by bit wear, several models were developed to predict the change in the penetration rate due to the polishing of the bit and the bit wear rate (Ziaja and Miska (1982)). Strebig et al. (1971) described the rate of penetration V in terms of bit life by the statistical theory of reliability using Weibull distribution:

$$V = V_o e^{-\lambda(S-\gamma)^B} \tag{2.13}$$

where V_o is the initial penetration rate, λ is the failure rate, B is the shape parameter, and γ is the location parameter. This method allowed the relative performance of the drill under sub-optimal conditions to be tested without direct measurement of wear.

Siribumrungsukha (1980) described the progressive decrease in penetration rate due to diamond wear through the production of wear flats:

$$S = V_o/b \cdot (1 - e^{-b\mathcal{T}}) \tag{2.14}$$

where b is a coefficient related to the rate of decrease in penetration rate, and $\mathcal{T}$ is the test duration. This model is used to predict how the wear of the diamonds on the bit affects the drilling performance, and it suggests that the penetration rate decreases over time following an exponential decay curve.

Goktan and Gunes Yılmaz (2017) relates the wear rate of impregnated diamond tool to rock hardness. The Knoop hardness of the rock (HK) was determined by applying a specified load to the surface of a test sample using a pyramidal-shape diamond indenter. The projected area of the resulting residual impression was then measured with a high-powered microscope. The specific wear rate (SWR) corresponds to the height loss of the bit per unit area:

$$\text{SWR} = 0.0631(\text{HK}) - 128.68 \tag{2.15}$$

Ersoy et al. (2005) performed multi-variable linear regression analysis to investigate the relationship between 19 independent variables deemed relevant to the wear of the diamond tools. These variables included Schmidt rebound hardness, specific energy, silica content, etc. Quacquarelli et al. (2021) proposed a multi-scale model to predict the wear of the matrix around the diamond.

These models oversimplify the bit wear mechanisms while drilling: the Weibull distribution assumes that the bit wear mechanism is governed solely by the drilling distance, neglecting factors like rock and bit properties and depth of cut. Siribumrungsukha (1980) focuses primarily discusses diamond polishing wear mechanism, without addressing diamond fracturing and pull-out wear mechanisms. Goktan and Gunes Yılmaz (2017) assumes a linear relationship between Knoop hardness and the specific wear rate without accounting for other factors, such as mineral composition and abrasiveness, which can significantly affect the wear rate.

2.5.4 Phenomenological model

The phenomenological model describes the physical processes involved in drilling operations, and has been used to model the drilling action of ID grinding wheel (Malkin and Cook (1971)), ID circular saws (Ersoy and Waller (1995b); Ersoy et al. (2005)) and PDC bits (Detournay and Defourny (1992)). Following the suggestion (Fairhurst and Lacabanne (1957)) that the bit-rock interaction is characterised by the coexistence of rock cutting and frictional contact, the weight on bit and torque on bit are each decomposed into two components associated with these basic processes.

$$W = W_c + W_f \tag{2.16}$$

$$T = T_c + T_f \tag{2.17}$$

where the subscript c denotes the cutting process and f denotes the frictional process.

The cutting components are proportional to the cross-sectional area A_c of the cut:

$$W_c = \zeta \varepsilon A_c \tag{2.18}$$

$$T_c = r \varepsilon A_c \tag{2.19}$$

where $A_c = d(r_o - r_i)$, ε is the intrinsic specific energy, and ζ characterises the inclination of the cutting force acting on the cutting face.

The intrinsic specific energy (ε) quantifies the minimum amount of energy required to cut a unit volume of rock, reflecting the complex process of rock destruction. This value generally depends on the mechanical properties of the rock, i.e., the uniaxial compressive strength of the rock (q) (Richard et al. (1998)). The inclination of the cutting force (ζ) depends on the design of the bit, approximately 1 for PDC bits (Detournay and Defourny (1992)) and about 3 for ID bits (Chan (2022)).

The frictional components are proportional to the wear flat area of the tool A and read as:

$$W_f = \sigma A \tag{2.20}$$

$$T_f = \mu \sigma A \tag{2.21}$$

where σ and μ represents contact stress and friction coefficient between wear flat and rock, respectively.

Malkin and Cook (1971) observed that forces increase linearly with the wear flat area, indicating that contact pressure and friction coefficient are invariant for a given combination of bit and rock. Franca et al. (2015) later extended this model to ID bits, decomposing the frictional process into diamond rubbing and

matrix rubbing. As a result, forces acting on the bit read as:

$$T = r(\varepsilon A_c + \mu_d \sigma_d A_d + \mu_m \sigma_m A_m) \tag{2.22}$$

$$W = \zeta \varepsilon A_c + \sigma_d A_d + \sigma_m A_m \tag{2.23}$$

where the subscript d corresponds to diamond and m to matrix.

The model effectively differentiates parameters associated with the operating conditions (ζ,ε,σ, and μ) and bit wear state (A_d and A_m). However, accurate measurement of wear flats is essential for deriving model parameters, and isolating the effect of bit wear is crucial for obtaining reliable results. To address these challenges, Franca et al. (2015) developed a specialised test procedure that involves drilling rock at various depths of cut in a short period of time. Consequently, the bit wear state is characterised by a quasi-nil rate of change during the test, and the effect of bit wear on forces is minimised.

A drilling response model is established based on relationships between weight, torque, and depth of cut at a given state of wear. It consists of three distinct cutting regimes, each governed by different processes, see Figure 2.9. In regime I, forces associated with rock fragmentation, diamond frictional, and matrix frictional processes increases with depth of cut. The friction force mobilised on the diamond/rock wear flat levels off at the end of regime I and remains constant thereafter as conformal contact between the diamond wear flat and the rock is established. In regime II, both the matrix friction force and the pure cutting force continue to increase with the depth of cut. Regime III starts at a high depth of cut because of cleaning issues (excessive three-body contact) that matrix fictional force increases with depth of cut at a higher rate. More details of the model are presented in Chapter 3.

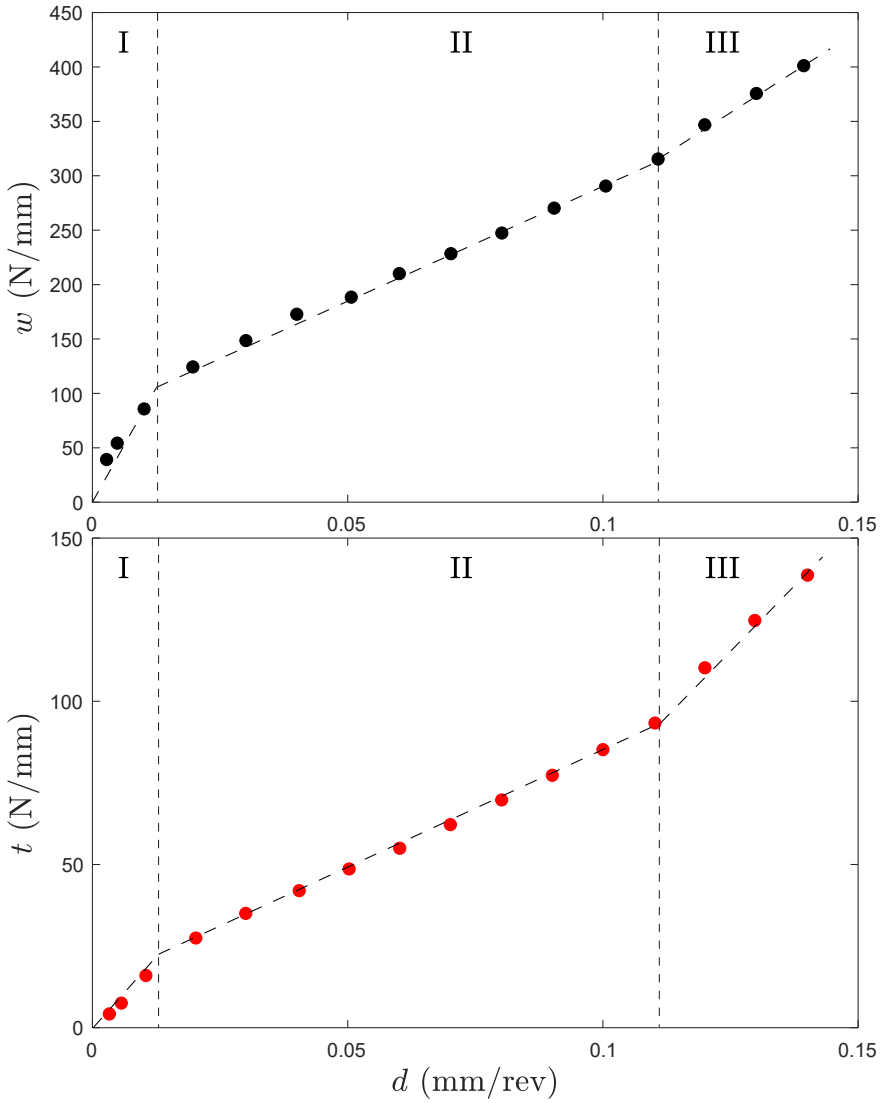

Figure 2.9: An example of drilling responses fitted with the model characterised by three different regimes with two critical depths of cut. Results are obtained in drilling American Black granite using an ID bit (redrawn from Mostofi (2014)).

2.6 Shortcoming

The experimental results indicate that the drilling performance of ID bits is influenced by a combination of factors: bit design, rock properties, operating parameters, and bit wear state. Despite this understanding, there appears to be a lack of research focused specifically on how bit wear state affects drilling response. This gap suggests that the detailed relationship between physical wear and geometric

changes in the bit and the resulting performance during drilling has not been thoroughly explored and quantified.

The wear process of the bit under different drilling conditions remains largely qualitative. The existing literature primarily identifies and describes different wear mechanisms, such as diamond polishing and fracturing, as well as matrix abrasion and erosion. However, how the bit wear state and wear rate evolve over time under varying drilling conditions have not been studied in detail. The specific changes in the bit wear state and how these changes impact drilling performance over time have not been quantitatively analysed.

Chapter 3

Phenomenological model and research methodology

3.1 Introduction

In this chapter, four nominal lengths are introduced to characterise the bit wear state and how these nominal lengths can affect the drilling response are discussed. A conceptual model is also proposed to capture how nominal lengths and bit wear rate evolve under different drilling conditions. The model can be used as a tool to help identify the optimal depth of cut at which a balance between penetration rate and bit life is achieved.

An experimental workflow is designed to validate the proposed model that consists of three components: (i) scanning of the bit face to measure nominal lengths (quantify bit wear state), and derive bit wear rate, (ii) drilling (step) tests to capture the drilling response at a given bit wear state, and (iii) extended drilling (wear) tests to produce a change in the bit wear state.

3.2 Bit wear state and drilling response

3.2.1 Concept of equivalent blade and nominal lengths

At scale of a single diamond, the rock is fragmented into cuttings at the front of the diamond. Cuttings mix with drilling fluid to form a slurry that erodes the matrix and creates a crater at the front of the diamond and a tail behind the diamond (as the diamond protected the matrix behind from erosion), see Figure 3.1a. Figure 3.1b shows the 2D image of a single diamond in a mix of true- and pseudo-colour views. The colour bar helps evaluate the diamond's geometry by correlating the height with different colours. The matrix wear flat at the crater is set as the datum (0 mm). The diamond wear flat and the matrix wear flat at the tail are at the same height, around 0.2 mm. The height difference between matrix wear flat at the crater and diamond wear flat is defined as the diamond protrusion (p).

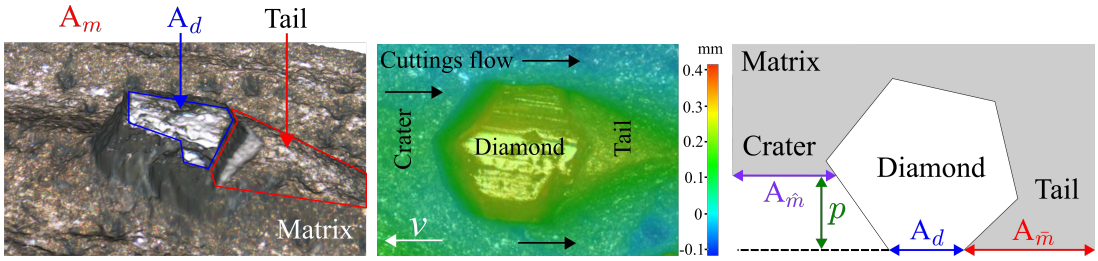

(a) 3D image. (b) 2D image. (c) Conceptual drawing.

Figure 3.1: Single diamond geometry.

The geometry of a single diamond can be characterised by a diamond wear flat area (A_d) and a matrix wear flat area (A_m). The matrix wear flat area can be divided further into matrix wear flat area at the crater ($A_{\hat{m}}$), and at the tail ($A_{\bar{m}}$), see Figure 3.1c.

The cutting face of an ID bit consists of many diamonds with different geometry (p, A_d, $A_{\bar{m}}$, and $A_{\hat{m}}$), see Figure 3.2. Instead of trying to model the interaction of all diamonds on the bit face with the rock, we reduce the bit cutting structure to a single equivalent blade (Peterson (1976)) with a width equal to that of the

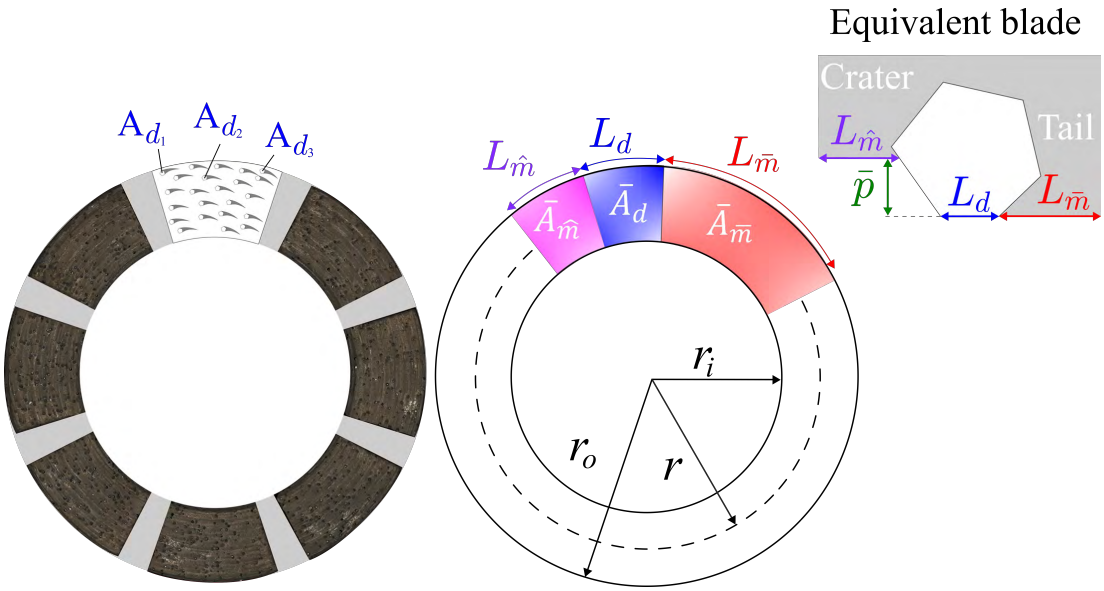

Figure 3.2: Concept of an equivalent blade. All diamonds on the bit are reduced to a single equivalent blade characterised by four equivalent (nominal) lengths, $\bar{p}$, L_d, $L_{\bar{m}}$, and $L_{\hat{m}}$.

segment on the bit. Diamond protrusion ($\bar{p}$), diamond wear flat area ($\bar{A}_d$), matrix wear flat area at the tail ($\bar{A}_{\bar{m}}$) and at the crater ($\bar{A}_{\hat{m}}$) of the equivalent blade read as follows:

$$\bar{A}_d = \sum_{i=1}^{n} A_{d_i} \tag{3.1}$$

$$\bar{A}_{\bar{m}} = \sum_{i=1}^{n} A_{\bar{m}_i} \tag{3.2}$$

$$\bar{A}_{\hat{m}} = \sum_{i=1}^{n} A_{\hat{m}_i} \tag{3.3}$$

$$\bar{p} = \frac{\sum_{i=1}^{n} p_i}{n} \tag{3.4}$$

with n the total number of diamonds.

We assume the wear flats are uniformly distributed across the blade width

and then introduce nominal length-scales of the equivalent blade as:

$$L_d = \frac{\bar{A}_d}{r_o - r_i} \tag{3.5}$$

$$L_{\bar{m}} = \frac{\bar{A}_{\bar{m}}}{r_o - r_i} \tag{3.6}$$

$$L_{\hat{m}} = \frac{\bar{A}_{\hat{m}}}{r_o - r_i} \tag{3.7}$$

where L_d, $L_{\bar{m}}$, and $L_{\hat{m}}$ represent the nominal length of the diamond wear flat area, matrix wear flat area at the tail and at the crater of the equivalent blade, which will later be referred as the diamond wear flat length, the matrix wear flat length at the tail and at the crater, respectively, for simplicity.

While drilling, the equivalent blade cuts a thickness of rock equal to the total depth of cut d. The forces acting on the bit is scaled by the width of the blade or segment to arrive scaled forces - force per unit width - read as:

$$w = \frac{W}{r_o - r_i} \tag{3.8}$$

$$t = \frac{2T}{r_o^2 - r_i^2} \tag{3.9}$$

where w and t are scaled weight and scaled torque acting on the equivalent blade, respectively.

3.2.2 Effective contact lengths

While drilling, the bit is forced into contact with a rock through effective contact lengths that transmit loads and generate friction. Figure 3.3 conceptually illustrates the effective contact lengths formed from the contact between the wear flat lengths of an equivalent blade and a rock. In tribology, the effective contact length (ℓ) formed by two-body contact is generally smaller than the wear flat length (L) because of surface unevenness. However, if these two surfaces fit each other perfectly without any gap, a conformal contact is established ($\ell = L$).

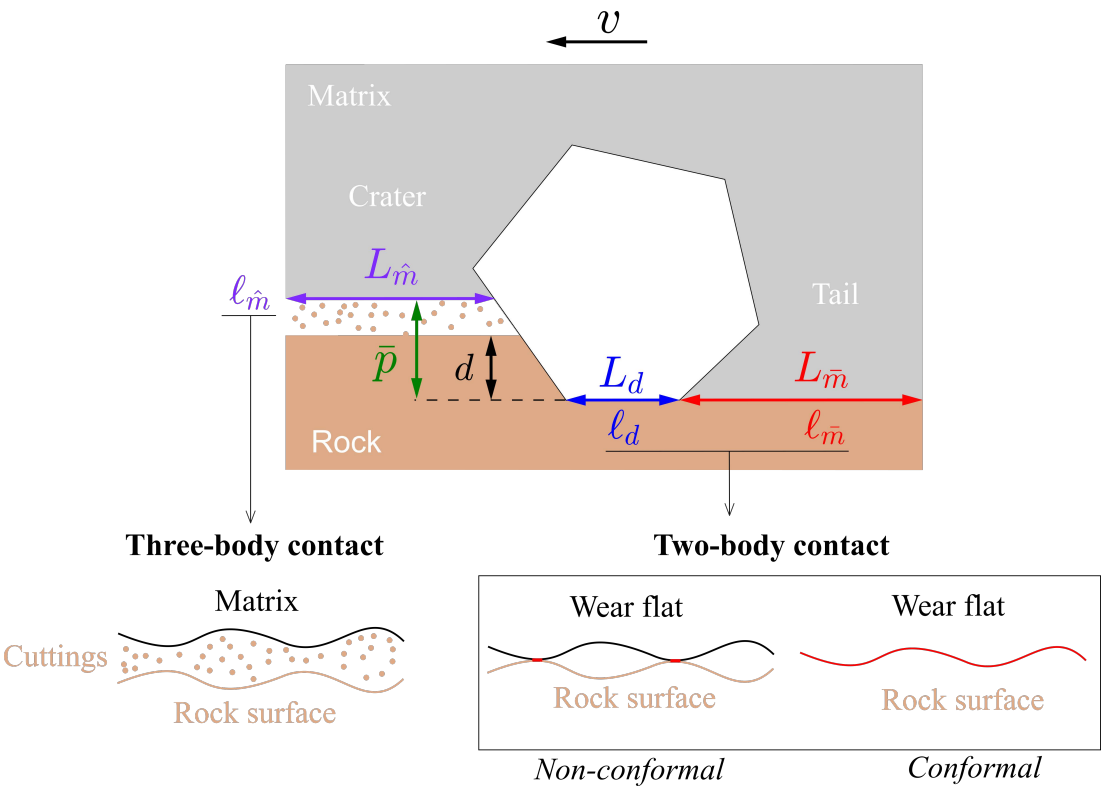

Figure 3.3: Two types of effective contact lengths formed at the interface between an equivalent blade and a rock (conceptual drawing).

Contact between the diamond wear flat or the matrix wear flat at the tail and the rock is a two-body contact characterised by a degree of conformity (Archard (1953)) that increases with depth of cut to eventually reach a plateau (Franca et al. (2015)). However, whether this plateau ($\hat{\ell}$) is equal to the wear flat length (L) is still questionable because part of the wear flat area may never touch the rock.

$$\ell \leq \hat{\ell} \leq L \tag{3.10}$$

Contact at the crater is a three-body contact where the cutting/fluid slurry acts as the third body. The magnitude of this three-body contact also increases with depth of cut, not by increasing the degree of conformity, but by increasing the number of cuttings that are in contact with the matrix. Thus, the relationships between the diamond frictional contact length (ℓ_d), the matrix frictional contact

length at the tail ($\ell_{\bar{m}}$) and at the crater ($\ell_{\hat{m}}$) and the depth of cut read as follows:

$$\ell_d = \begin{cases} \kappa_d d, & d < d_* \\ \hat{\ell}_d & d_* \leq d \end{cases} \tag{3.11}$$

$$\ell_{\bar{m}} = \kappa_{\bar{m}} d \tag{3.12}$$

$$\ell_{\hat{m}} = \begin{cases} 0, & d \leq d_{**} \\ \kappa_{\hat{m}}(d - d_{**}) & d_{**} < d \end{cases} \tag{3.13}$$

where κ_d, $\kappa_{\bar{m}}$, and $\kappa_{\hat{m}}$ are coefficients that represent the variation of effective diamond and matrix frictional contact length with d, d_* and d_{**} (the depths of cut at the onset of regime II and regime III, respectively).

The diamond frictional contact length (ℓ_d) increases with depth of cut and eventually reaches a plateau ($\hat{\ell}_d$) when depth of cut passes beyond the depth of cut (d_*) at the onset of regime II, see Figure B.2. The matrix frictional contact length (ℓ_m) initially increases linearly with depth of cut and suddenly increases at a larger rate when d exceeds d_{**}. This sudden change in slope is owned to additional contact caused by inadequate evacuation of cuttings. As mentioned earlier, cuttings only contribute to the matrix frictional contact at the crater, thus we can assume that as depth of cut increases, two-body contact takes place, and $\ell_{\bar{m}}$ increases, but $\ell_{\hat{m}}$ equals zero because of adequate cleaning - all cuttings leave the bit-rock interface without touching the matrix at the crater (see Figure 3.5), as the depth of cut continues to increase, more cuttings are produced, the space in the crater region narrows, and eventually cleaning problem occurs when d passes beyond d_{**}, three-body contact occurs, and $\ell_{\hat{m}}$ increases, and thus the matrix frictional contact (ℓ_m) increases at a higher rate.

3.2.3 Nominal lengths and drilling response parameters

There are experimental observations in the literature that suggest the drilling response is governed by nominal wear flat lengths. Mostofi (2014) conducted

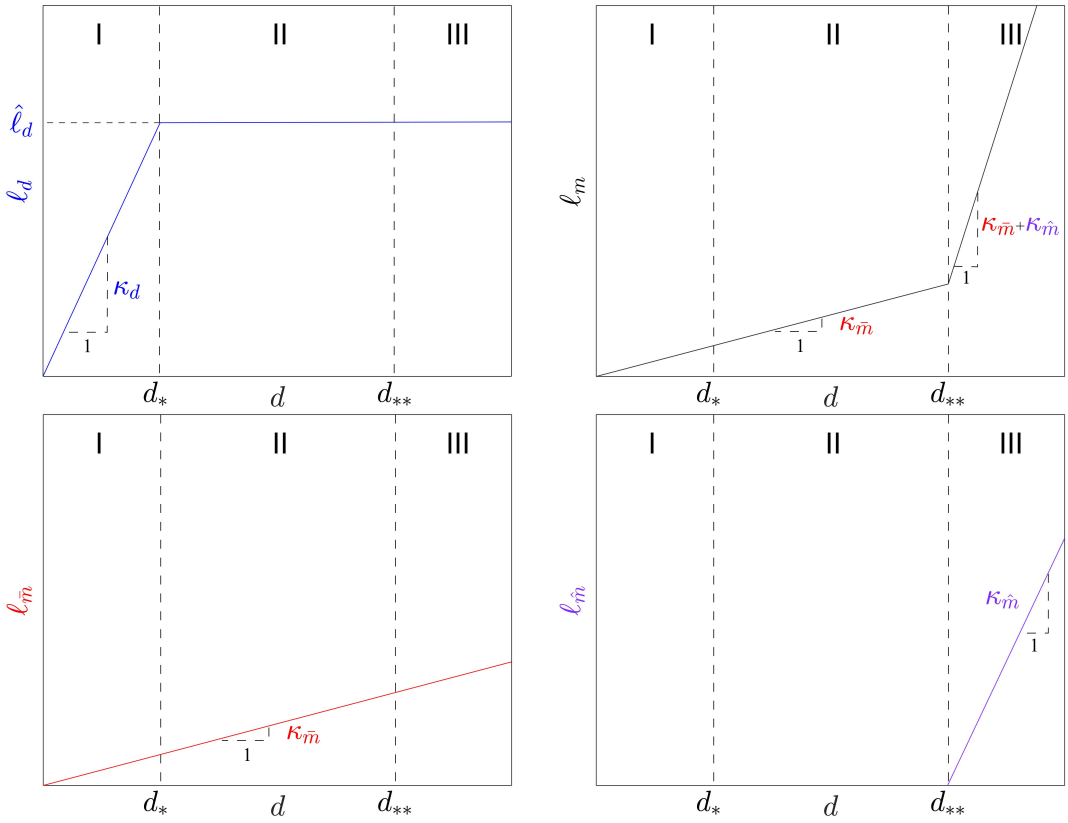

Figure 3.4: Conceptual model of diamond frictional contact length, matrix frictional contact length with d at a given state of wear (L_d,L_m).

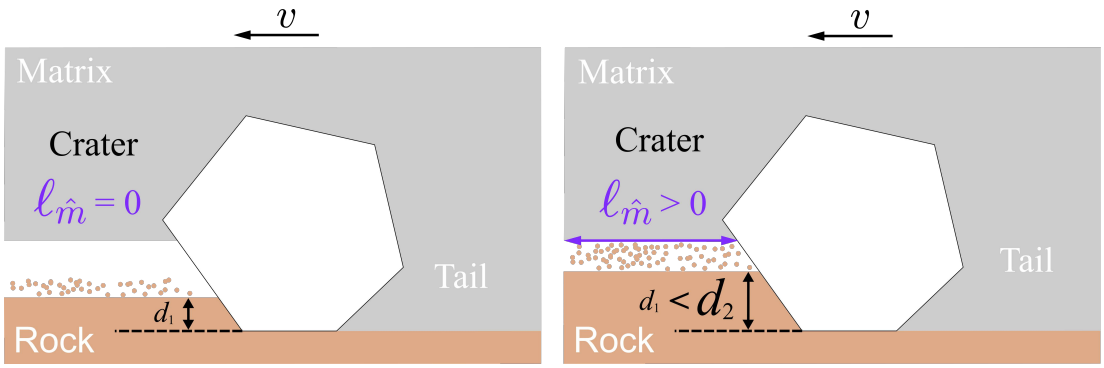

Figure 3.5: Sketch of the matrix frictional contact at the crater ($\ell_{\hat{m}}$) at $d < d_{**}$ (left) and $d > d_{**}$ (right).

cutting tests with a segment in two different wear states ($L_{d_2} > L_{d_1}$). Figure 3.6 shows the cutting responses of the segment; the response with a larger flat diamond wear length (L_{d_2}) shows a higher intercept of regime II. Given that the scaled normal force in regime II read as: $f_n = (\zeta\epsilon + \sigma_m\kappa_m)d + \sigma_d\hat{\ell}_d$, we can

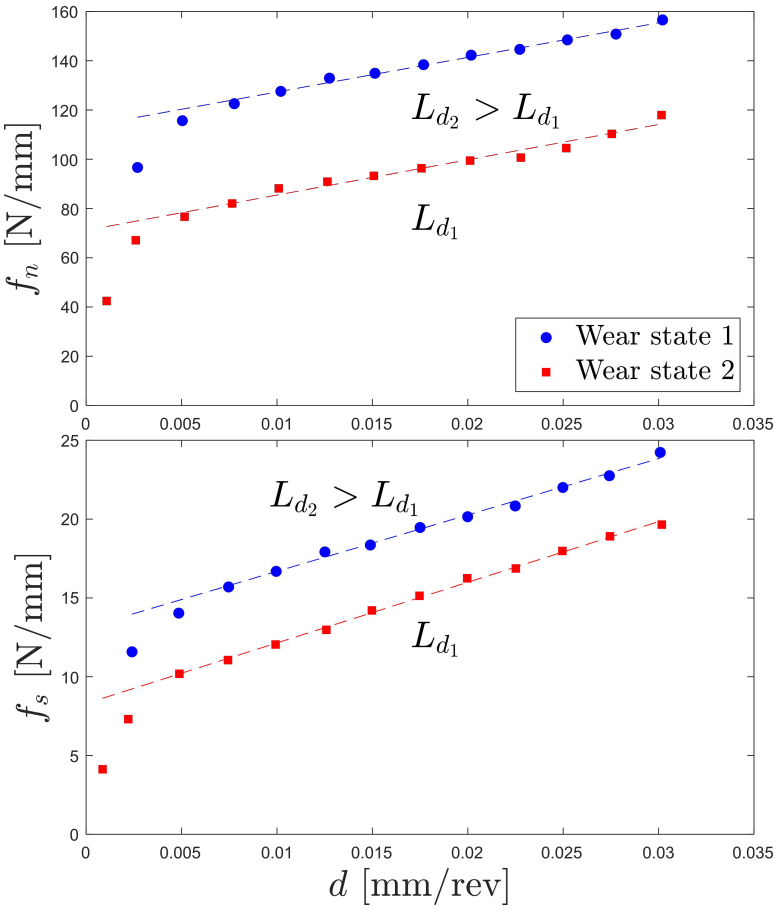

Figure 3.6: The cutting responses of a modified segment in two different wear states (redrawn from Mostofi (2014)).

conclude that the conformal diamond frictional contact length ($\hat{\ell}_d$) increases with the diamond wear flat length (L_d). Even though regime I only contains two data points, we can still observe that the coefficient (κ_d) representing the variation of diamond frictional contact length increases and the depth of cut (d_*) at the on set of regime I extends from 0.005 to 0.007 mm/rev when the diamond wear flat length increases. Based on the results, we can infer that:

$$\frac{\delta d_*}{\delta L_d} > 0 \tag{3.14}$$

$$\frac{\delta \kappa_d}{\delta L_d} > 0 \tag{3.15}$$

Similar to diamond frictional contact length, the matrix frictional contact length at the tail ($\ell_{\bar{m}}$) is expected to increase with matrix wear flat length ($L_{\bar{m}}$) at a given depth of cut meaning that $\kappa_{\bar{m}}$ increases with $L_{\bar{m}}$.

For the matrix frictional contact length at the crater ($\ell_{\hat{m}}$), it is legitimate to assume that the depth of cut (d_{**}) at the onset of regime III increases with increasing diamond protrusion ($\bar{p}$), increasing diamond protrusion widens the space between matrix and rock at the crater and thus accommodates more cuttings without matrix-cuttings contact and therefore delay the onset of regime III. Similarly, within regime III, for a given depth of cut, the bit with higher diamond protrusion leads to a smaller matrix frictional contact length at the crater ($\ell_{\hat{m}}$).

Figure 3.7 conceptually illustrates the effect of bit wear state on the model parameters of the drilling responses. The next step is to investigate how nominal lengths ($\bar{p}$, L_d, $L_{\bar{m}}$, and $L_{\hat{m}}$) evolve with time (wear) under different drilling conditions.

3.3 Bit wear

3.3.1 Dominant wear mechanisms and controlling parameters

Diamonds wear through two different mechanisms: polishing and fracturing, see Figure 3.8. Diamond polishing leads to a loss of material and the development of a wear flat on the diamond tip. The diamond wear flat area (A_d) increases with the cutting distance (s), and the diamond height (h) decreases. Fracturing causes the diamond to shatter into smaller fragments leaving the diamond surface covered with multiple sharp points. The diamond wear flat area (A_d) either remains the same or decreases. The diamond height loss ($\dot{h}$) is much higher during fracturing

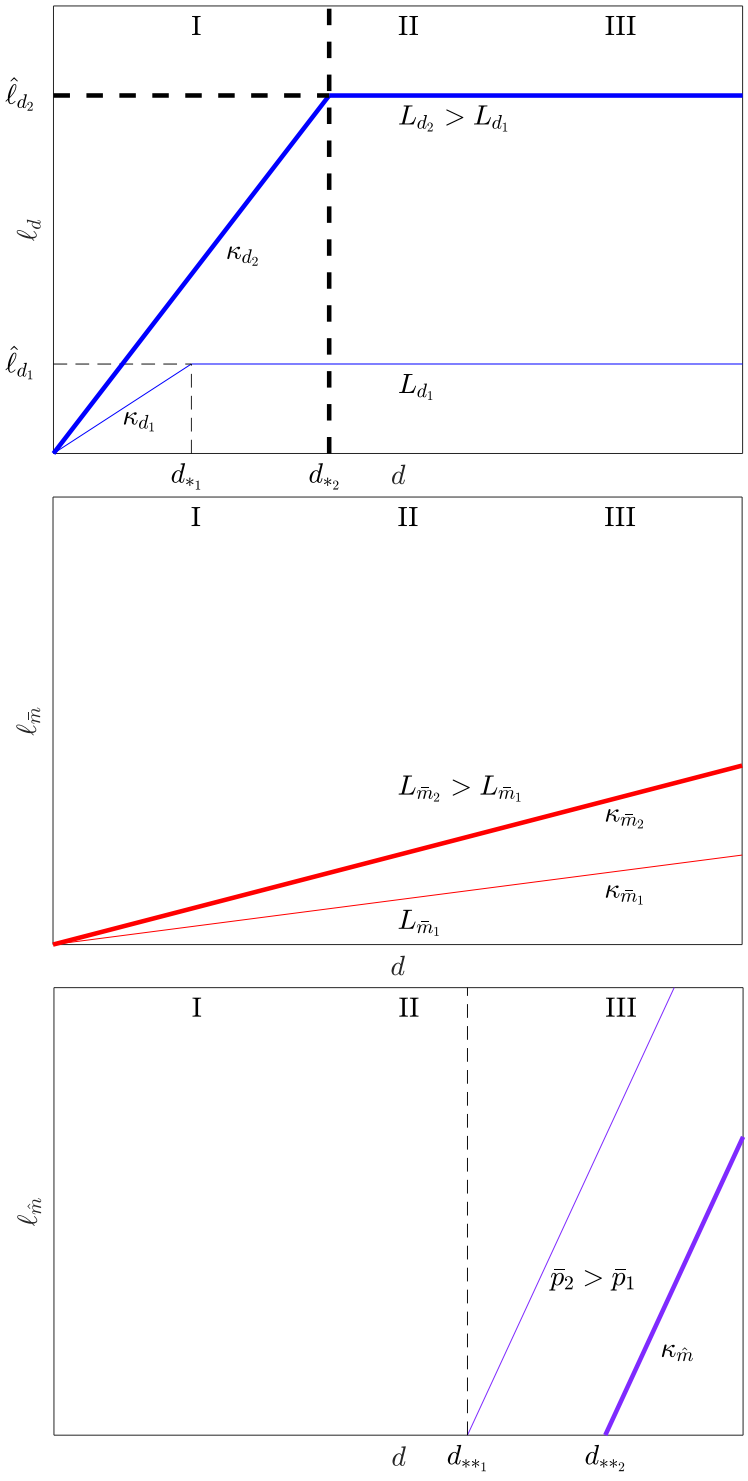

Figure 3.7: Conceptual drawing of the effect of bit wear state ($\bar{p}$, L_d, and $L_{\bar{m}}$) on the model parameters of drilling responses.

and is read as:

$$\dot{h} = \frac{\delta h}{\delta s} \tag{3.16}$$

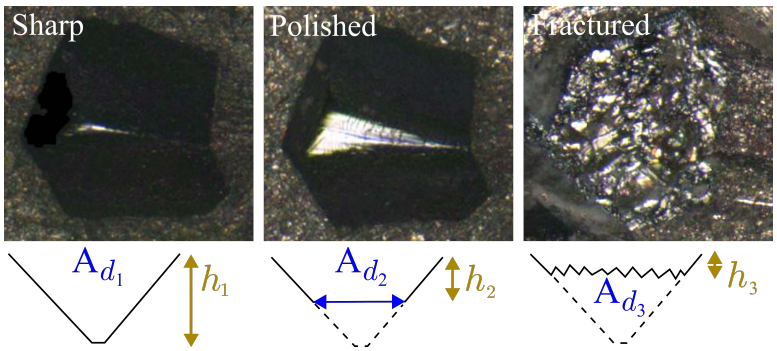

Figure 3.8: An example of a sharp (left), a polished (middle), and a fractured (right) diamond with the conceptual drawing of their geometry.

The surrounding matrix wear through two-body abrasion at the tail and three-body erosion at the crater. The matrix wear flat area at the tail ($A_{\bar{m}}$) increases with diamond wear flat area (A_d), see Figure 3.9. Because $A_{\bar{m}}$ is formed due to diamond protection, the wider the diamond wear flat area, the larger the matrix wear flat area at the tail is formed.

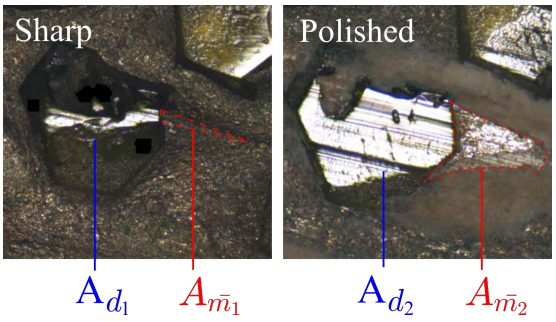

Figure 3.9: An example of change in the matrix wear flat area at the tail ($A_{\bar{m}}$) caused by diamond polishing.

The matrix at the crater is evenly eroded by the third body to expose the diamond. The matrix wear flat area at the crater ($A_{\hat{m}}$) may remain unchanged, but the diamond protrusion (p) increases with cutting distance. Figure 3.10

shows that the diamond protrusion (p) increases with cutting distance (s) due to three-body erosion but decreases when the diamond is fractured.

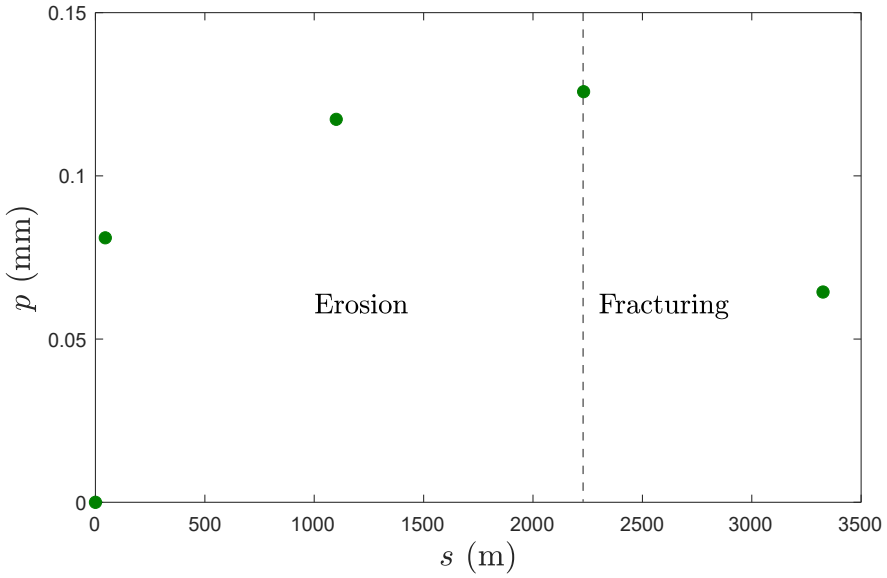

Figure 3.10: The evolution of diamond protrusion (p) as a function of cutting distance (s) (Quacquarelli et al. (2021)).

When the diamond protrusion (p) increases, the ability of that matrix to hold the diamond in place decreases. Di Ilio and Togna (2003) suggests the maximum diamond protrusion is about 50% of its height (h). In other words, the diamond will be pulled out when $p/h > 0.5$. Figure 3.11 shows that the diamond is removed when the diamond protrusion (p) increases beyond 0.15mm ($h = 0.3$ mm) leaving a pit on the cutting face. After diamond loss, two-body abrasion becomes the only wear mechanism to expose a new diamond.

The dominance of each wear mechanism is controlled by weight on bit or depth of cut. Miller and Ball (1991) conducted drilling experiments with an ID bit at different weights on bit. The result shows that the percentage of diamond polishing decreases by 20% with increasing the weight on bit while the percentage of diamond fracturing increases by 25%, see Figure 3.12. The depth of cut gradually decreases at 800 N weight on bit as diamond polishing causes an increase in the diamond wear flat length (L_d), while it remains steady when the weight

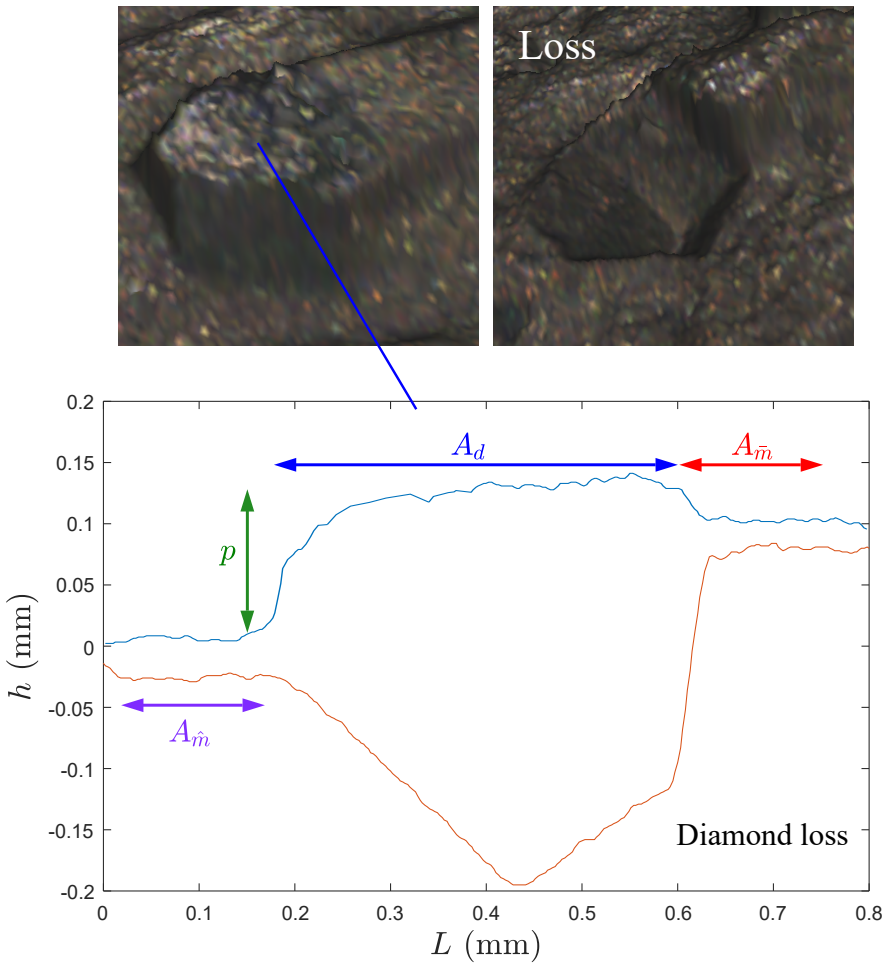

Figure 3.11: An example of diamond loss and comparison of depth profile before and after.

on bit is higher than 2000 N (L_d is balanced by fracturing).

Mostofi et al. (2018) conducted drilling experiments at a given depth of cut. Figure 3.13 shows the scaled forces (w and t) increase with the cutting distance (s), but stabilise when the depth of cut increases. The steady increase in w and t at a shallow depth of cut is due to an increase in the diamond frictional contact length (ℓ_d), which results from the growing diamond wear flat length (L_d). At larger depths of cut, these two lengths remain constant as the responses transitioned from the polishing dominant to the fracturing dominant regime. It is worth to highlight that, at depth of cut 0.03 mm/rev, even the weight on bit increases to more than 20000 N (calculated from $W = w(r_o - r_i)$), diamonds

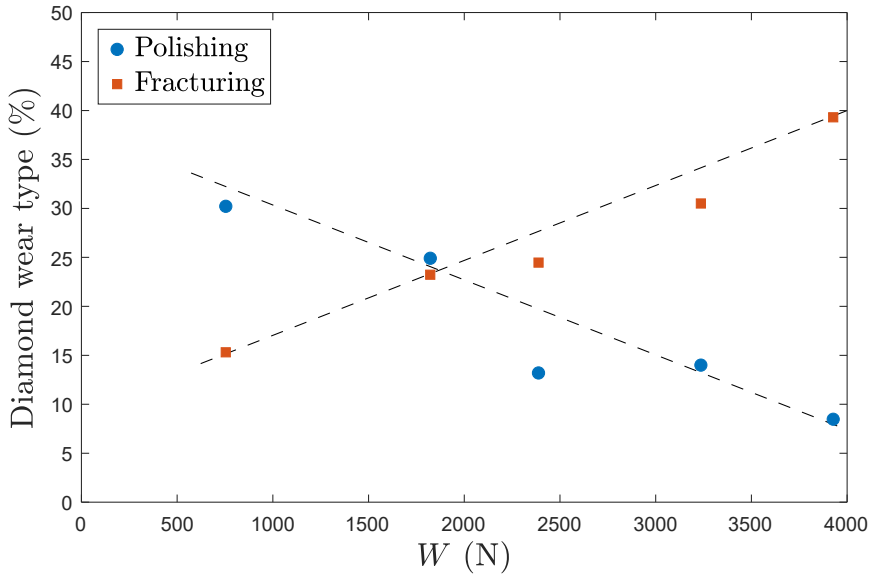

Figure 3.12: The relationship between percentage of diamond wear type and weight on bit. Drilling tests were carried out in norite (redrawn from Miller and Ball (1991)).

still undergo polishing wear, which means that the dominant wear mechanism is controlled by depth of cut rather than weight on bit.

Two-body abrasion between matrix and rock persistently occurs at the tail and becomes dominant when diamonds are pulled out, the spikes in t at 0.09 mm/rev depth of cut indicate localised two-body abrasion contacts. As the depth of cut continues to increase and passes beyond the depth of cut ($d_{**} = 0.1$ mm/rev) at the onset of regime II, the forces fluctuate around a mean value and a much higher wear rate ($\dot{H}$) is observed (Mostofi et al. (2018)). It indicates a continuous matrix rock frictional contact that includes two-body and three-body contacts when $d > d_{**}$ causing an increase in the number of diamonds pulled out.

3.3.2 Conceptual model

A conceptual model can be established in terms of dominant wear mechanisms, see Figure 5.1. For simplicity, I define a depth of cut, d_f, as the transition from polishing dominant wear to fracturing dominant wear. In the example shown in

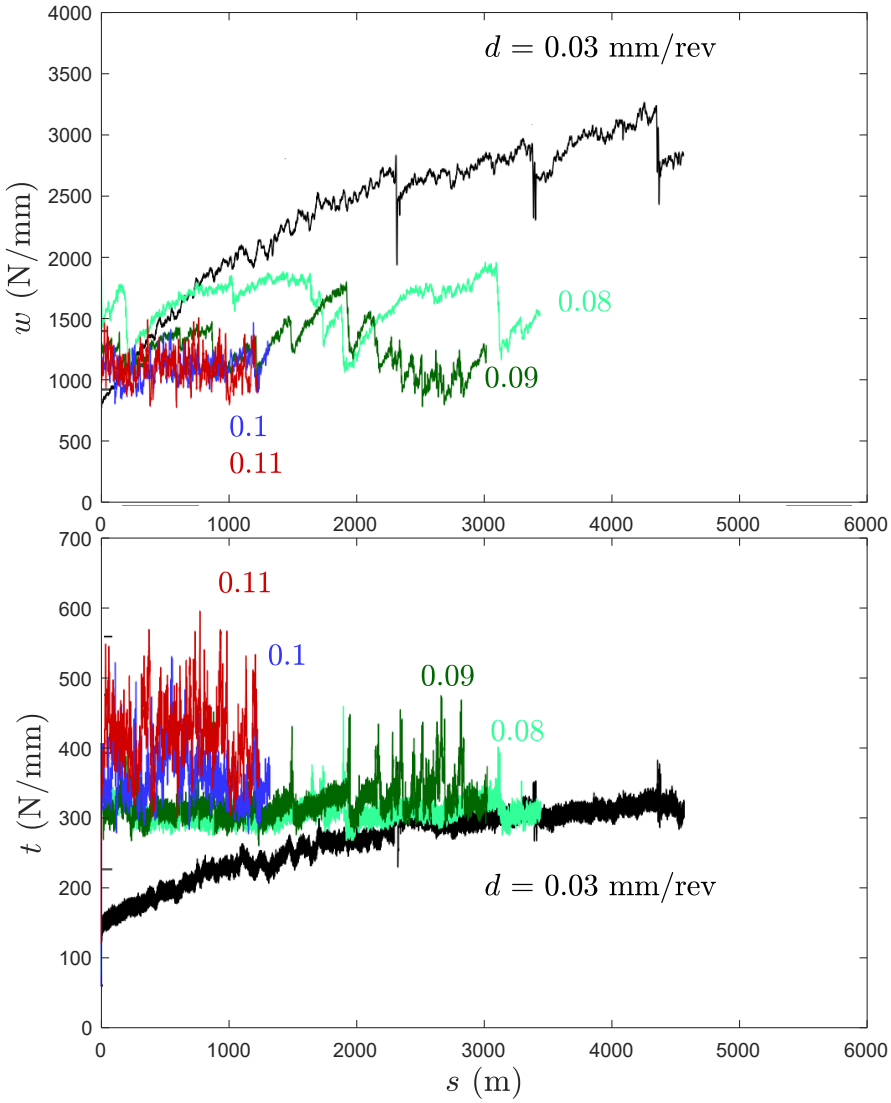

Figure 3.13: The variation of scaled forces (w and t) in drilling Radiant Red granite at different depth of cut(redrawn from Mostofi et al. (2018)).

Figure 3.13, diamond fracturing occurs at 0.08 mm/rev depth of cut while, based on the drilling response, d_{**} is around 0.1 mm/rev depth of cut, I assume $d_f < d_{**}$. When d passes beyond d_{**}, matrix three-body erosion overtakes diamond wear and eventually can lead to excessive diamond loss, thus d_{**} is defined as the transition from fracturing dominant regime to pull-out regime.

It is important to note that the cutting depth of each diamond on the bit may vary due to differences in their geometry and location. As a result, few

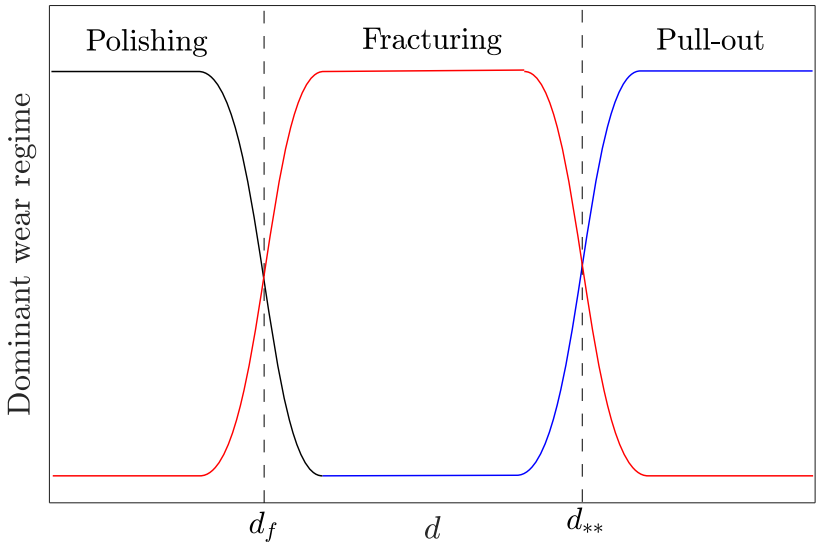

Figure 3.14: Conceptual model of change in dominant wear mechanisms with depth of cut.

diamonds with low protrusion (p) may undergo polishing wear when drilling at both fracturing dominant and pull-out dominant regimes. For simplicity, this model focuses on the predominant wear mechanisms.

3.3.2.1 Polishing dominant regime ($d < d_f$)

Figure 3.16 conceptually illustrates how nominal lengths change with cutting distance in drilling at the polishing dominant regime, and the wear state of the equivalent diamond blade at a selected cutting distance.

In this regime, the diamond blade only wears through the polishing mechanism. The diamond wear flat length (L_d) and the matrix wear flat length at the tail ($L_{\bar{m}}$) increase with the cutting distance (s_0 to s_1). Because $d < d_{**}$, there is no three-body contact at the crater, $\ell_{\hat{m}} = 0$. Thus, the matrix wear flat length at the crater ($L_{\hat{m}}$) remains unchanged, but the diamond protrusion ($\bar{p}$) decreases steadily due to the decrease in diamond height (h) caused by polishing.

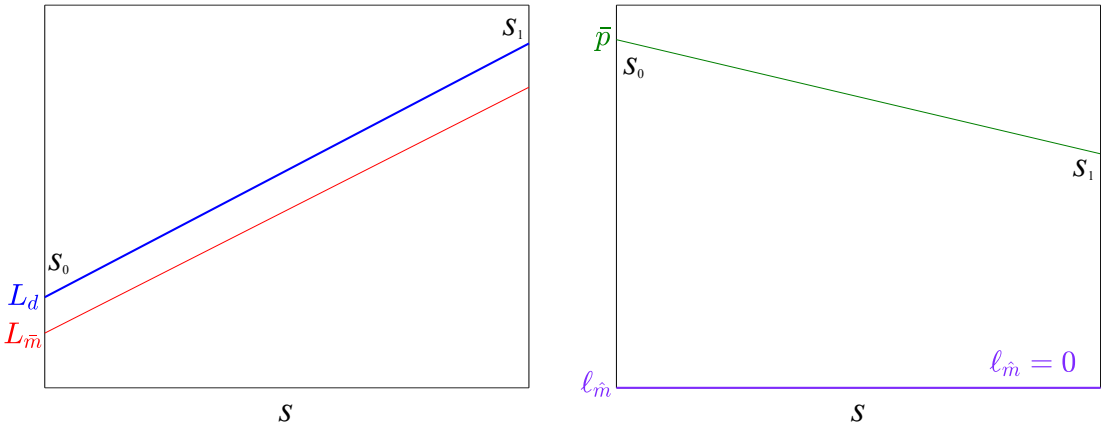

(a) Variation of nominal lengths.

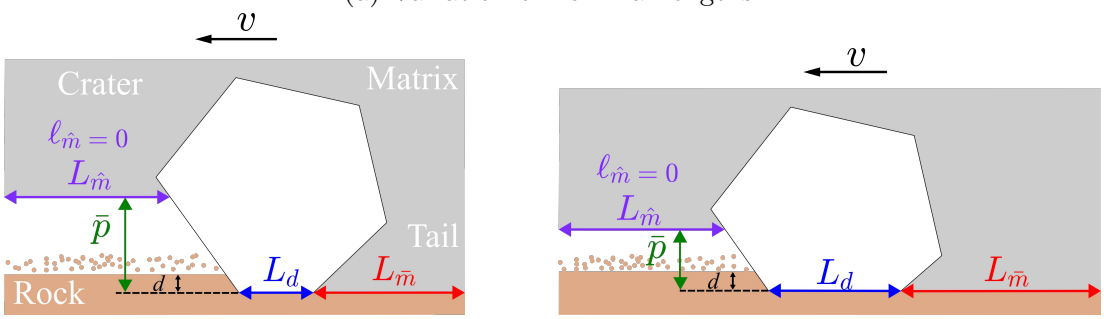

(b) s_0: initial wear state.

(c) s_1: diamond polishing.

Figure 3.15: Conceptual drawing of change in the cutting face geometry in polishing dominant regime.

3.3.2.2 Fracturing dominant regime ($d_f \leq d < d_{**}$)

In the fracturing dominant regime, most of the diamonds on the bit face undergo fracturing wear. We assume a sharp bit drills the rock at d_f. Figure 3.16 shows that, as $d < d_{**}$, $\ell_{\hat{m}} = 0$ (s_0). However, when the diamond blade fractures, there is an abrupt decrease in the diamond protrusion ($\bar{p}$), leading to the formation of the three-body contact at the crater, $\ell_{\hat{m}} > 0$ (s_1). Because we assume a sharp bit, the diamond wear flat length (L_d) and the matrix wear flat length at the tail ($L_{\bar{m}}$) are minimal, diamond fracturing does not significantly affect these two lengths. The third body at the crater evenly erodes the matrix, as a result, increasing the diamond protrusion while decreasing the matrix frictional contact length at the crater ($\ell_{\hat{m}}$). Once the diamond protrusion returns to its initial value, the three-body contact stops and $\ell_{\hat{m}} = 0$ (s_2).

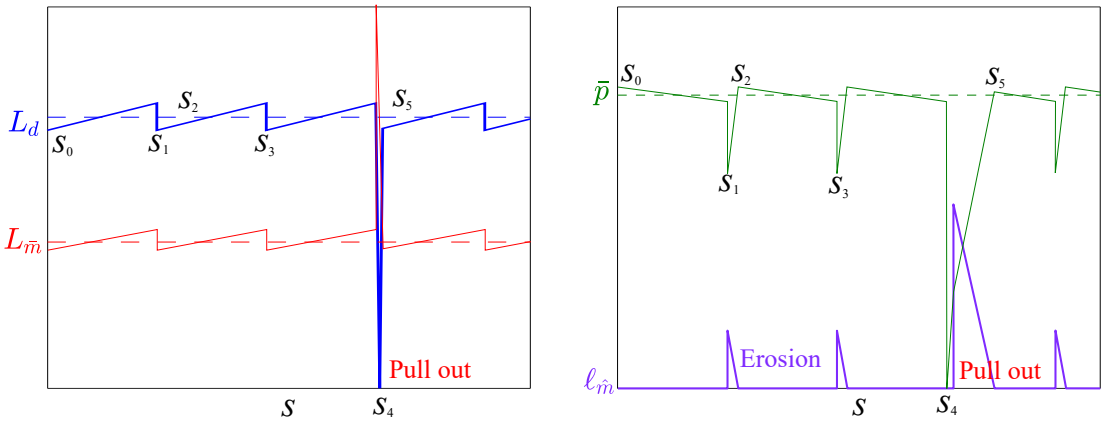

(a) Variation of nominal lengths.

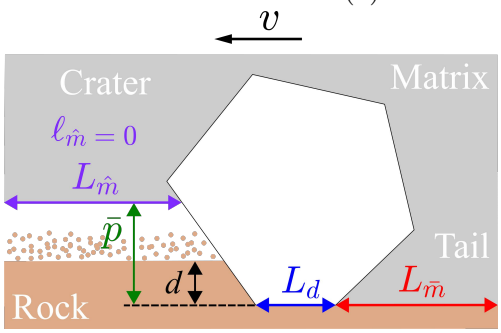

(b) s_0: initial wear state.

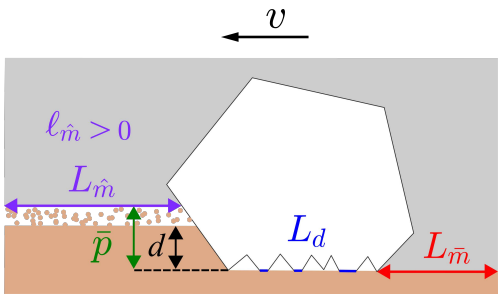

(c) s_1: diamond fracturing.

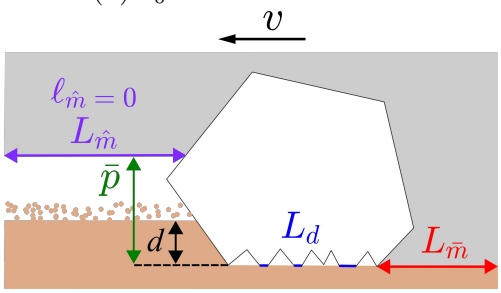

(d) s_2: three-body erosion.

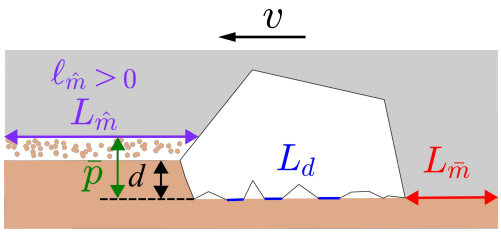

(e) s_3: diamond fracturing.

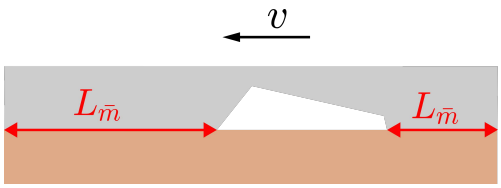

(f) s_4: diamond being pulled out.

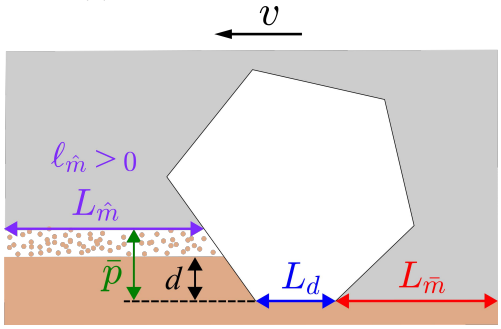

(g) s_5: new diamond exposing.

Figure 3.16: Conceptual drawing of change in the cutting face geometry in fracturing dominant regime.

The three-body erosion resumes when the diamond blade fractures again (s_3) until the diamond protrusion exceeds half of the current diamond height ($\frac{\hat{p}}{h} > 0.5$), eventually leading to diamond pull out (s_4). After the diamond blade is pulled out, the diamond protrusion and the matrix wear flat at the crater both drop to zero, while the matrix/rock two-body contact at the maximum until a new diamond blade is exposed (s_5). Despite the diamond pull-out event that occurs on a very small time scale, the diamond protrusion ($\bar{p}$), the diamond wear flat length (L_d), and the matrix wear flat length at the tail ($L_{\bar{m}}$) fluctuate around a mean value.

3.3.2.3 Pull-out regime ($d > d_{**}$)

When the depth of cut passes beyond the depth of cut (d_{**}) at the onset of regime III, the three-body contact at the crater takes place regardless of the diamond blade wear state, $\ell_{\hat{m}} > 0$ (s_0). In this regime, the diamond blade may still experience fracturing wear, but persistent matrix erosion at the crater may lead to early diamond loss even before it fractures. For illustration purposes, let us assume that the diamond is pulled out before fracturing occurs.

Figure 3.17 shows that, during the cutting process, the third body at the crate consistently erodes the matrix, causing the diamond protrusion ($\bar{p}$) to increase (s_0 to s_1). As the diamond protrusion increases, the matrix frictional contact length at the crater ($\ell_{\hat{m}}$) decreases but does not reach zero. This ongoing erosion significantly reduces the diamond retention ability and eventually leads to the diamond pull out (s_1 to s_2). Following the diamond blade removal, the two-body abrasion wear between the matrix and the rock exposes the next layer of diamond (s_2 to s_3). Similar to the fracturing dominant regime, the overall diamond wear flat (L_d), matrix wear flat at the tail ($L_{\bar{m}}$), and diamond protrusion ($\bar{p}$) fluctuates around a mean value. However, continuous three-body erosion and frequent diamond loss result in a much higher overall bit wear rate in the pull-out regime.

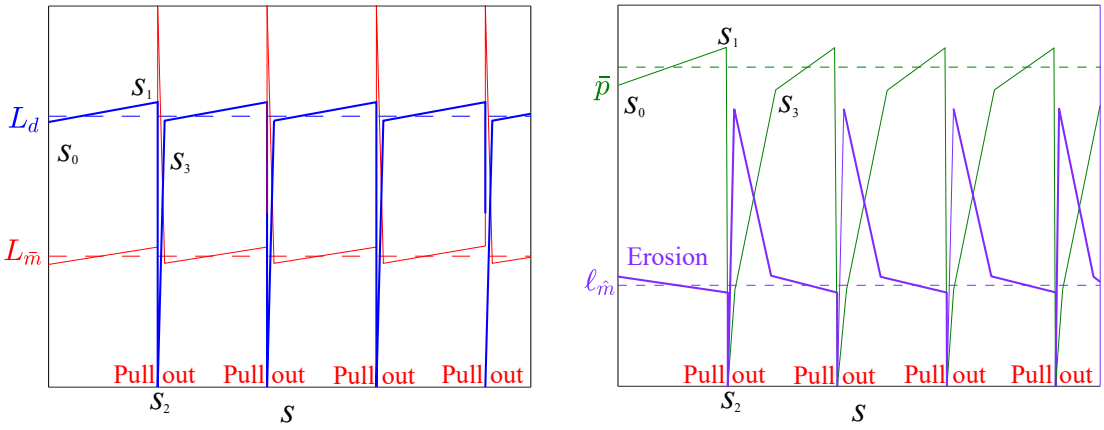

(a) Variation of nominal lengths.

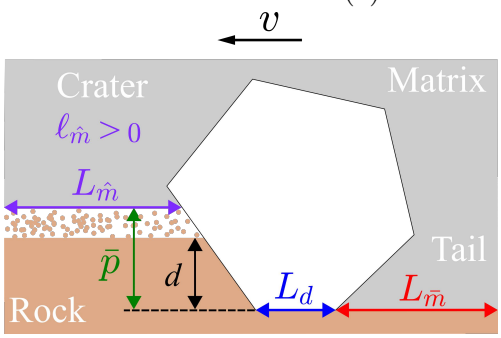

(b) s_0: initial wear state.

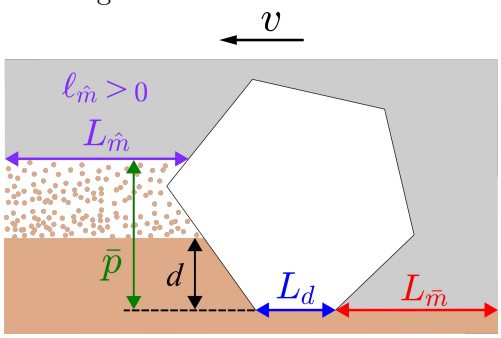

(c) s_1: three-body erosion.

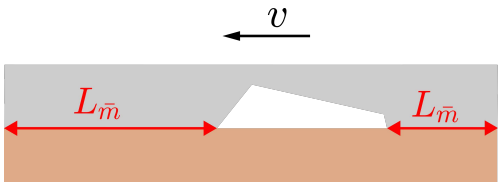

(d) s_2: diamond pull out.

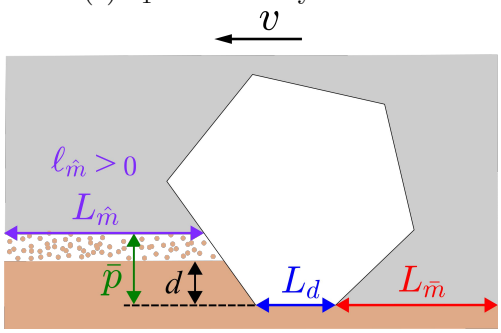

(e) s_3: new diamond exposing.

Figure 3.17: Conceptual drawing of change in the cutting face geometry in pull-out dominant regime.

3.3.2.4 Bit life

Besides change in bit wear state, the bit wear rate is another important metric for evaluating bit performance. In this research, it is defined as the bit height

loss per unit distance that the cutting structure travels:

$$\dot{H} = \frac{\delta H}{\delta s} \tag{3.17}$$

where H is the height of the impregnated section of the bit.

Unlike the change in nominal lengths ($\bar{p}$, L_d, and L_m) which reflect on forces, the bit wear rate cannot be inferred directly from the surface measurements. However, we can conceptually model $\dot{H}$ under different dominant wear mechanisms.

Mostofi (2014) measured the wear rate of the bit in drilling Radiant Red granite at different depths of cut, as shown in Figure 3.18, which illustrates the relationship between the rate of height loss and the depth of cut. Based on the wear response shown in Figure 3.13, we can identify two critical depths of cut: $d_f = 0.08$ mm/rev and $d_{**} = 0.1$ mm/rev. In the polishing dominant regime at $d = 0.03$ mm/rev, the bit wear rate is minimal, with $\dot{H} = 10^{-5}$ mm/m. As the depth of cut increases and pushes the response into the fracturing dominant regime, the height loss increases to around 10^{-4} mm/m at a depth of cut of 0.09 mm/rev. As the depth of cut continues to increase beyond d_{**}, the bit wear rate increases eightfold. This exponential trend is consistent with the conceptual model that diamond fracturing causes a higher diamond height loss than polishing and the frequent diamond pull out leads to a much higher wear rate.

3.3.3 Effect of rock and drilling fluid properties

Besides depth of cut, rock properties also play an important role in the wear of ID bits. Figure 3.19 shows that the force increases faster in drilling Radiant Red granite than in American Black granite at the same depth of cut. Given that the quartz content is 39% in Radiant Red granite, which is ten times higher than in American Black granite, the diamond polishing process is amplified, leading to a faster increase in the diamond wear flat length (L_d). However, the effect

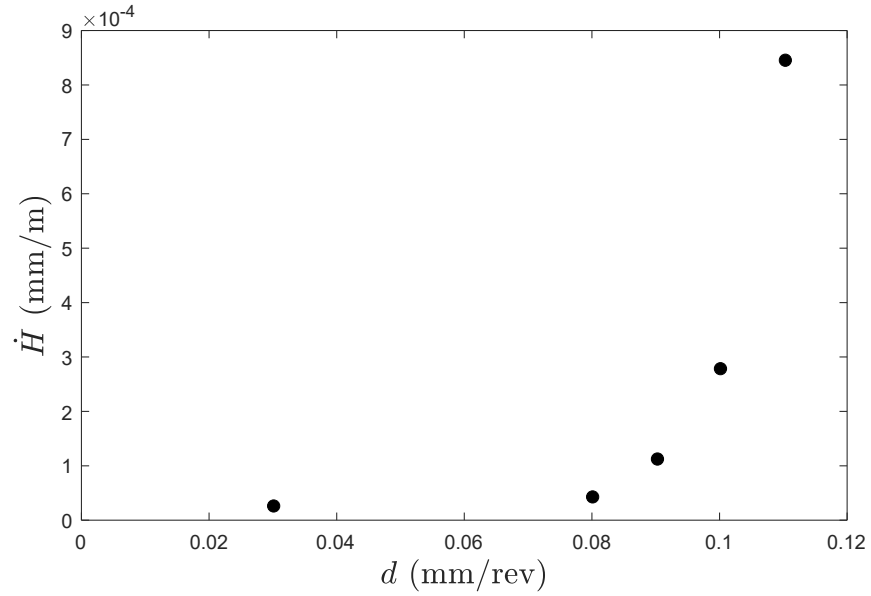

Figure 3.18: Bit wear rates in the form of height loss ($\dot{H}$) in drilling Radiant Red granite at various depths of cut (redrawn from Mostofi (2014)).

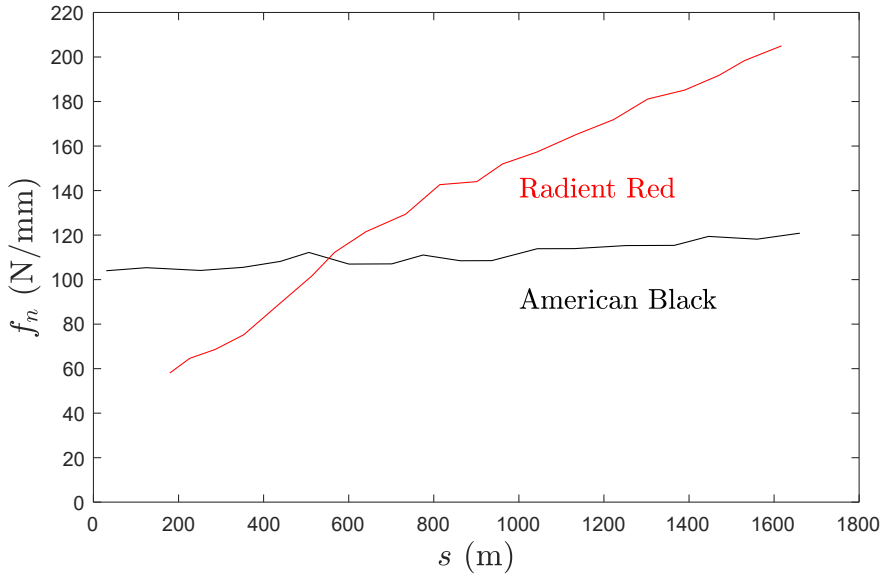

Figure 3.19: The wear responses carried out at $d = 0.0025$ mm/rev on two different rock material using the ID segment H3 (redrawn from Mostofi (2014)).

of rock properties on the diamond fracturing process is not well studied in the literature, particularly regarding the rock properties that control the transition between polishing wear and fracturing wear. It is reasonable to suggest that a

high quartz content may amplify the fracturing process due to its high Mohs hardness.

When drilling through soft rock, such as sandstone, the minerals are loosely bonded by cement, resulting in low rock strength and hardness. Although sandstone typically contains larger quartz grains, it can erode the matrix through three-body contact, causing diamonds to pull out before fracturing occurs. Therefore, it is critical to focus on quantifying the impact of various rock properties on both polishing and fracturing wear processes.

The polishing rate is also affected by the properties of the drilling fluid (Strebig et al. (1971), Selim et al. (1969)). Figure 3.20 shows that, when drilling at a given

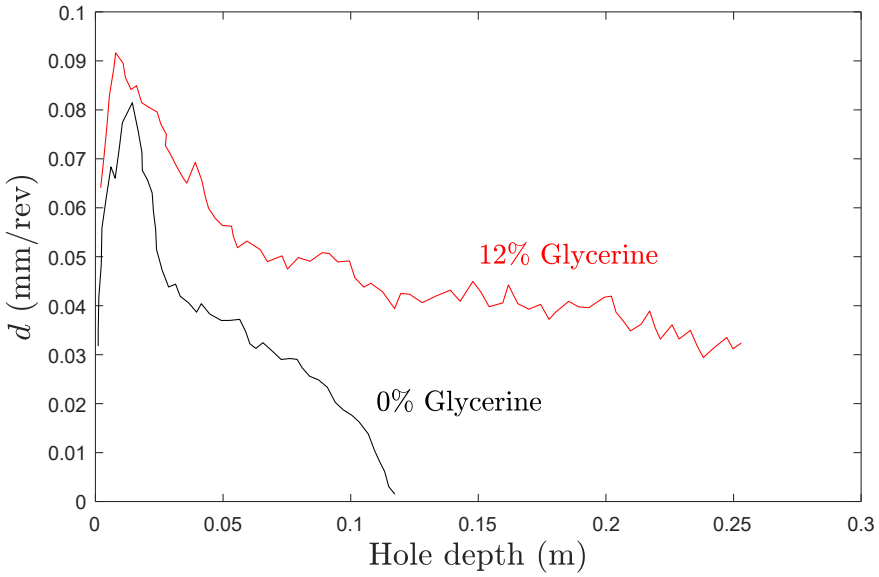

Figure 3.20: The effect of Glycerine (lubricant) concentration on the variation of depth of cut at a given weight on bit, $W = 2670$ N (redrawn from Selim et al. (1969)).

weight on bit, the rate of decrease in the depth of the cut slows down with the presence of glycerine, which acts as a wetting agent, increasing the heat transfer from the diamonds to the coolant and therefore inhibited their wear by oxidation and graphitisation. The drilling fluid is part of the third body that may affect the three-body contact at the crater, but there is no research on how the properties

of the fluid affect the three-body erosion mechanism and consequently the wear rate.

In summary, it is important to quantify the variation in bit wear state and wear rate in different dominant wear regimes and drilling conditions to better understand the wear process of the bit.

3.4 Methodology

3.4.1 Experimental workflow

An experimental workflow is designed to validate the proposed conceptual model. This workflow is divided into three sections: preparation, testing, and data analysis.

In the preparation section, the test material (bit, rock, and drilling fluid) and the operating parameters (depth of cut, rotation speed, flow rate, and cutting distance) are selected based on the research objective. Once the bit is selected, a sharpening test is performed by drilling a synthetic rock (40% metal shard) at 0.03 mm/rev depth of cut for 2 minutes to remove blunt diamonds on the bit face. The sharpened bit is checked by microscope to make sure that all blunt diamonds on the cutting face are removed and also to record the initial bit wear state.

In the test section, see Figure 3.21, a step (drilling) test is conducted on a Bluestone granite to obtain the drilling response of the bit (L_d, L_m, $\bar{p}$, and H remain unchanged). During the test, the depth of cut is increased by increments of 0.03mm/rev (0.01 mm/rev increment for ID segments) until the torque on bit reaches 90% of the sensor limit. The depth of cut is reduced at the same step but each depth of cut is offset by 0.015 mm/rev. At each step, the depth of cut is maintained constant, for long enough time interval as to record stationary weight and torque signals.

After the step test, the bit is removed from the rig for a surface scan to

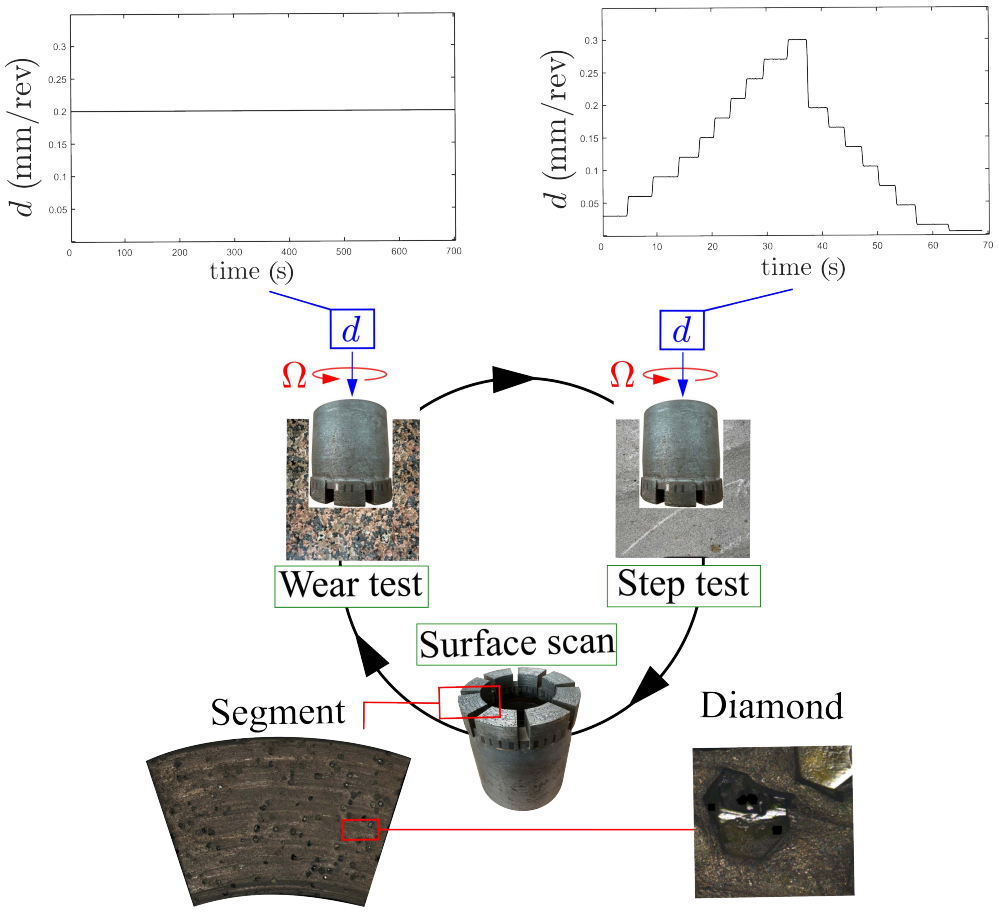

Figure 3.21: Test section: experimental workflow.

capture the bit wear state (L_d, L_m, $\bar{p}$, and H are recorded). A comparison of the scanning results before and after the step test shows no change in the bit wear state, confirming that no wear occurred during the test. By combining the drilling responses obtained from the step test with the estimates of nominal wear length scales, relationships between the nominal lengths and the model parameters can be constructed.

A wear (drilling) test, performed after the surface scan, involves drilling a selected rock at a constant depth of cut to wear the bit (L_d, L_m, $\bar{p}$, and H vary). After the wear test, the step test combined with the surface scan is repeated to measure the variation in the nominal lengths ($\dot{L}_d$, $\dot{L_m}$, $\dot{\bar{p}}$, and $\dot{H}$) and the new drilling response.

By repeating the test cycle, the full image of how the nominal lengths vary

with the cutting distance and how the variation of the nominal lengths affects the drilling response can be obtained.

3.4.2 Deriving model parameters from drilling response

3.4.2.1 Drilling response and transition regime

Figure 3.22 shows a typical drilling response (test carried out in Bluestone granite). It can be seen that the $w-d$ space is characterised by three regimes but with a curve connecting regime I and II. This curve is also seen in the $t-d$ space. As the transition from regime I to regime II is characterised by the variation of the diamond frictional contact length (ℓ_d), it indicates that the diamond frictional contact length increases with the depth of cut not linearly, but at a decreasing rate and eventually converges to the conformal contact ($\hat{\ell}_d$). This transition is governed by the geometry of the diamonds wear flats.

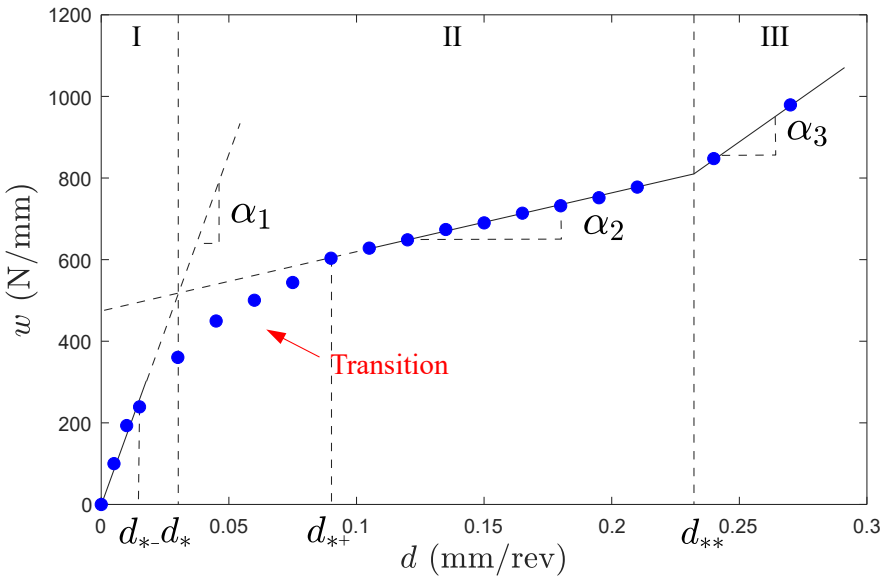

Figure 3.22: An example of drilling response fitted with the model showing a transient regime between regime I and II. Drilling tests were conducted using an NQ-size bit in drilling Bluestone granite.

Figure 3.23 shows that the diamond wear flat area (A_d) is characterized by small unevenness with a total size of 0.36 mm^2. Assuming that a depth of cut is

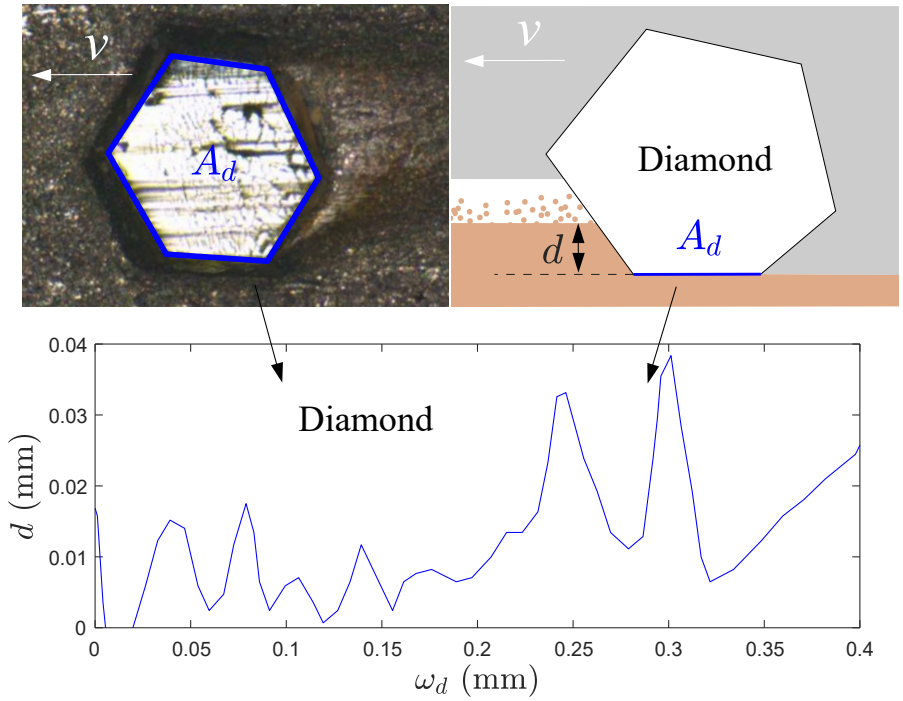

Figure 3.23: An example of the wear state of a diamond wear flat.

applied on the diamond at an increment of 0.005 mm, the diamond/rock contact area increases with depth of cut at a decreasing rate and eventually converge to the size of the diamond wear flat area, see Figure 3.24.

The result confirms that the transition curve observed in the drilling responses is caused by the unevenness of the diamond wear flat. To fully understand and model this curve, a precise measurement of the bit wear state is required, which is beyond the scope of this research. However, it is taken into account when deriving model parameters.

3.4.2.2 Minimisation function with a quadri-linear constraint

The quadri-linear model is developed which treats the drilling responses as a four consecutive linear regimes, and the scaled weight in each regime is calculated

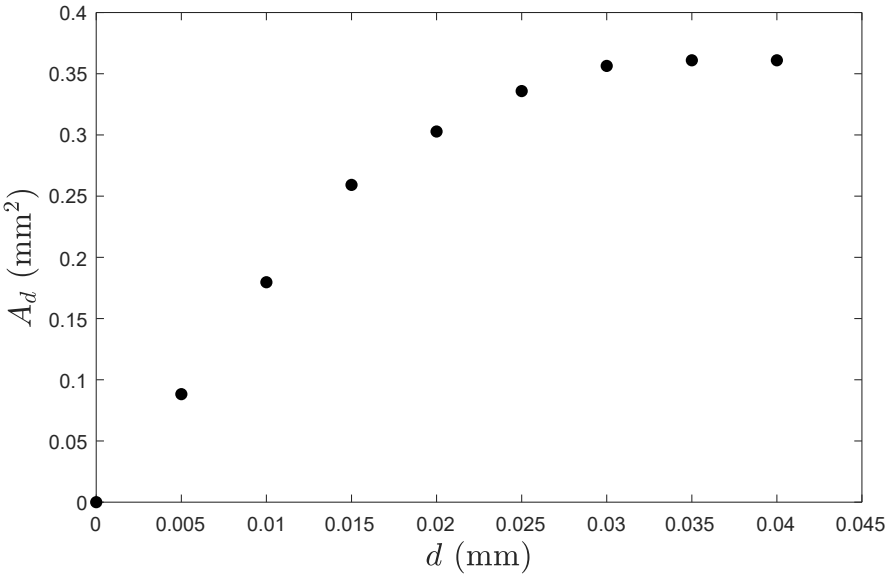

Figure 3.24: The relationship between the diamond frictional contact length (ℓ_d) and the depth of cut (d).

based on seven parameters:

$$w = \begin{cases} \alpha_{\mathrm{I}} d & d \leq d_{*-} \\ \alpha_{\mathrm{t}}(d - d_{*-}) + \alpha_{\mathrm{I}} d_{*-} & d_{*-} < d \leq d_{*+} \\ \alpha_{\mathrm{II}}(d - d_{*+}) + \alpha_{\mathrm{t}}(d_{*+} - d_{*-}) + \alpha_{\mathrm{I}} d_{*-} & d_{*+} < d \leq d_{**} \\ \alpha_{\mathrm{III}}(d - d_{**}) + \alpha_{\mathrm{II}}(d_{**} - d_{*+}) + \alpha_{\mathrm{t}}(d_{*+} - d_{*-}) + \alpha_{\mathrm{I}} d_{*-} & d_{**} < d \end{cases} \tag{3.18}$$

where α_t is the slope of the transition regime with d_{*-} and d_{*+} representing the beginning and end of the transition regime.

Then I use the minimisation function (fmincon) in MATLAB software to identify the best-fit parameters of the quadri-linear model. The fmincon function takes an initial guess of the seven parameters and attempts to find the best fit that minimises the sum of squared errors (SE) between the estimated scaled

weight of the model ($\hat{w}$) and the actual scaled weight (w).

$$SE = \sum_{i=1}^{n} (w_i - \hat{w}_i)^2 \tag{3.19}$$

where n is the total number of depth of cut.

Figure 3.25 illustrates examples of the drilling responses fitted with the model in two different wear states. It can be seen that the model overestimates the forces in the transition regime. To be specific, in wear state 2, the scaled weight at 0.03 mm/rev is estimated to be around 850 N/mm while the actual value is 700 N/mm. However, the model successfully captures the forces in both regime II and III and accurately identifies the depth of cut (d_{**}) at the onset of regime II, which is sufficient for this research.

3.4.2.3 Deriving model parameters associated with bit wear state

Each regime in the drilling response model read as:

$$\mathrm{I} = \begin{cases} w & = \alpha_{\mathrm{I}} d = (\zeta\varepsilon + \sigma_d\kappa_d + \sigma_m\kappa_{\bar{m}})d \\ t & = \beta_{\mathrm{I}} d = (\varepsilon + \mu_d\sigma_d\kappa_d + \mu_m\sigma_m\kappa_{\bar{m}})d \end{cases} \tag{3.20}$$

$$\mathrm{II} = \begin{cases} w & = \alpha_{\mathrm{II}} d + w_o = (\zeta\varepsilon + \sigma_m\kappa_{\bar{m}})d + \sigma_d\hat{\ell}_d \\ t & = \beta_{\mathrm{II}} d + t_o = (\varepsilon + \mu_m\sigma_m\kappa_{\bar{m}})d + \mu_d\sigma_d\hat{\ell}_d \end{cases} \tag{3.21}$$

$$\mathrm{III} = \begin{cases} w & = \alpha_{\mathrm{III}} d + w_o - \sigma_m\kappa_{\hat{m}}d_{**} = [\zeta\varepsilon + \sigma_m(\kappa_{\bar{m}} + \kappa_{\hat{m}})]d + \sigma_d\hat{\ell}_d - \sigma_m\kappa_{\hat{m}}d_{**} \\ t & = \beta_{\mathrm{III}} d + t_o - \mu_m\sigma_m\kappa_{\hat{m}}d_{**} = [\varepsilon + \mu_m\sigma_m(\kappa_{\bar{m}} + \kappa_{\hat{m}})]d + \mu_d\sigma_d\hat{\ell}_d - \mu_m\sigma_m\kappa_{\hat{m}}d_{**} \end{cases} \tag{3.22}$$

where β are the slope of different regimes in $t-d$ space. t_o represents the intercept of regime II in the $t-d$ space.

The model parameters can be categorised into two groups: 1. parameters associated with the bit wear state (d_*, d_{**}, κ_d, $\kappa_{\bar{m}}$, $\kappa_{\hat{m}}$, and $\hat{\ell}_d$); 2. parameters associated with rock and bit matrix properties (ζ and ε, σ_d, σ_m, μ_d, and μ_m).

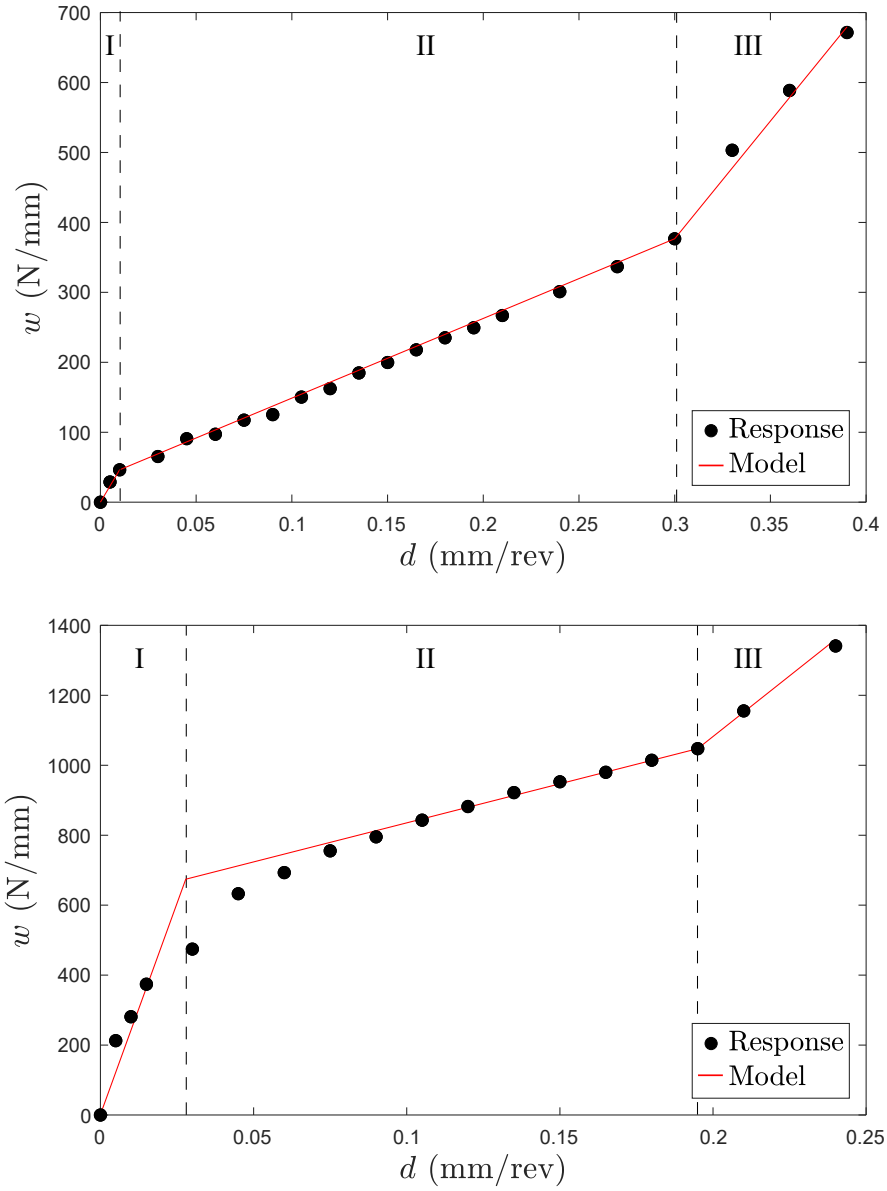

Figure 3.25: Examples of $w - d$ space modelled using the quadri-linear function with seven variables specified in two different wear states. Wear state 1: $L_d = 0.4$ mm (upper), wear state 2: $L_d = 3.9$ mm (bottom).

The matrix contact stress, σ_m, is not necessary the same for two-body and three-body contact due to the differing mechanisms of stress distribution. However, for simplicity, the same symbol is used to represnt it in both case. The effects of bit design and rock properties are isolated by drilling in one type of rock using bits with the same matrix properties. The model parameters in the first groups are

fixed and can be estimated as follows:

- The intrinsic specific energy (ε) and the number (ζ) are estimated from the slope of regime II (α_{II}) of the drill response of the bit with a modified wear state such that the matrix-rock contact is eliminated. Figure 3.26 shows a sandblasted (modified) bit, for which the matrix around the diamond has been eroded by sandblasting, especially the wear flat along the matrix tail behind the diamond ($L_{\bar{m}} = 0$). As a result, $\kappa_{\bar{m}} = 0$, and therefore the slope of regime II in the $w - d$ and $t - d$ spaces consists of only $\zeta\varepsilon$ and ε, respectively. For Bluestone granite the results yield $\zeta = 4$ and $\varepsilon = 400$ MPa (Chan (2022)).

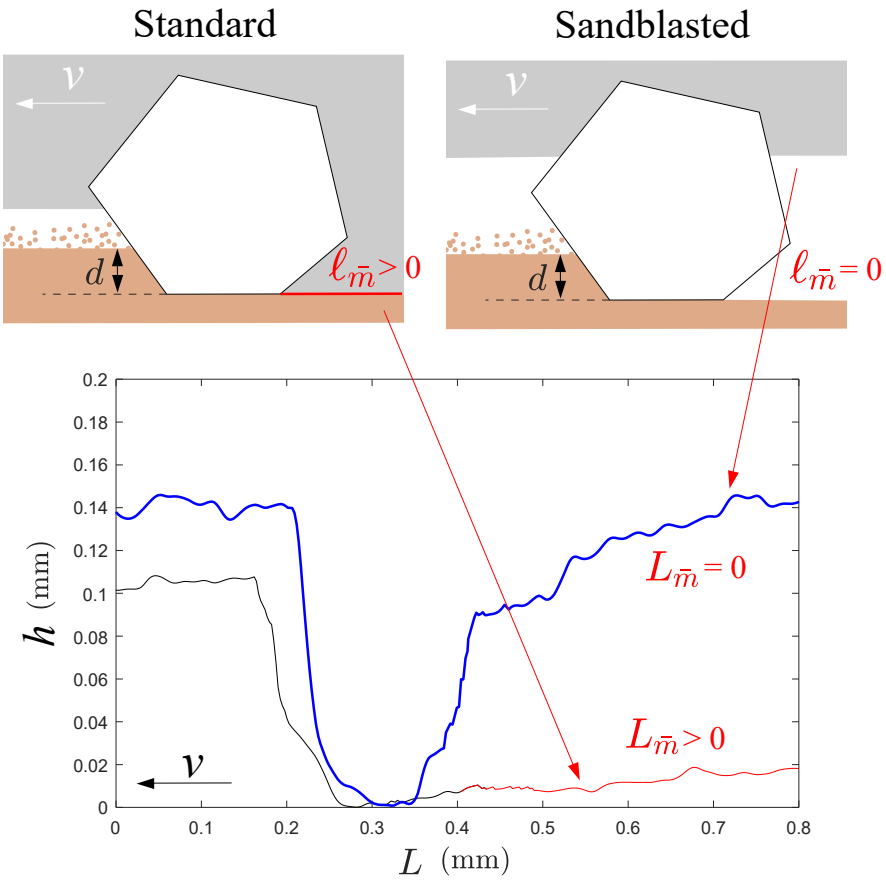

Figure 3.26: Comparison of wear states between standard and sandblasted bits.

- The diamond/rock contact stress (σ_d) can be estimated from the intercept of regime II (w_o) of the drilling response. However, this calculation requires

the assumption that the conformal diamond frictional contact length is equal to the nominal diamond wear flat length ($\hat{\ell}_d = L_d$). Based on this assumption, the diamond/rock contact stress can be expressed as:

$$\sigma_d = \frac{w_o}{L_d} \tag{3.23}$$

To increase the repeatability of the results, step tests were performed using an ID segment of 10 mm width on 10 different types of rock under two different wear states. Wear State 1; The total diamond wear flat area was approximately 3 mm^2, resulting $L_d = 0.3$ mm. Wear State 2: The total diamond wear flat area increased to 4 mm^2, giving $L_d = 0.4$ mm. Table 3.1 summaries the values of w_o for two wear states across all 10 rock types. The final diamond/rock contact stress (σ_d) was averaged from the results calculated for the two wear states. Taking Bluestone as an example, the calculated diamond/rock contact stress (σ_d) is 138 MPa which is in the same order of magnitude of its uniaxial compressive strength (q). As shown in Figure 3.27, there is a strong and consistent correlation between the diamond/rock contact stress and the uniaxial compressive strength of various rock types.

Table 3.1: The intercept of regime II (w_o) obtained from drilling response of an ID segment in drilling different rocks in two different wear states ($L_{d_1} = 0.3$ mm and $L_{d_2} = 0.4$ mm).

Rock	q [MPa]	w_{o_1} [N/mm]	w_{o_2} [N/mm]	σ_d [MPa]
Austin Chalk	11	3	4	10
Indiana	24	6	8	20
Grey Berea	42	12	15	39
Donnybrook Sandstone	72	18	24	60
Crab Orchard	117	29	42	101
Bluestone granite	126	45	66	158
Guelph dolomite	152	29	44	103
Calca Red granite	155	78	106	263
Austral Black granite	170	65	79	207
Verde Austral	181	79	92	247

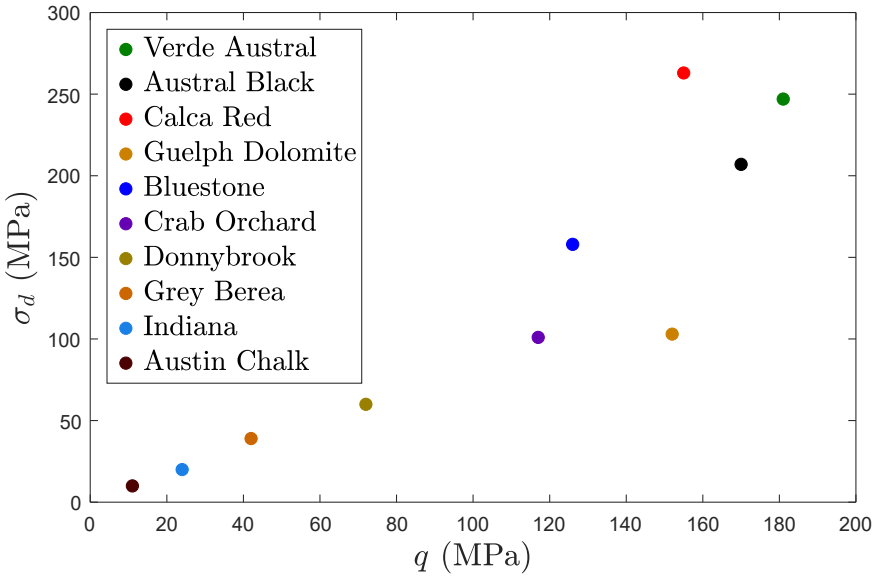

Figure 3.27: The relationship between the diamond/rock contact stress (σ_d) and the unaxial compressive strength of the rock (q).

- The matrix/rock contact stress (σ_m) can be estimated from the wear test carried out using a standard bit. The increase in the weight on bit is caused by the increase in both the cumulative diamond wear flat area and the cumulative matrix wear flat area at the tail and reads:

$$\delta W = \sigma_d \delta \bar{A}_d + \sigma_m \delta \bar{A}_{\bar{m}}. \tag{3.24}$$

  The matrix/rock contact stress can be calculated once $\delta \bar{A}_d$ and $\delta \bar{A}_{\bar{m}}$ have been estimated from the scanning results. However, accurately measuring $A_{\bar{m}}$ is challenging. According to Figure 3.28, the cumulative diamond wear flat area, approximately 0.05 mm^2, can be easily measured due to its high color contrast, whereas the matrix wear flat at the tail is difficult to measure. Therefore, instead of measuring $\delta \bar{A}_{\bar{m}}$ to calculate σ_m, I use $\sigma_m \kappa_{\bar{m}}$ and $\sigma_m \kappa_{\hat{m}}$ as the coefficient representing the variation of matrix frictional contact length at the tail and at the crater, respectively.

Based on the model, the parameters associated with the bit wear state can be

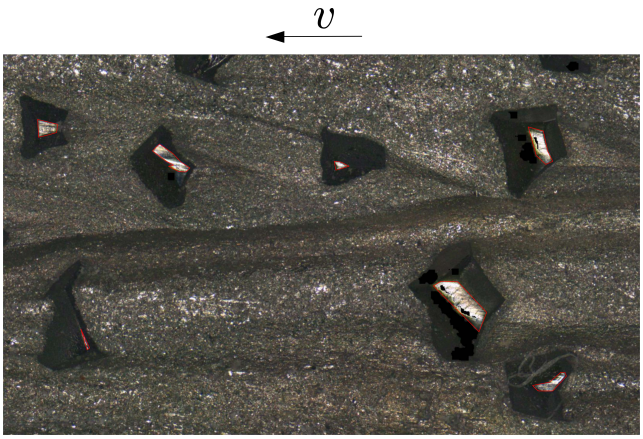

Figure 3.28: An example of the cutting face geometry of an ID bit.

obtained from the $w - d$ space using the following equations:

$$\hat{\ell}_d = \frac{w_o}{\sigma_d} \tag{3.25}$$

$$\kappa_d = \frac{\alpha_{\mathrm{I}} - \alpha_{\mathrm{II}}}{\sigma_d} \tag{3.26}$$

$$\sigma_m \kappa_{\bar{m}} = \alpha_{\mathrm{II}} - \zeta\varepsilon \tag{3.27}$$

$$\sigma_m \kappa_{\hat{m}} = \alpha_{\mathrm{III}} - \alpha_{\mathrm{II}} \tag{3.28}$$

3.4.3 Experiment setup

This section introduces the machines, ID tools, and materials used in this research.

3.4.3.1 Drilling rig, Echidna

A lab-scale drilling rig, Echidna, is used to carry out drilling experiments with field-size bits, see Figure 3.29. Echidna comprises a frame, a feed drive system, a rotary drive system, and a fluid flow system. During experiments, the LabView interface (Echidna GUI) is used to control the penetration rate (v), the bit angular velocity ($\Omega = 400$ rpm) and the flow rate ($Q = 30$ L/min). The computer communicates with the Galil motion controller to control the motors of both the feed and rotary drive systems.

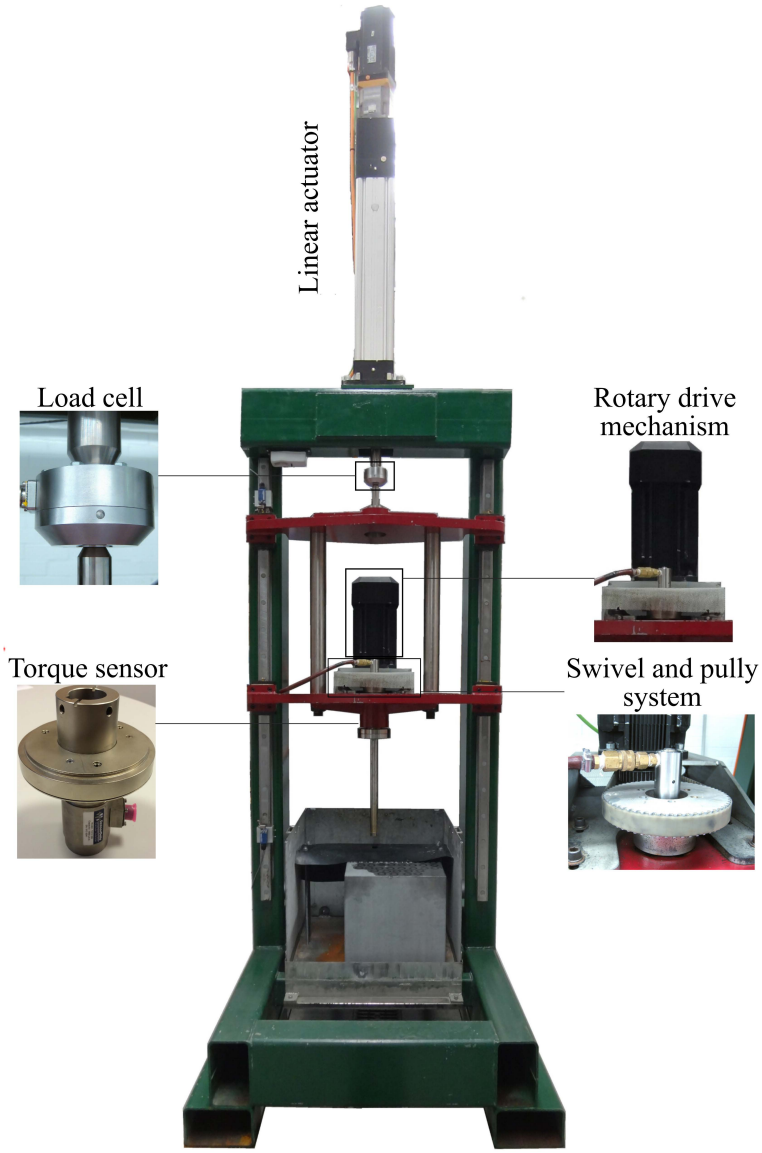

Figure 3.29: Drilling rig, Echidna.

Echidna is equipped with several sensors connected to an HBM MGCPlus data acquisition system to measure operating parameters at a sampling rate of 2.4 kHz. Reactive forces (W and T) are recorded by an HBM load cell (model: 1U10M / 50kN) and a SensorData torque sensor (model: T211-106), respectively. The head position and the angular position of the bit are measured by a linear displacement sensor and a rotary encoder. The depth of cut is calculated using the ratio of the derivatives of both measurements with respect to the time required

to complete one bit revolution.

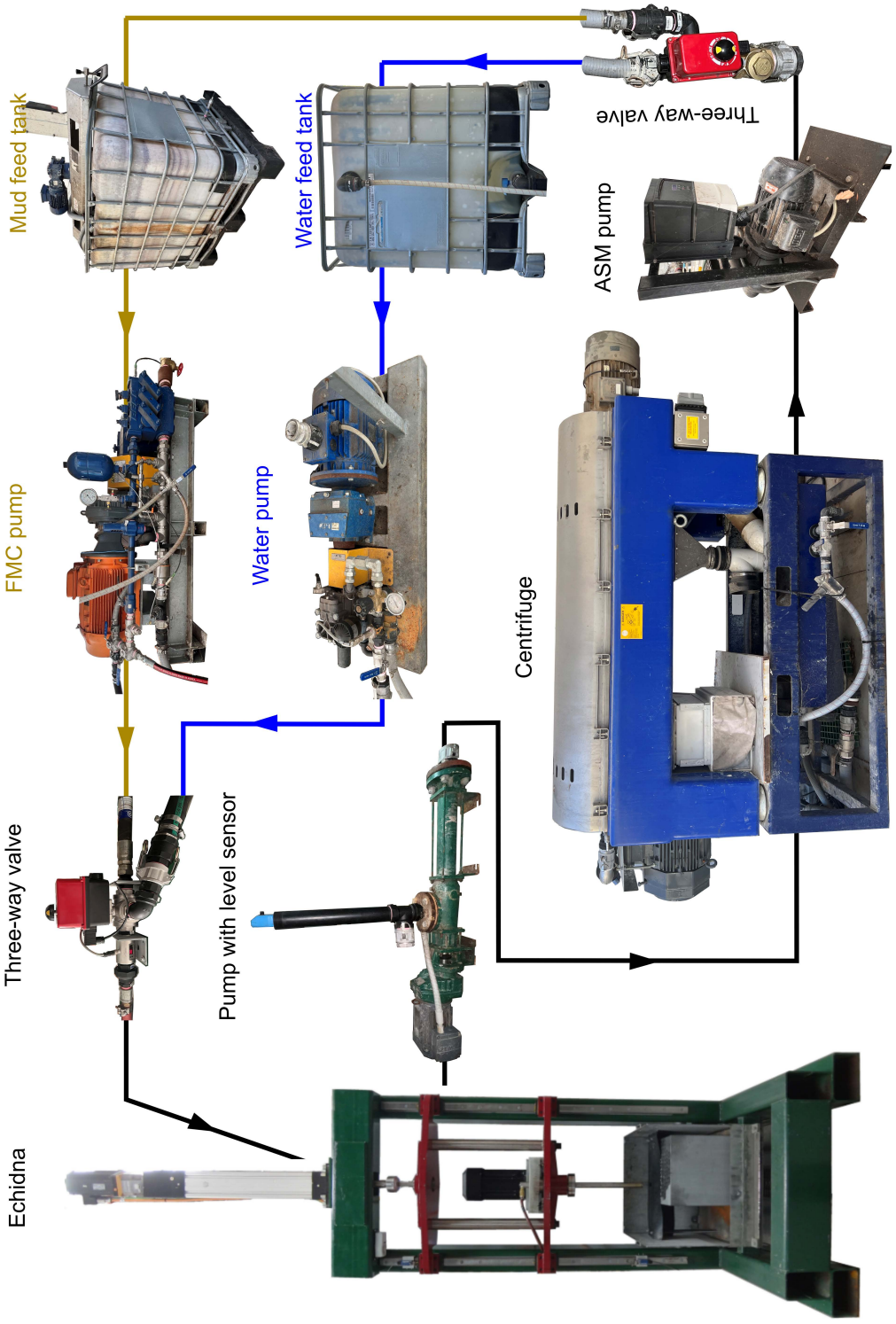

Figure 3.30: The fluid flow system of Echidna.

For the fluid flow system, depicted Figure 3.30, two IFM pressure sensors (model: PT5443) are installed at the bottom of the water and mud feed tank (1000L capacity) to monitor fluid levels. A spray pump and an FMC bean pump deliver water and drilling fluid to Echidna, respectively. Two 40-bar pressure sensors are installed at the pump to monitor operating pressure (2 bar when running water at 30 L/min and 5 bar when running drilling fluid). The pump outlets are connected via an electrical three-way valve, allowing the system to switch between water and mud by simply clicking a button on the interface. After the valve, a flow metre measures the flow rate to the machine. To recycle discharge fluid, waste water/mud flows through a centrifuge operating at 3600 RPM to remove cuttings. The cleaned fluid is then returned to the feed tanks, ready for the next experiment.

3.4.3.2 Cutting rig, Thor

Thor is a modified CNC lathe designed to study the cutting performance of ID segments, see Figure 3.31. The machine can accommodate cylindrical rock ranging from the size of an NQ core sample (45 mm in diameter) up to 200 mm in diameter and 400 mm in length. In this research, large rock samples are used to allow for cutting up to 5 layers of 350 mm length from the outer diameter. Unlike Echidna, where the bit rotates, Thor has the rock sample mounted on a chuck that rotates at a constant angular velocity. A segment (10 mm in width) is attached to a tool post and is moved along the edge of the cross-section of the rock using a servo actuator.

Similar to Echidna, Thor is also kinematically controlled via a computer (MATLAB GUI) that interfaces with a Galil motion controller. The system controls the penetration rate and angular velocity, while the normal and tangential forces acting on the segment are measured with a triaxial piezoelectric force sensor. The angular velocity of the rock is set at 0.9 m/s, which matches the angular velocity of the bit on Echidna. The linear position of the cutter and

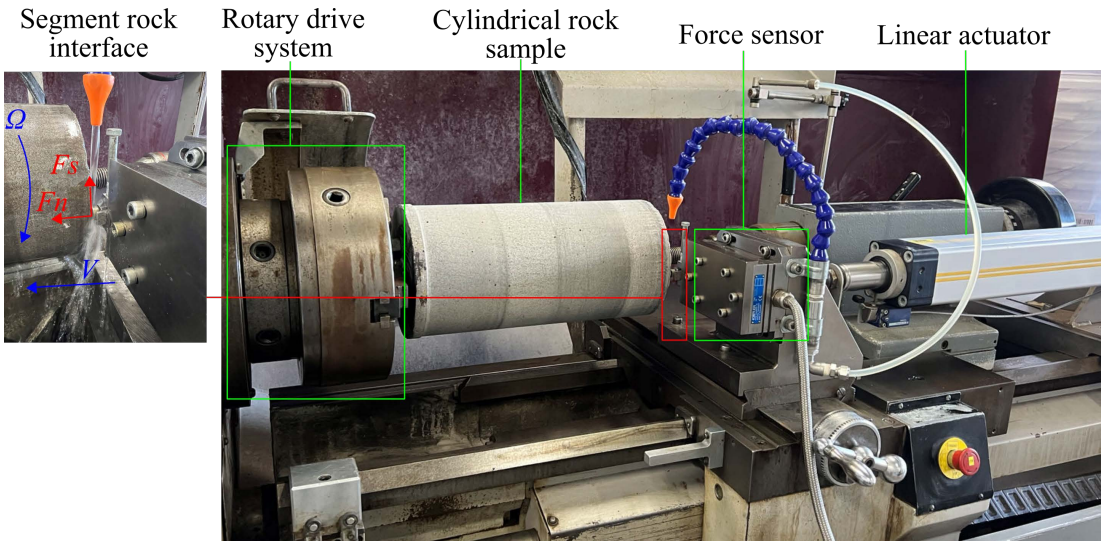

Figure 3.31: Cutting rig, Thor.

the angular position of the rock are measured by encoders. A centrifugal pump injects water at a rate of 5 L/m to cool down the segment and flush the cuttings. All data are recorded at a frequency of 2.4 kHz.

3.4.3.3 Optical microscope, Alicona

An optical microscope, Alicona, is used to scan the cutting face geometry of ID tools, as shown in Figure 3.32. It has demonstrated significant advantages in evaluating the wear of other cutting tools (Kapłonek et al. (2016); Seid Ahmed et al. (2017); Michaels (2021)). Alicona uses the Focus Variation technique, which captures images at multiple focal planes and constructs a 3D model of the surface.

To scan, the tool is first positioned under the lens of Alicona (X5 magnification). The lens is moved along the z-axis to its upper limit, and the current position is set as the datum. By doing this, all scanning results have the same reference plane, which helps to calculate height and volume differences between different scanning results. The top left corner of the cutting face is set as the origin of the scan, and the length, width, and height of the scan are determined to include the entire cutting face. Then the scanning process is initiated. The duration of a scan depends on the size of the sample. Scanning an ID segment

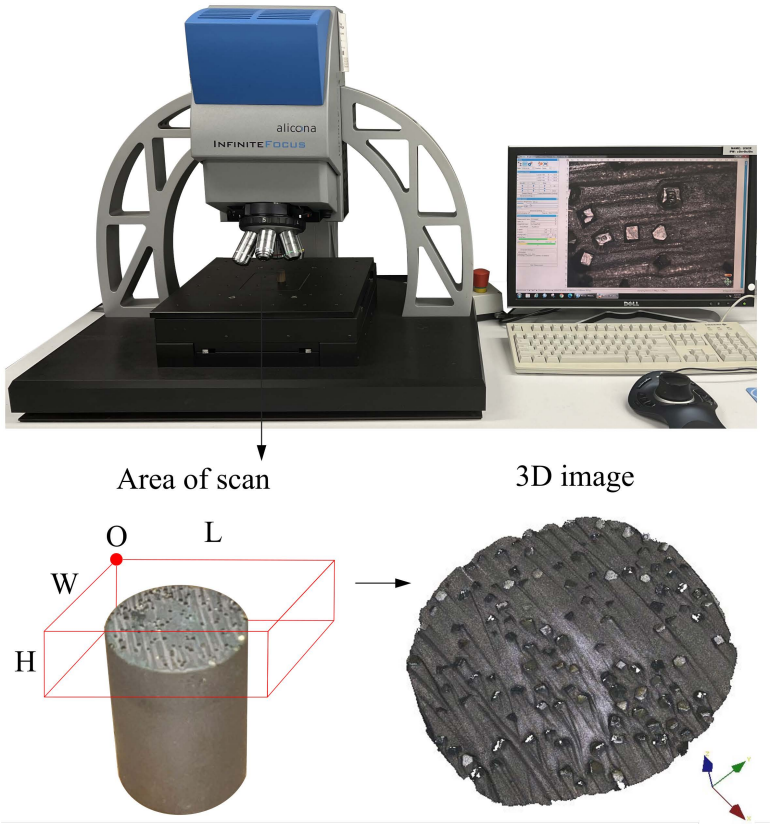

Figure 3.32: Optical microscope (Alicona) and an example of scanning result.

(10 X 10mm) takes about half an hour.

3.4.3.4 Calculating nominal lengths from scanning result

Based on the scanning result from Alicona, diamond protrusion (p) and diamond wear flat area (A_d) of all diamonds on the bit face and bit volume loss (δV) can be measured to calculate nominal lengths ($\bar{p}$ and L_d) of the equivalent blade and bit wear rate ($\dot{H}$).

The Alicona measurement software (IF-Measure Suite) is used to measure diamond exposure and bit volume loss. Figure 3.33 shows the depth profile of the cross-sectional area of a diamond. Diamond exposure is the height difference between the diamond tip and the matrix level at the crater. The average diamond exposure $\bar{p}$ of an ID segment is computed as the average value of all diamonds exposure on the cutting face, with around 50 to 200 diamonds per

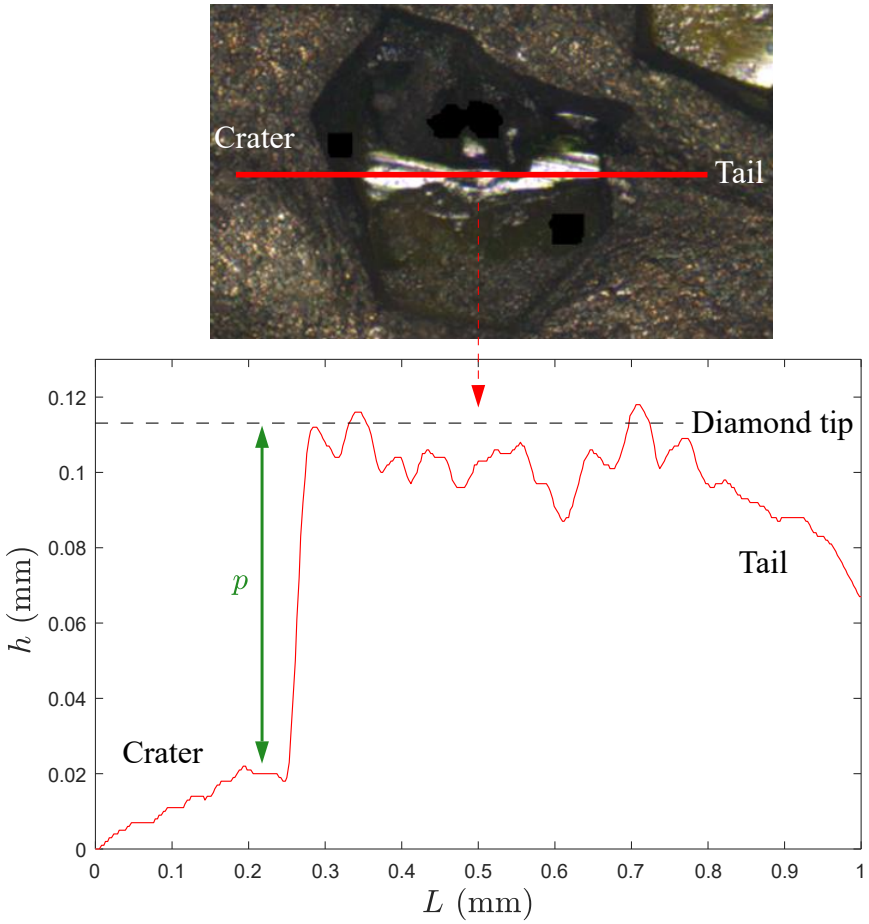

Figure 3.33: An example of the depth profile of a diamond.

segment depending on the size of the segment.

The Difference Measurement module is used to assess the volume differences between two scanning results. This module determines how much one dataset differs from the second dataset by measuring deviations. The first scanning result is selected as the reference, and the second scanning result is aligned with it. After alignment, it depicts the difference and calculates the volume beneath the reference surface (δV). The wear rate (height loss) of the tool ($\dot{H}$) is then calculated using the following equation:

$$\dot{H} = \frac{\delta V}{\mathcal{A}} \cdot \frac{1}{s} \tag{3.29}$$

where $\dot{H}$ is the rate of bit height loss. $\mathcal{A}$ is the cross-sectional area of the bit cutting face. δV is the volume loss after cutting for distance s.

Image processing software - ImageJ - is used to measure the diamond wear flat area (A_d) of all diamonds on the bit face. First, the scale of all images is set to millimetres to ensure accurate and consistent measurement. The diamond wear flat area is outlined as shown in Figure 3.34. The software then provides

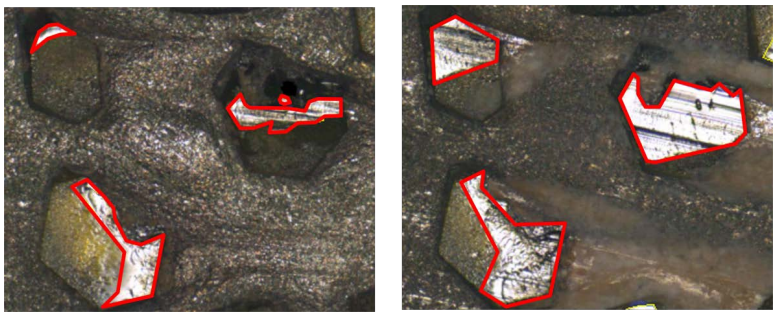

Figure 3.34: Measurement of diamond wear flat area (A_d) in different wear states.

measurements for each selected area. The cumulative diamond wear flat area ($\bar{A}_d$) is obtained by summing all measured areas, which is subsequently scaled by the segment width to calculate the diamond wear flat length (L_d) of the equivalent blade.

3.4.3.5 ID tools

The ID tools used in this research are supplied by HARDCORE, featuring diamond sizes of 25/35 (0.6 mm) and a concentration of 15%, as shown in Figure 3.35. For cutting tests on Thor, ID segments with a 10 mm width are employed. For drilling tests on Echidna, both NQ-size bits and TT56-size bits with a smaller outer radius (r_o) are used. Compared to the NQ-size bit, using a smaller bit allows higher scaled forces ($w = \frac{W}{r_o - r_i}$) and larger wear flat lengths (L_d and L_m) to reach within the operating limits of the machine.

Figure 3.35: ID tools of three different sizes.

3.4.3.6 Rocks properties

This research investigates four rocks, including three types of granite and one type of sandstone. Their properties are detailed in Table 3.2, and representative samples are shown in Figure 3.36.

Figure 3.36: Rock sample: Donnybrook, Bluestone, Austral Black, and Calca Red (from left to right).

Table 3.2: Rock properties. Besides Mohs hardness, all other rock properties are obtained from Chan (2022)'s work.

Rocks	Mohs hardness	q [MPa]	Quartz content [%]	Grain size [mm]
Calca Red	8	155	37	0.8
Austral Black	7	170	0.9	1.39
Bluestone	3	126	2	0.1
Donnybrook	2	72	80	1.3

Although the uniaxial compressive strength (q) is commonly used rock property to assess drilling performance and is well correlated with intrinsic specific energy (ε) and diamond-rock contact stress (σ_d), the rock failure mode observed in UCS test differs from that in drilling with an ID bit.

The Mohs hardness of the rock plays a crucial role in the bit wear process and is measured using a Mohs hardness test kit, as illustrated in Figure 3.37. The

Figure 3.37: Mohs hardness test kit.

kit includes eight hardness picks, each corresponding to a Mohs hardness ranging from 2 to 9. The test involves selecting a pick and placing it on a smooth rock surface. Apply downward pressure and drag the pick across the surface. If the pick scratches the rock, it indicates that the rock is softer than the hardness of the pick. Continue this process with progressively softer picks until no visible groove is made on the rock surface.

Figure 3.38 illustrates the relationship between the uniaxial compressive strength (q) of the rock and its Mosh hardness. Among the four rocks, Austral Black granite has the highest strength among all four rocks, Calca Red has a higher Mohs hardness, probably due to its higher quartz content. Bluestone, with slightly lower strength that Calca Red and Austral Black, has a Mohs hardness comparable to Donnybrook. Consequently, it is anticipated that drilling Bluestone will result in significantly less diamond polishing or fracturing. Donnybrook, although having the lowest strength and hardness, has the highest quartz content with the

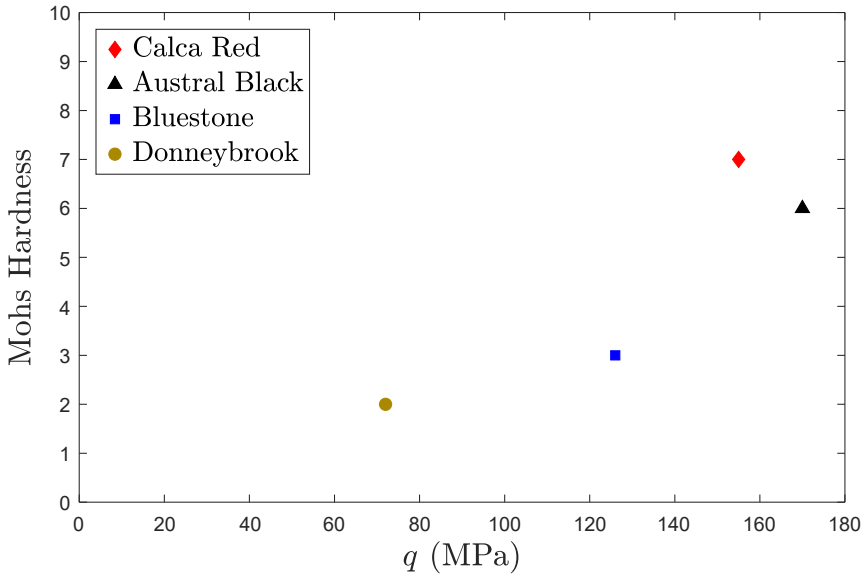

Figure 3.38: The relationship between uniaxial compressive strength (q) and Mohs hardness of different rocks.

largest grain size. This may lead to excessive three-body erosion of the matrix.

Chapter 4

Bit wear state (topology) and drilling response

4.1 Introduction

In this chapter, we establish relationships between the bit wear state and the drilling response from experimental results. For example, the depth of cut (d_{**}) at the onset of regime III is found to be proportional to the diamond protrusion ($\bar{p}$), which means it is important to maintain an adequate diamond protrusion while drilling to extend the range of regime II, and limit the occurrence of regime III.

I first perform a drilling test to obtain the drilling response and derive the model parameters (slopes of the different regimes, the intercept of regime II, and the depths of cut at the onset of regime II and III). Then a microscopy scan of the bit cutting face is performed to capture the bit wear state and calculate the nominal lengths, including diamond wear flat length (L_d) and diamond protrusion ($\bar{p}$). By repeating the same test procedure using drill bits in different wear states, we can map out how the model parameters change with the variation of the nominal wear lengths.

4.2 Diamond wear flat length (L_d)

Following the conceptual relationship between bit wear state and drilling response outlined in Chapter 3, the parameters associated with diamond frictional contact (d_*, κ_d, and $\hat{\ell}_d$) are expected to increase with the diamond wear flat length (L_d), see Figure 4.1.

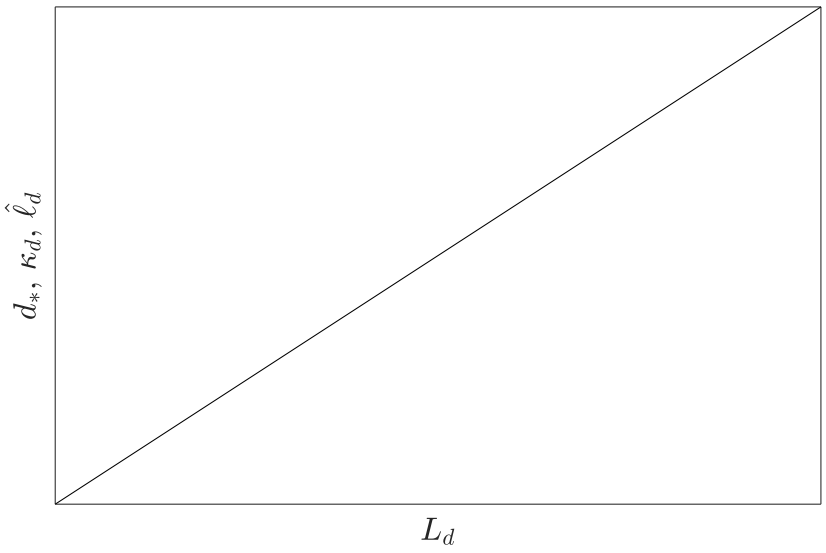

Figure 4.1: Conceptual model of how the critical depth of cut (d_*), the coefficient (κ_d), and the conformal contact length ($\hat{\ell}_d$) vary with the diamond wear flat length (L_d).

To test the proposed model and validate the concept of equivalent blade, I conducted drilling experiments with ID bits of different sizes: NQ-size (outer diameter 75 mm and inner diameter 45 mm) and TT56-size (same inner diameter as the NQ-size bit but smaller outer diameter of 55 mm).

Figure 4.2 compares the cumulative diamond wear flat area ($\bar{A}_d$) and the diamond wear flat length (L_d) of these two bits at different wear states. Although the total diamond wear flat area is larger for the NQ-size bit, the equivalent diamond wear flat lengths of the two bits are quite comparable. In wear state 1, the total diamond wear flat area of the NQ-size bit is 6 mm^2, three times larger than that of the TT56-size bit, after scaling, the diamond wear flat length of

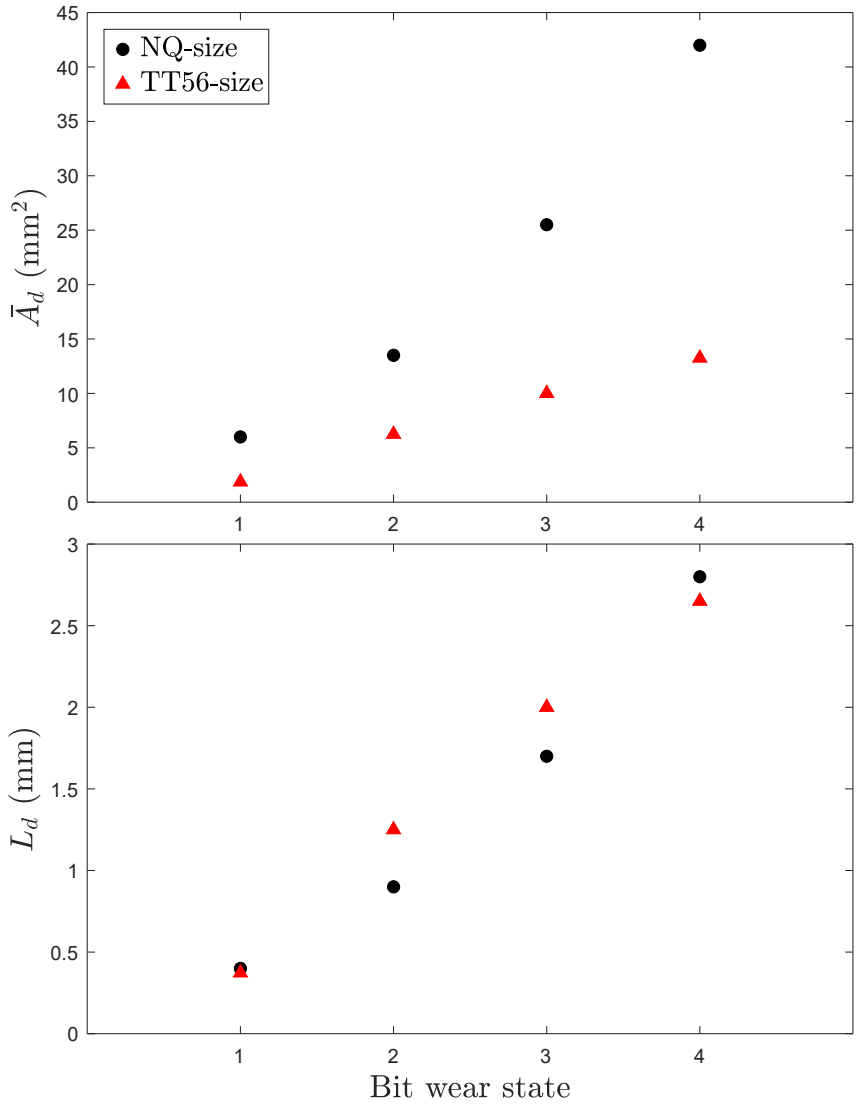

Figure 4.2: Cumulative diamond wear flat area ($\bar{A}_d$) and diamond wear flat length (L_d) of ID bits with different sizes.

these two bits is approximately the same around 0.4 mm.

Figure 4.3 compares the drilling responses of the two bits at different wear states. All the drilling responses are characterised by both regime I and II and the scaled forces at each depth of cut increase with the diamond wear flat length regardless of bit size. The intercepts of regime II estimated from both $w - d$ space ($\sigma_d \hat{\ell}_d$) and $t - d$ space ($\mu_d \sigma_d \hat{\ell}_d$) increase with diamond wear flat length. In wear state 1, where two bits share the same diamond wear flat length but

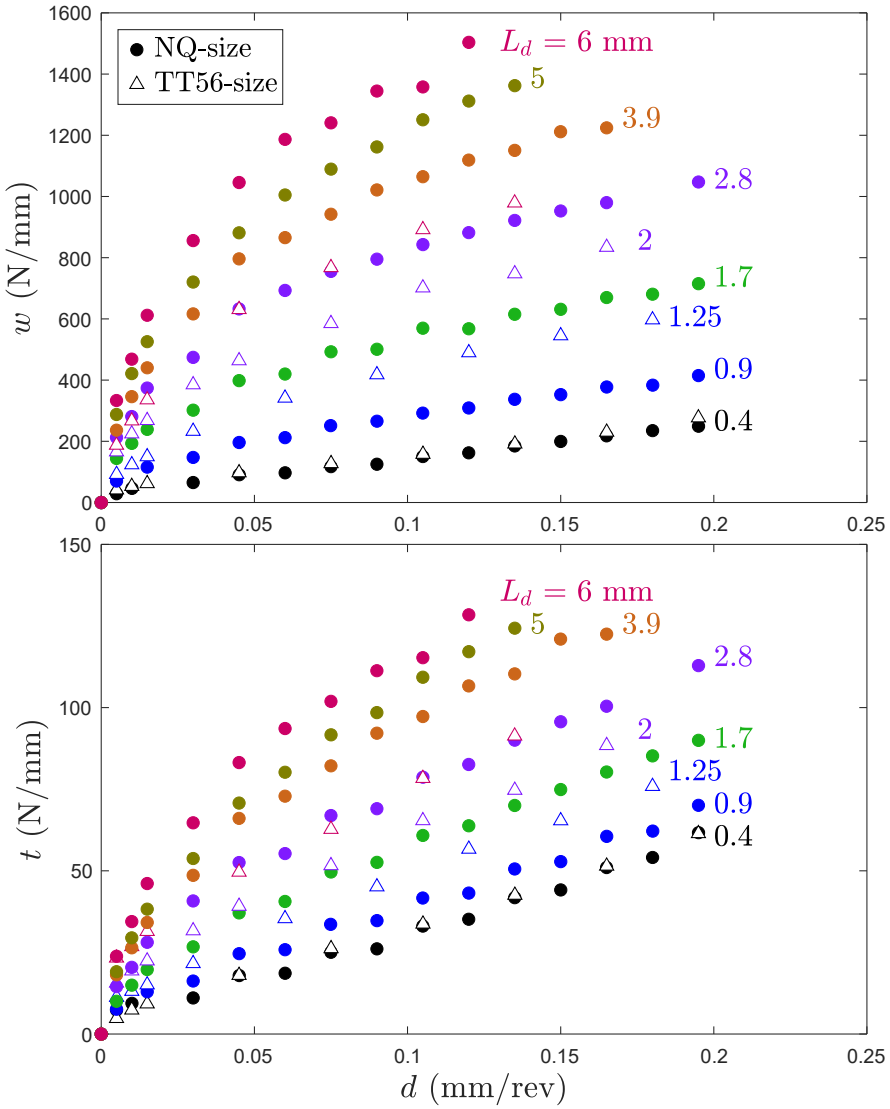

Figure 4.3: The effect of diamond wear flat length (L_d) on the drilling responses of an NQ-size bit (solid) and a TT56-size bit (hollow). Tests were conducted in Bluestone granite.

different diamond wear flat area, the intercepts of regime II are identical, 30 N/mm in $w - d$ space and 2 N/mm in $t - d$ space. As diamond contact stress (σ_d) and diamond frictional coefficient (μ_d) can be considered invariant for the same combination of bit rock, we can conclude that diamond frictional contact length (ℓ_d) is proportional to diamond wear flat length (L_d).

The model parameters of the drilling response are calculated using the method

Table 4.1: Model parameters derived from the drilling responses of an NQ-size bit at different diamond wear states.

L_d [mm]	d_* [mm/rev]	α_{I} [$\times 10^3$ MPa]	α_{II} [$\times 10^3$ MPa]	w_o [N/mm]
0.4	0.0085	4.9	1.12	31
0.6	0.009	14	1.39	103
0.9	0.0119	14.1	1.32	153
1.3	0.014	12	1.44	268
1.7	0.0186	21.3	1.79	363
2.2	0.0225	22	1.97	452
2.8	0.0251	31.1	2.19	620
3.9	0.026	32.2	2.79	776
5	0.0235	38.7	4.1	813
6	0.024	44.4	4.23	965

outlined in Chapter 3, they are summarized in Table 4.1. As shown in Figure 4.4, the depth of cut (d_*) at the onset of regimes II initially increases linearly with the diamond wear flat length and eventually saturates at around 0.023 mm/rev. The conformal diamond frictional contact length ($\hat{\ell}_d$) was calculated using the intercept of regime II and the diamond/rock contact stress obtained from Chapter 3 ($\sigma_d = 158$ MPa for Bluestone). The results show that $\hat{\ell}_d$ is of the same order of magnitude as the diamond wear flat length (L_d), supporting the assumption that the conformal diamond frictional contact length is equals to the diamond wear flat length. The coefficient (κ_d) representing the variation of the frictional contact length also increases linearly with diamond wear flat length at a rate of 37. In addition, the parameters obtained from bits with two different sizes are comparable.

The results confirm the proposed model that the frictional contact length (ℓ_d) is controlled by the diamond wear flat length (L_d). As the bit polishes, not only the effective diamond frictional contact length (ℓ_d) increases, the onset of regime II (where conformal contact occurs) is delayed (d_* increases).

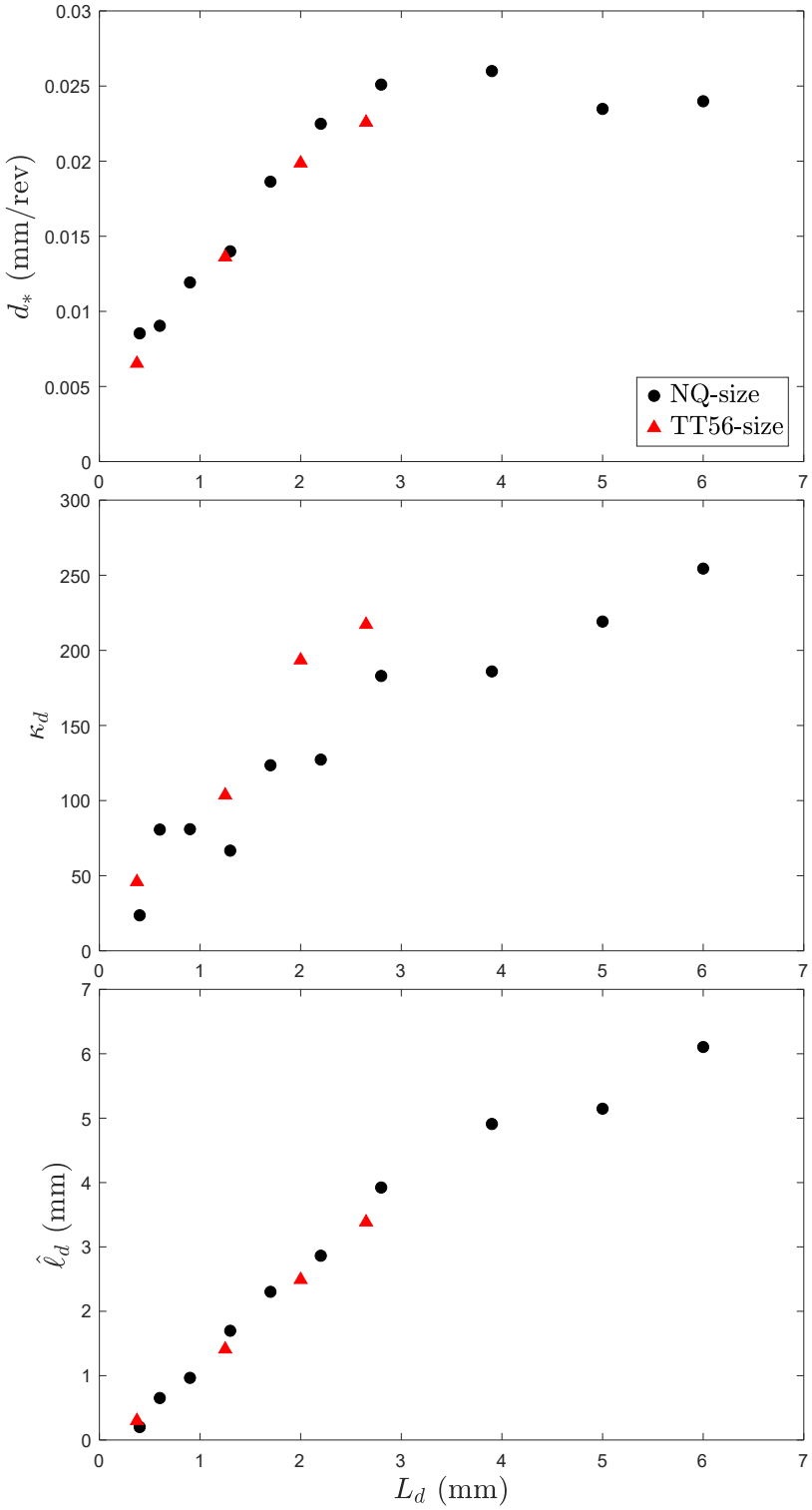

Figure 4.4: Relationships between model parameters associated with diamond frictional contact length and the diamond wear flat length.

4.3 The matrix wear flat length at the tail ($L_{\bar{m}}$)

In Chapter 3, we assumed the coefficient ($\kappa_{\bar{m}}$) representing the variation of matrix wear flat effective length at the tail changes with the matrix nominal wear flat length at the tail ($L_{\bar{m}}$), see Figure 4.5.

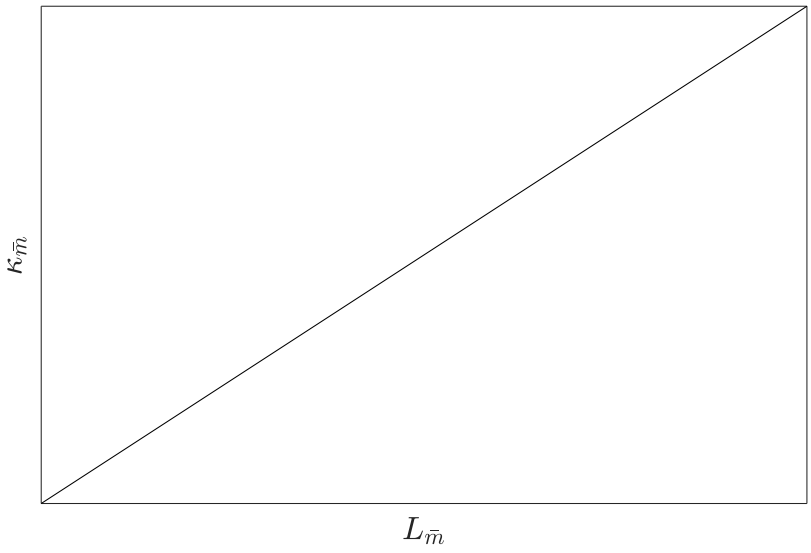

Figure 4.5: Proposed relation between the coefficient ($\kappa_{\bar{m}}$) and the matrix wear flat length at the tail ($L_{\bar{m}}$).

According to Table 4.1, the slope of regime II (α_{II}) increases with the diamond wear flat length (L_d). With the term $\zeta\varepsilon$ a constant ($\zeta\varepsilon = 1200$ MPa) we can estimate the term $\sigma_m\kappa_{\bar{m}} = \alpha_{\mathrm{II}} - \zeta\varepsilon$ which increases linearly with diamond wear flat length, see Figure 4.6. The contact stress is most likely independent of the bit topology and we can thus conclude that the term $\kappa_{\bar{m}}$ increases with the matrix wear flat length at the tail ($L_{\bar{m}}$).

Based on the scanning result, see Figure 4.7, the diamond wear flat area (A_d) increased by 0.34 mm^2 and the matrix wear flat area at the tail ($A_{\bar{m}}$) increased by 0.2 mm^2 which causes the increase in the variation of matrix frictional contact length at the tail. It confirms our argument that the parameter associated with matrix frictional contact length at the tail is controlled by the matrix wear flat at the tail ($L_{\bar{m}}$) that increases with the diamond wear flat length due to diamond

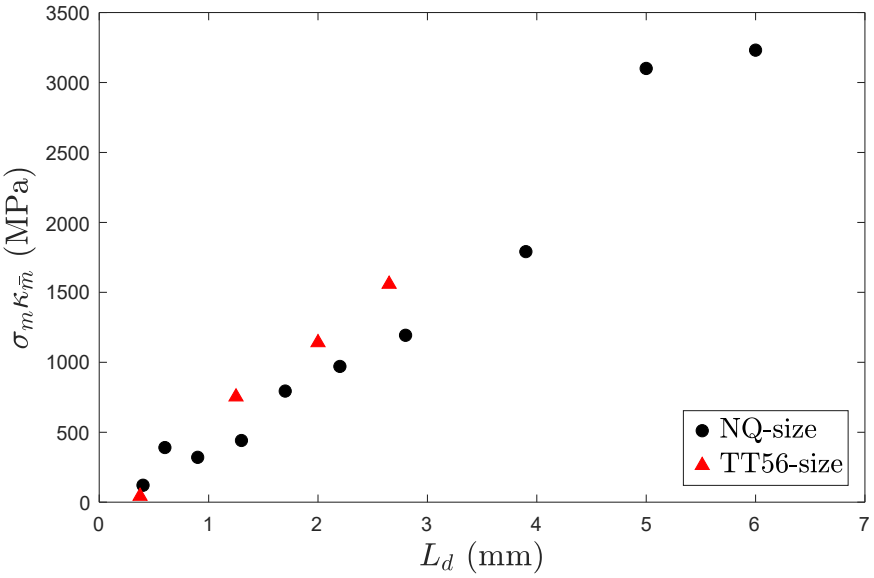

Figure 4.6: The relationship between ($\sigma_m \kappa_{\bar{m}}$) and the diamond wear flat length (L_d).

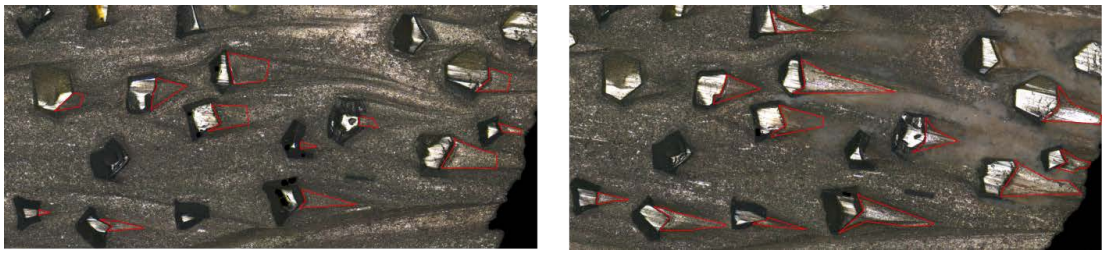

Figure 4.7: Picture of a section of the bit cutting face at two different wear states, with highlights on the section of the comet tails rubbing against the rock surface.

protection. Moreover, Figure 4.6 shows that $\kappa_{\bar{m}}$ is around 0 when the diamond wear flat length is small, which means that the matrix wear flat at the tail is close to 0 when the bit is sharp. These results stress how diamond polishing affects drilling performance by increasing both the diamond wear flat length and the matrix wear flat length.

4.4 Diamond protrusion ($\bar{p}$)

In Chapter 3, we argue that the depth of cut (d_{**}) at the onset of regime III is characterized by the occurrence of the three-body contact at the crater and is expected to increases with the diamond protrusion ($\bar{p}$), see Figure 4.8.

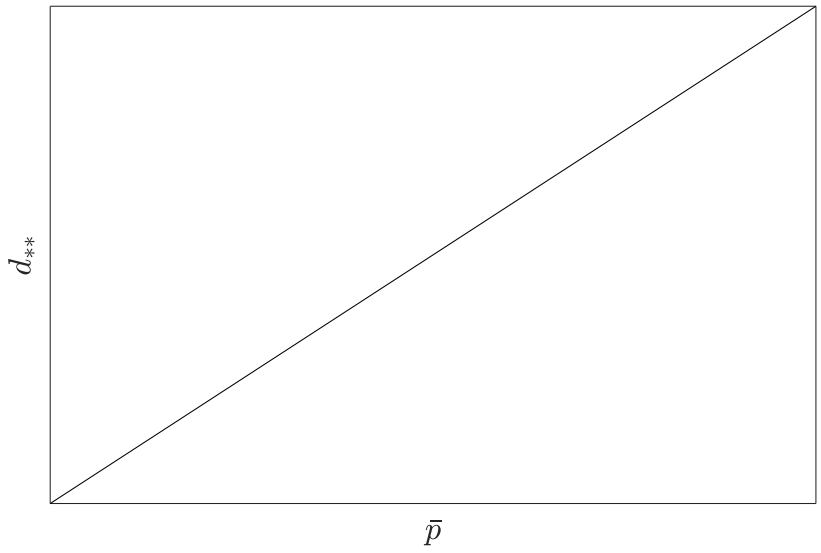

Figure 4.8: Proposed relation between the depth of cut (d_{**}) at the onset of regime III and the diamond protrusion ($\bar{p}$).

To validate our argument, drilling tests were conducted using the NQ-size bit at different wear states at depth of cut high enough to push the bit response into regime III. The diamond exposure was changed by gradually wearing the tip of the diamonds, while the matrix height at the crater was maintained. Figure 4.9 shows that the depth of cut (d_{**}) at the onset of regime III decreases as the diamond protrusion ($\bar{p}$) decreases.

The result aligns with our argument that the occurrence of regime III is caused by additional matrix frictional contact at the crater ($\ell_{\hat{m}}$) due to accumulation of cuttings at the bit-rock interface. One of the ways to confirm this is to measure the contact area of the bit face after cutting at different regimes. For this purpose, I coat the cutting face of an ID segment with nail polish, I then run a cutting test in a sample of Bluestone granite at different depths of cut: 0.1 mm/rev

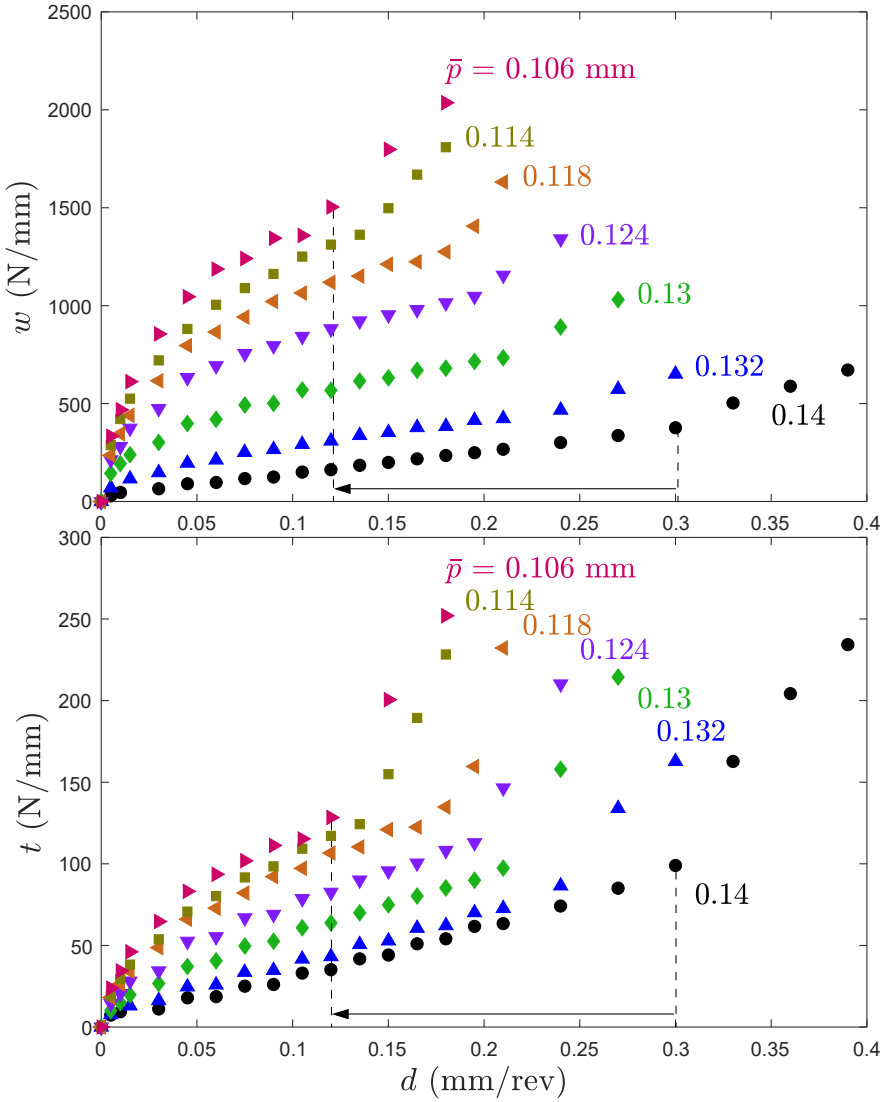

Figure 4.9: Effect of diamond protrusion ($\bar{p}$) on the drilling responses of the bit. Tests were conducted in a sample of Bluestone granite with the NQ-size bit.

(regime II), 0.2 mm/rev (d_{**}), and 0.25 mm/rev (regime III). Each cutting test lasted a minute to establish a stationary contact, and then the segment was taken for a scanning test to estimate the contact areas bit-rock. Figure 4.10 shows the cutting face coated with nail polish after cutting at different depths of cut. Initially, all diamonds and the matrix are coated with nail polish. After cutting at 0.01 mm/rev depth of cut, the nail polish on the diamonds is removed. When the depth of cut increases to 0.2 mm/rev, some of the nail polish on the matrix

tail is also removed. When the depth of cut increases to 0.025 mm/rev (beyond d_{**}), more than 90% nail polish on the matrix is removed and a layer of cuttings sticking on the bit face is observed confirming the occurrence of regime III is caused by additional three-body contact between matrix, rock, and cuttings.

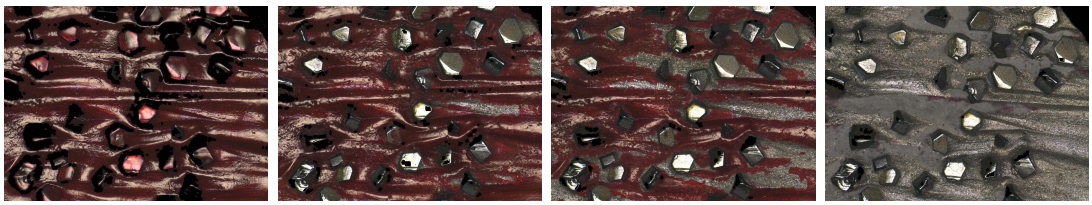

Figure 4.10: Identification of contact area after cutting at different regimes: initial state, regime II, d_{**}, regime III (left to right).

The drilling tests were repeated with a TT56-size bit and a single ID segment. Similarly to the NQ-size bit, the diamond protrusion of the TT56-size bit was changed by wearing the diamond tip. However, for the segment, the diamond protrusion increased by eroding the matrix at the crater to expose diamonds. According to Figures 4.11 and 4.12, for the TT56-size bit, the depth of cut at the onset of regime III decreases from 0.21 mm/rev to 0.06 mm/rev when the diamond protrusion decreases from 0.14 mm to 0.078 mm, and for the single segment, the depth of cut at the onset of regime III increases from 0.004 mm/rev to 0.023 mm/rev as the diamond protrusion increases.

Summarizing all the results, a linear constraint exists between the depth of cut (d_{**}) at the onset of regime III and the diamond protrusion ($\bar{p}$), see Figure 4.13, while the slope changes with bit size: 5 for the NQ-size bit, 2 for the TT56-size bit, and 0.33 for the segment. The difference in slope is caused by the number of active diamonds on the cutting face whose trajectory overlaps. As discussed in Chapter 3, during drilling, the overall depth of the cut of the bit (or the thickness of the rock removed by the bit over one revolution) is evenly shared by the diamonds located at the same radial distance from the centre of the bit (considering that the bit rotates around its axis of symmetry). Assuming, for the sake of simplicity, evenly spaced diamonds with the same protrusion, we can

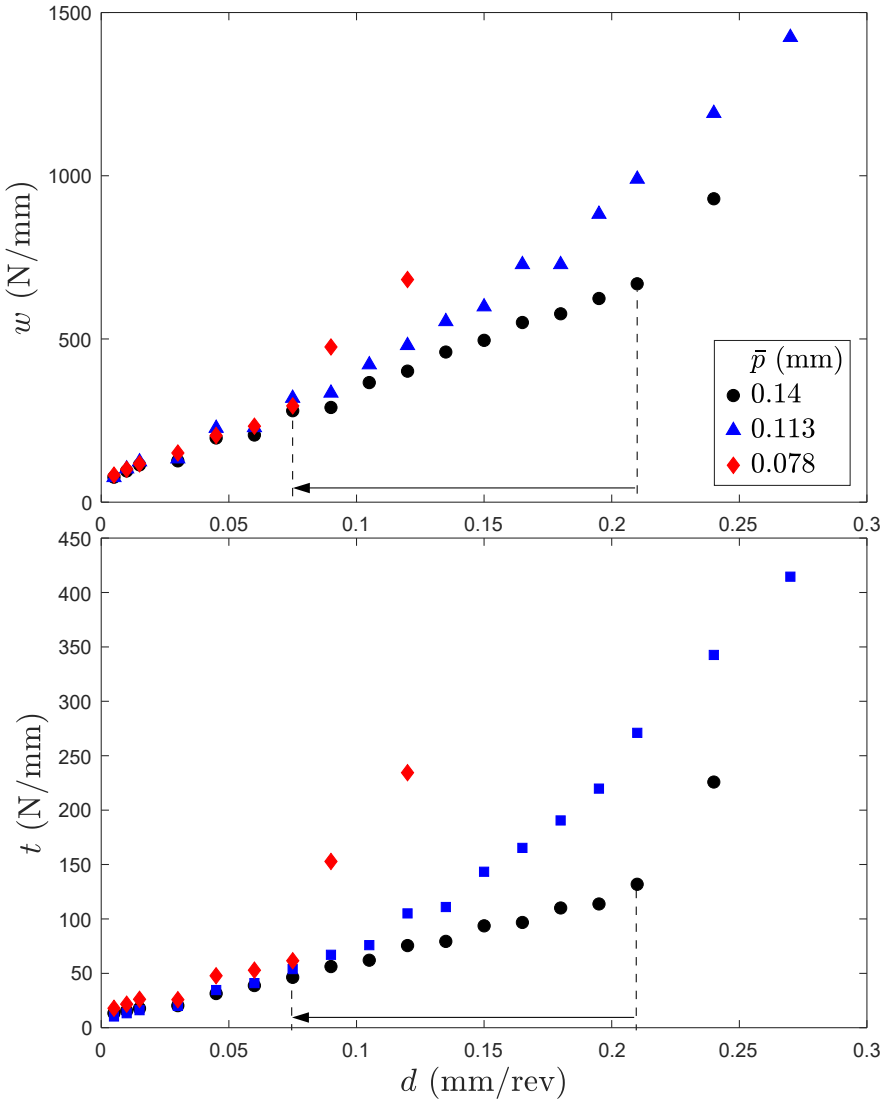

Figure 4.11: The effect of diamond protrusion ($\bar{p}$) on drilling responses. The tests were performed with a TT56-size bit on Bluestone granite.

write

$$d = \sum_{i=1}^{n} (d_d) = n d_d \tag{4.1}$$

where d_d is the depth of cut per diamond, and n is average number of diamonds whose trajectory overlaps. In other words, for a given depth of cut, the more diamonds on the same perimeter, the lower the depth of cut per diamond. Based

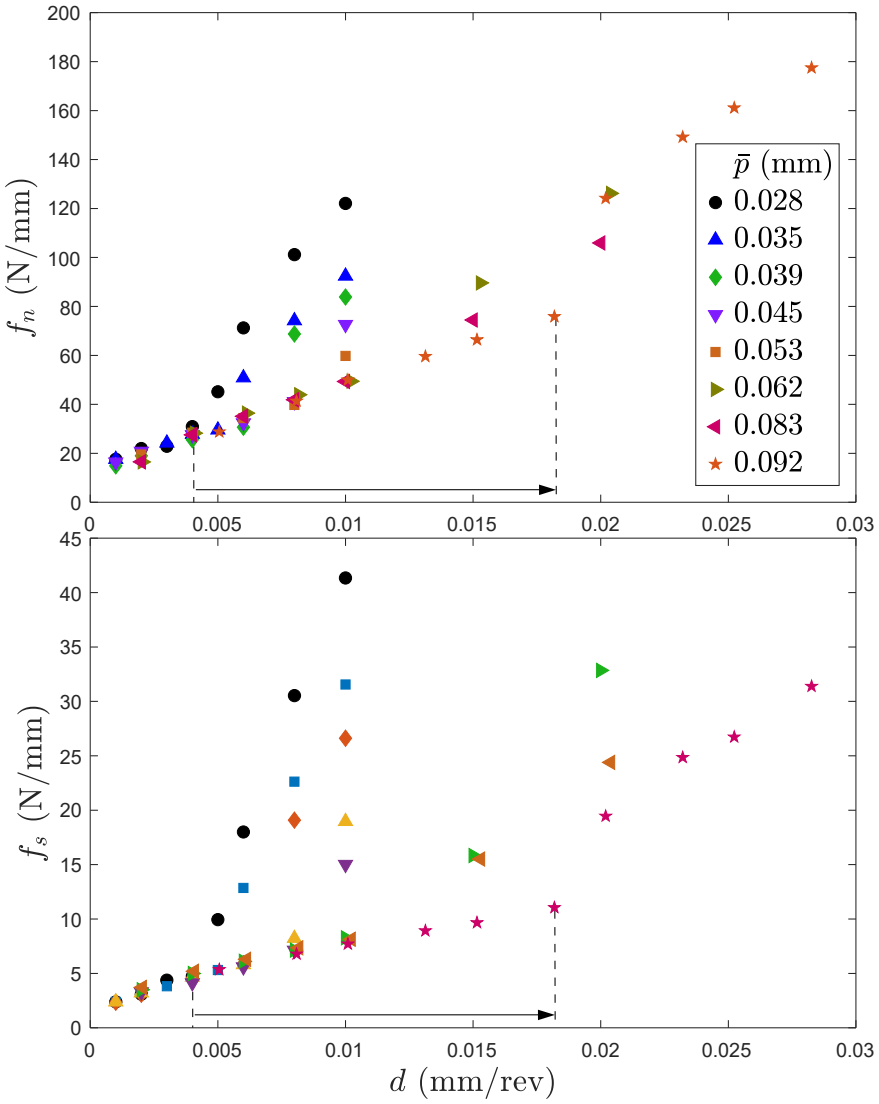

Figure 4.12: The effect of diamond protrusion ($\bar{p}$) on drilling responses. Tests were performed using an ID segment on a sample of Bluestone rock.

on the scanning results, the NQ-size bit has approximately 80 diamonds tracing the same groove, the TT56-size bit 50 diamonds, and the ID segment only 14 diamonds. Thus, the depth of cut per diamond for the segment is 6 times larger than the NQ-size bit and therefore may enter regime III at a smaller overall depth of cut. Figure 4.13 shows that the depth of cut at the onset of regime III increases with the diamond protrusion, scaled with the number of diamonds and thus likely with the diamond protrusion.

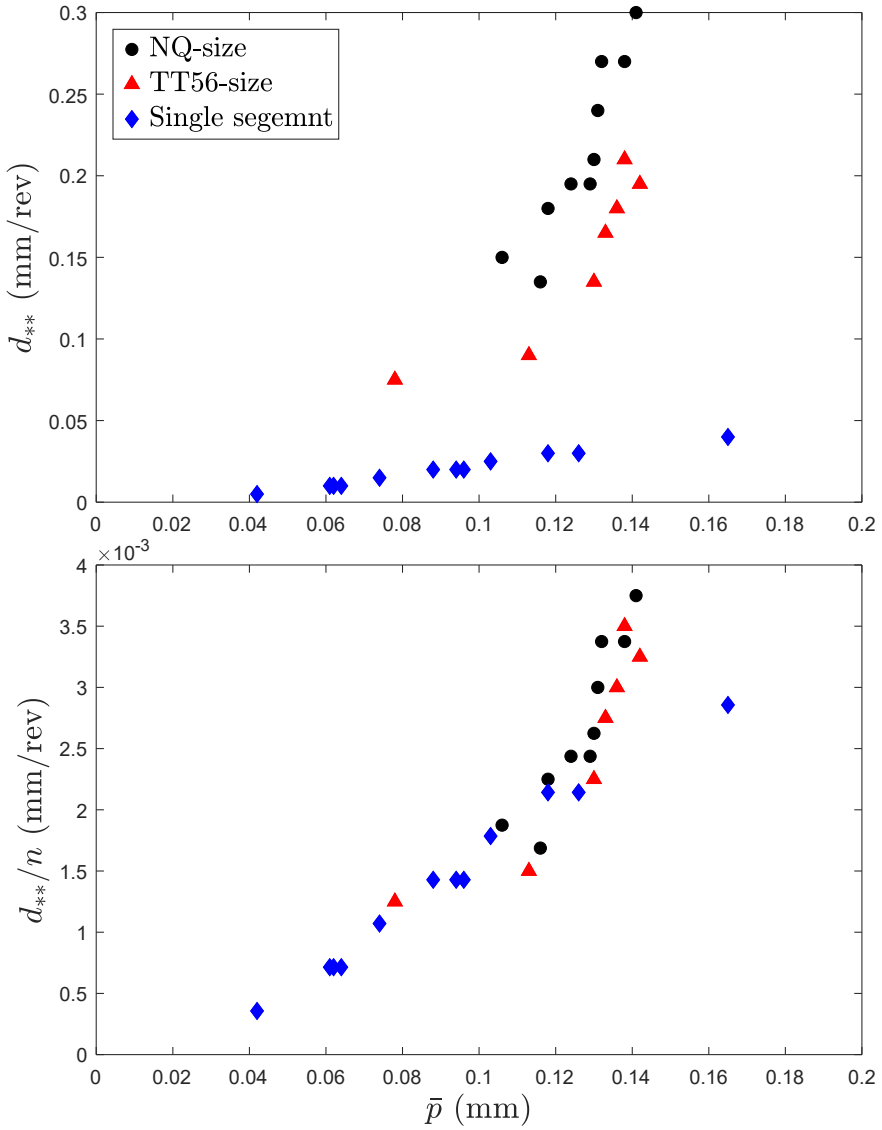

Figure 4.13: The relationship between the depth of cut at the onset of regime III and diamond protrusion.

4.5 The matrix wear flat length at the crater ($L_{\hat{m}}$)

The coefficient ($\kappa_{\hat{m}}$) representing the variation of matrix frictional contact at the crater is expected to change with the matrix wear flat length at the crater ($L_{\hat{m}}$), see Figure 4.14. Unfortunately, we are not able to measure the extent of contact

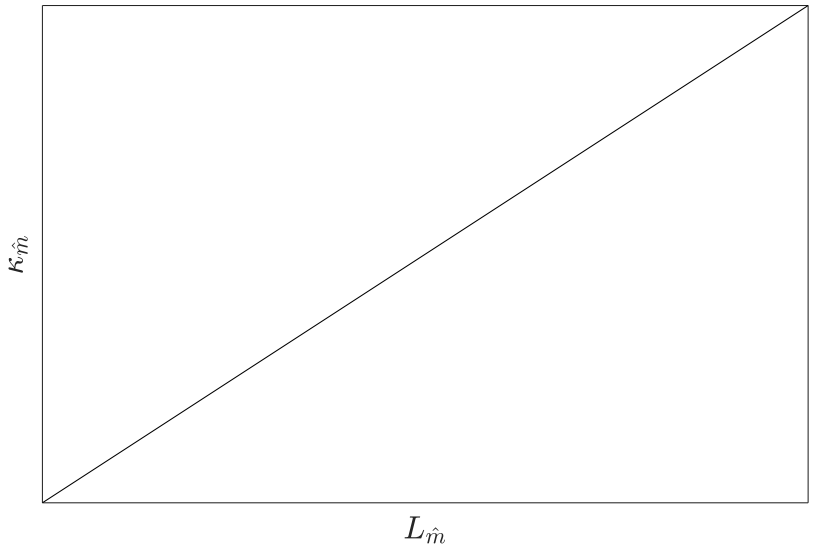

Figure 4.14: Effect of the diamond protrusion on the coefficient ($\kappa_{\bar{m}}$).

between rock debris and the matrix. Thus, I decided to consider the diamond protrusion ($\bar{p}$) rather than $L_{\hat{m}}$ to describe the geometry of the contact associated with regime III.

The coefficient ($\kappa_{\bar{m}}$) is derived from the differences in slopes in the space $w-d$ in regime II and regime III ($\alpha_{\mathrm{III}} - \alpha_{\mathrm{II}}$). The results in Figure 4.15 show some dispersion (as compared to other experimental results) in part caused by the smaller number of points in regime III (leading to a larger error in the estimate of the slope) but also likely related to the stochastic nature of the process.

Regime III is associated with three bodies contact, where the third body consists of a slurry drilling fluid and cuttings, the complex behaviours of viscous fluid flow filled with particle (turbulence, impact between cuttings..) can certainly explain the observed dispersion. Indeed, Figure 4.16 shows that for a given bit topology the forces in regime I and II are quite repeatable, while the force in regime III varies, leading the slope of regime III to range from 2000 MPa to 3000 MPa. However, the results suggest an overall decrease of $\sigma_m \kappa_{\hat{m}}$ with the diamond protrusion.

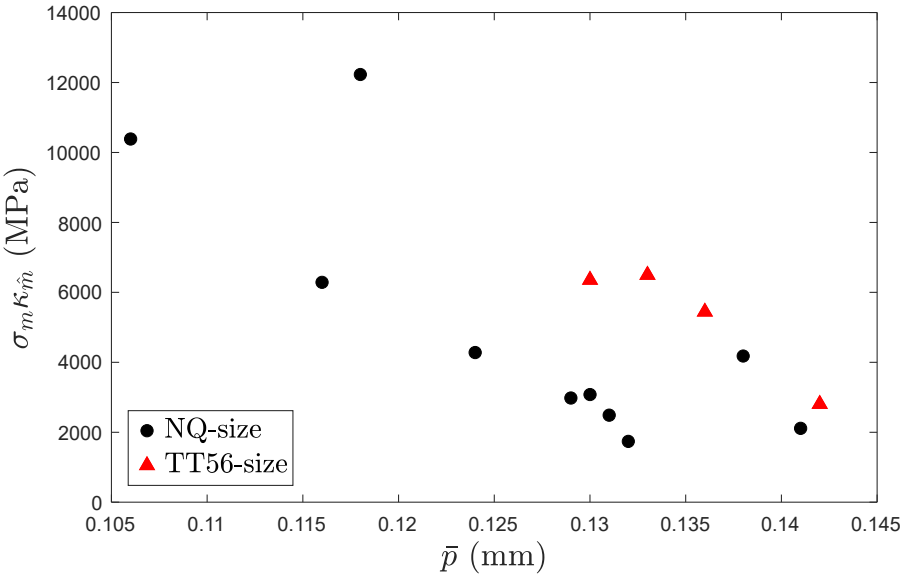

Figure 4.15: Effect of the diamond protrusion ($\bar{p}$) on the coefficient ($\kappa_{\hat{m}}$) representing the variation of matrix frictional contact length at the crater.

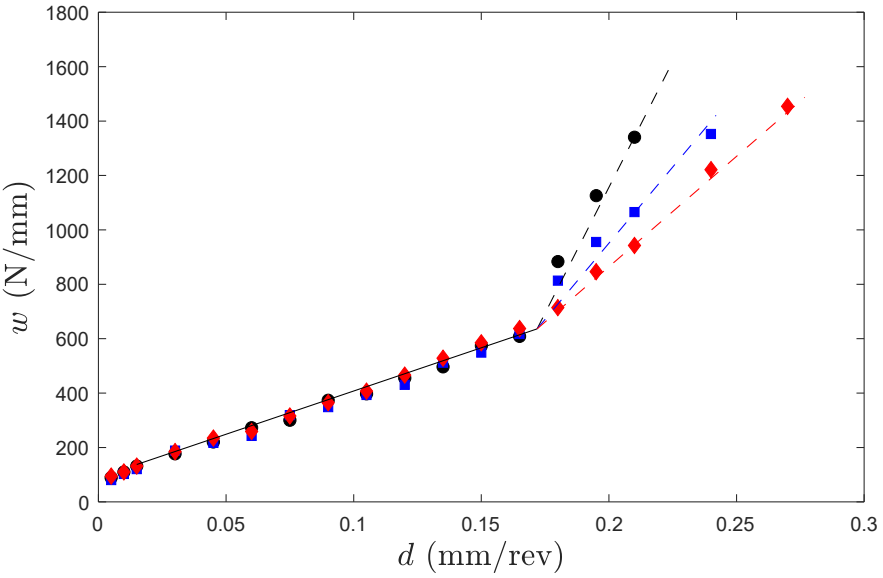

Figure 4.16: Variation in forces in regime III for a given state of wear. Tests were conducted with a NQ-size bit on Bluestone granite.

4.5.1 The effect of third body properties on drilling response

In three-body contact, the third body is a slurry made of cuttings and drilling fluid. It is reasonable to assume that variations in the properties of either cuttings or drilling fluid could influence the matrix frictional contact at the crater ($\ell_{\hat{m}}$), particularly the depth of cut (d_{**}) at the onset of regime III.

4.5.1.1 Rock properties

To investigate the effect of rock properties, I conducted drilling tests using a TT56-size ID bit on three different types of granite: Bluestone, Austral Black, and Calca Red. Austral Black, which has a mineral composition similar to that of Bluestone, differs primarily in its much larger grain size. Calca Red, while having a grain size comparable to Austral Black, contains 36% quartz, making it the hardest rock among the three. This variation in rock type and hardness provides a comprehensive basis for evaluating how different rock characteristics influence the drilling response.

The bit topology was measured before and after each drilling test using the Alicona microscope. Analysis of the scanning result revealed that the diamond wear flat length of the bit (L_d) increased by less than 5%, from 0.5 to 0.52 mm, and the diamond protrusion remained unchanged. This indicates that the bit wear state remained unchanged during the test.

Figure 4.17 compares the drilling responses for the three rocks and shows that all responses are characterised by three cutting regimes with $d_* = 0.04$ mm/rev and $d_{**} = 0.21$ mm/rev. This indicates that the onset of different regimes is not a function of rock type. The variation in the slope of each regime across different rocks is attributed to a change in the intrinsic specific energy (ε) and contact stress (σ).

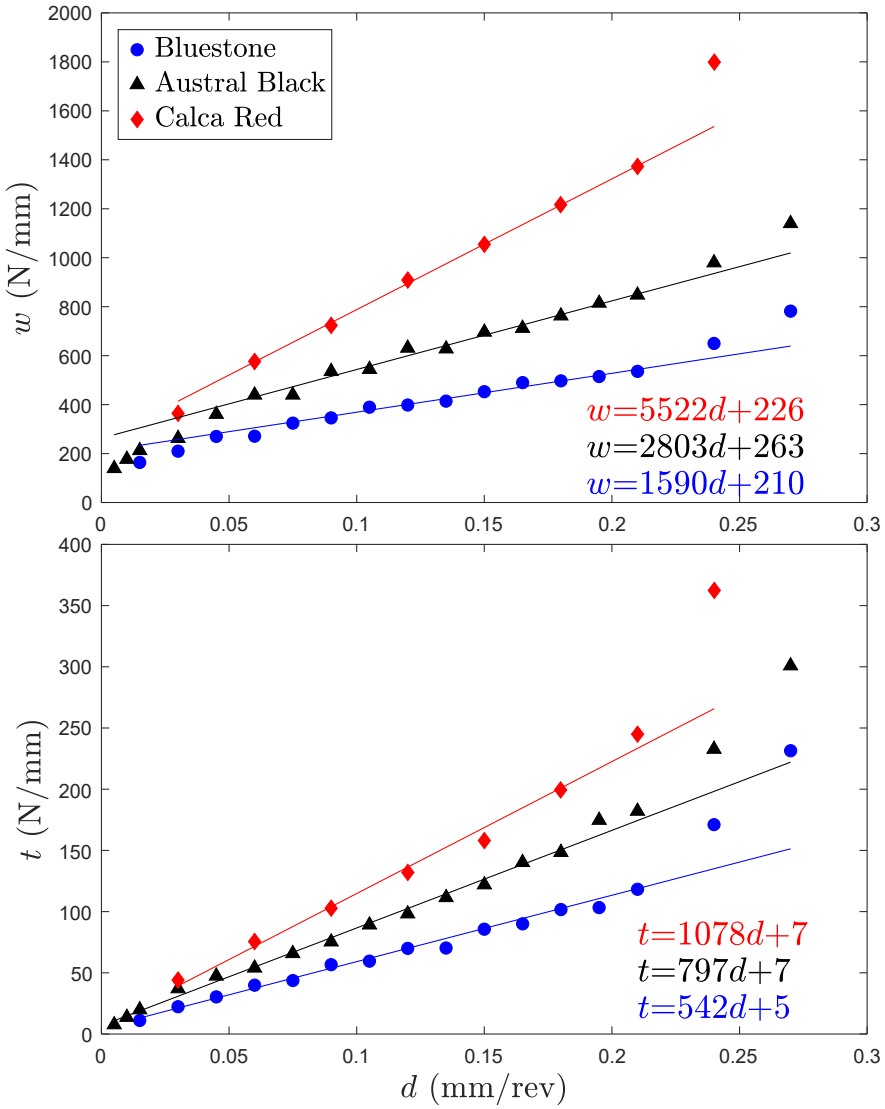

Figure 4.17: Effect of rock properties on the drilling responses of an ID bit.

4.5.1.2 Drilling fluid viscosity and type

Drilling fluid viscosity is often modified in diamond drilling to improve wellbore cleaning. Common additives such as polymer and bentonite are used to increase fluid viscosity. Polymers are long chains of repeating molecular units that interact with water to form a network that increases fluid viscosity. Bentonite, on the other hand, absorbs water and swells, forming a gel-like structure that thickens the fluid and increases its viscosity.

To investigate the effect of fluid viscosity on the drilling response, I conducted drilling experiments using an NQ-size bit on Bluestone granite, varying the marsh funnel viscosity from 30 s to 45 s (commonly used in the field) in increments of 5 s. As shown in Figure 4.18, the depth of cut (d_{**}) at the onset of regime III decreases from 0.14 to 0.04 mm/rev as the fluid viscosity increases. Once

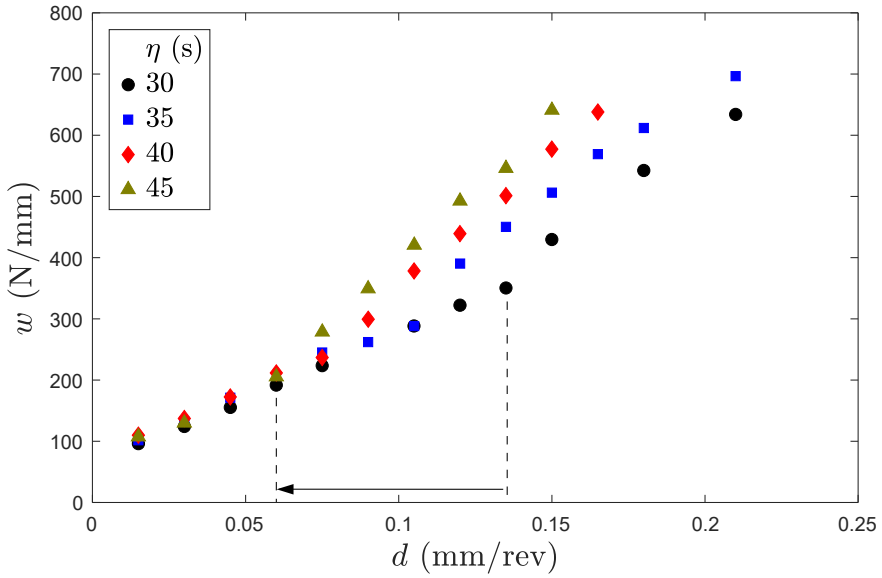

Figure 4.18: Effect of drilling fluid viscosity on drilling responses. Tests were carried out on Bluestone granite using an NQ-size bit .

we removed the bit from the rig after the test, we observed a layer of cuttings sticking to the bit face, with one of the waterways is blocked by the cuttings, see Figure 4.19. The accumulation of cuttings reduces the diamond protrusion ($\bar{p}$)

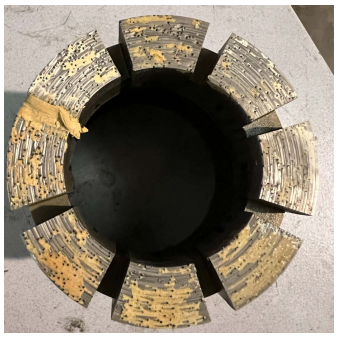

Figure 4.19: Cuttings stick on the bit face after the drilling test ($\eta = 45$ s).

which in turn causes three-body contact at the crater to occur at a smaller depth of cut. However, the forces in regime I and II are identical, indicating that the diamond frictional contact length (ℓ_d) and the matrix frictional contact length in the tail ($\ell_{\bar{m}}$) are not affected by the fluid viscosity. This observation confirms that three-body contact only occurs in regime III at the crater.

By extracting the depth of cut (d_{**}) at the onset of regime III from the drilling responses and plotting it against the fluid viscosity, we observe a linear constraint between two variables, see Figure 4.20.

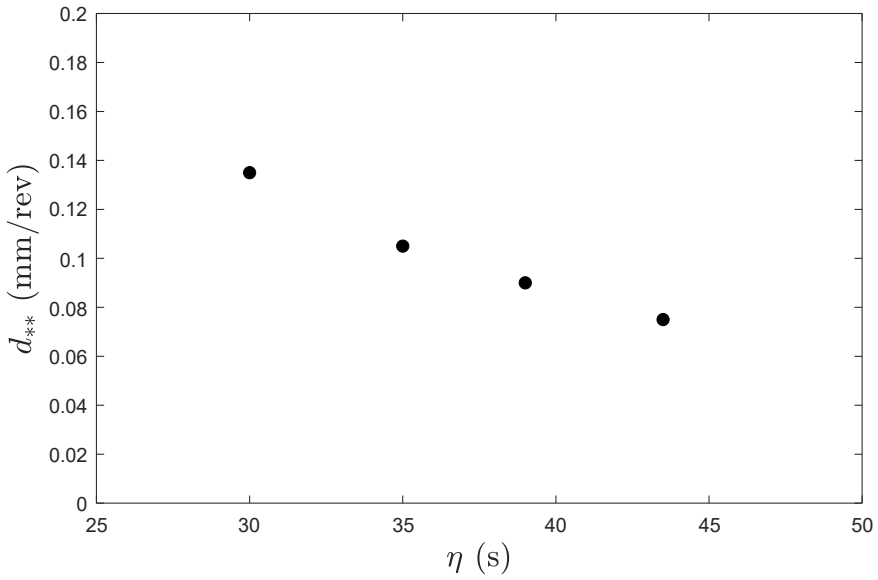

Figure 4.20: The relationship between the depth of cut at the onset of regime III (d_{**}) and fluid viscosity (η).

It is also important to investigate whether this relationship is controlled by the type fluid. Understanding how various additives affect drilling can provide valuable insight into optimising fluid formulations for better performance. Drilling fluids were formulated with three different additives - xanthan gum (bio-polymer), PAC R (synthetic polymer), and bentonite - each targeting a marsh funnel viscosity (η) of 35 s. Figure 4.21 shows the forces remain consistent across all three fluids, and the drilling response enters regime III at a depth of cut of 0.11 mm/rev. This consistency of drilling responses across different fluids simplifies performance

predictions and ensures more stable operations regardless of the type of fluid.

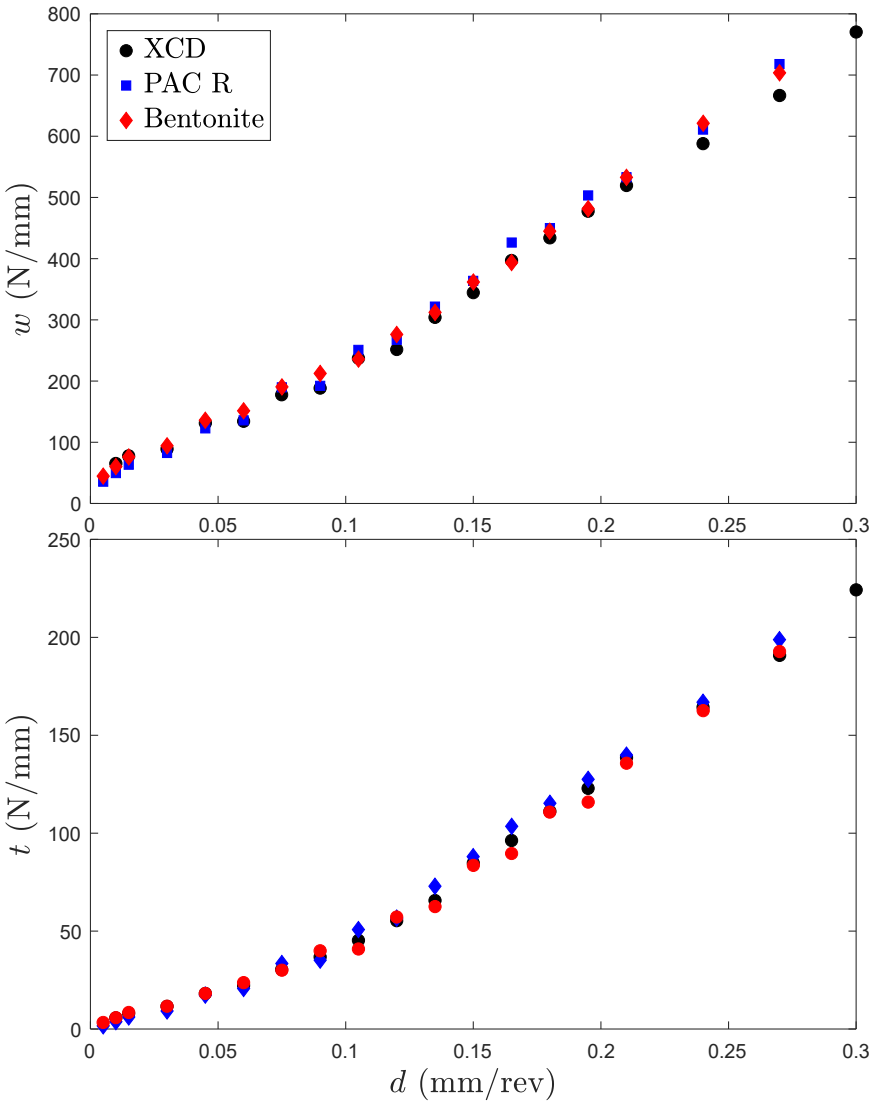

Figure 4.21: Effect of drilling fluid type on drilling responses. Tests were conducted with an NQ-szie bit on Bluestone granite.

4.6 Summary

In summary, in this chapter we established relationships between the bit wear state and the drilling response. We reduce the complex bit topology to a single equivalent blade that is characterised by four nominal (scaled) lengths: diamond

protrusion ($\bar{p}$), diamond wear flat length (L_d), matrix wear flat length at the tail ($L_{\bar{m}}$) and at the crater ($L_{\hat{m}}$). Drilling experiments using bits of different sizes shows that the scaled forces are controlled by the diamond wear flat length (L_d) rather than the cumulative diamond wear flat area ($\bar{A}_d$). This consistency validates the concept of equivalent blade, confirming its utility to predict drilling performance in different bit sizes.

The drilling responses are captured at different wear states, with the nominal lengths precisely quantified. The diamond wear flat length (L_d) controls the relationship between the diamond frictional contact length (ℓ_d) and the depth of cut. The model parameters (d_*, κ_d, and $\hat{\ell}_d$) are found to increase linearly with the diamond wear flat length. This means that as the bit polishes, the diamond frictional contact length (ℓ_d) at a given depth of cut increases, and the depth of cut at (d_*) the onset of regime II (where conformal contact occurs) is delayed.

The matrix frictional contact length at the tail ($\ell_{\bar{m}}$) is controlled by the matrix wear flat length at the tail ($L_{\bar{m}}$). The coefficient ($\kappa_{\bar{m}}$) representing the variation of the matrix frictional contact length at the tail increases with $L_{\bar{m}}$, which in turn increases with the diamond wear flat length (L_d) due to diamond protection. This highlights how diamond polishing affects drilling performance by increasing both the diamond wear flat length and the matrix wear flat length.

We confirmed that the higher slope in regime III is caused by the three-body contact between diamond, matrix, and cuttings that occurs in the crater. The depth of cut (d_{**}) at the onset of regime III increases with diamond protrusion ($\bar{p}$). The matrix frictional contact length at the crater ($\ell_{\hat{d}}$) and the coefficient ($\kappa_{\hat{m}}$) appear to be also affected by the diamond protrusion. However, more results are needed to confirm this due to the limited number of points in regime III and the stochastic nature of the process.

Besides bit wear state, the effect of rock and fluid properties is also investigated. The rock properties do not affect the parameters associated with the bit wear state but do influence the intrinsic specific energy (ε) and the contact stress

(σ), resulting in a change to the slopes (α). The depth of cut (d_{**}) at the onset of regime III was found to decrease linearly with increasing fluid viscosity (η). This is due to cuttings building up and sticking to the matrix wear flat at the crater, which reduces the diamond protrusion.

Understanding the relationships between bit wear state and drilling response is highly valuable because it allows us to estimate the bit wear state from surface measurement. This capability allows for real-time monitoring of the bit, facilitating timely adjustments to optimize drilling performance and enhance overall efficiency.

Chapter 5

Bit Wear

5.1 Introduction

This chapter aims to validate the conceptual model of wear and establish the relationship between the change in both nominal lengths and bit wear rate with depth of cut. For this purpose, I conducted drilling tests following the workflow proposed in Chapter 3, which involves drilling a rock at a constant depth of cut to wear the bit while monitoring the change of bit topology by frequently pausing the test at predetermined intervals for microscope scanning. The effect of rock and fluid viscosity on bit wear rate was also investigated.

5.2 Dominant wear mechanisms

We proposed a wear model consisting of three dominant wear regimes based on the relationship between the wear mechanism of both the diamonds and the matrix with the depth of cut, as illustrated in Figure 5.1. Diamonds experience polishing at small depths of cut ($d < d_f$). As the depth of cut increases to the depth of cut d_f at the onset of the fracturing dominant regime, diamonds undergo fracturing wear. With further increases in the depth of cut, the response enters regime III, where a constant three-body contact at the crater erodes the matrix, resulting in

excessive diamond loss, characterising the pull-out dominant regime.

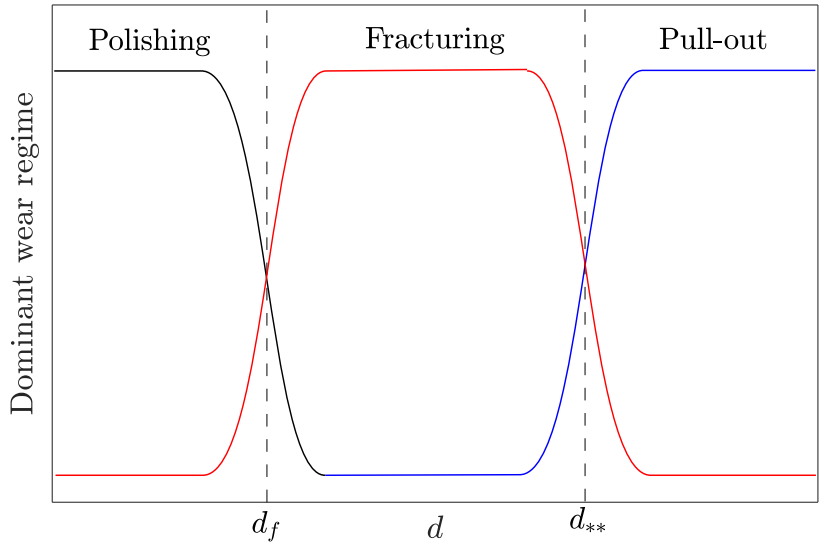

Figure 5.1: Conceptual wear model consisting three dominant wear regimes: polishing, fracturing and pull-out.

Drilling experiments were conducted using the TT56-size bit on three different types of granite (Calca Red, Austral Black, and Bluestone) and one type of sandstone (Donnybrook) at various depths of cut to validate the proposed model. The dominant wear mechanism of the bit at each depth of cut is investigated by evaluating the wear mechanism of all diamonds on the bit face, classified as polishing, fracturing, and pulling out, see Figure 5.2.

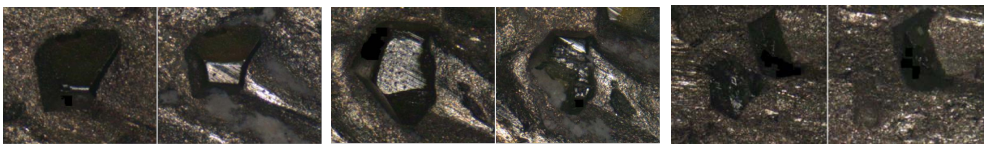

(a) Polishing (b) Fracturing (c) Pull-out

Figure 5.2: Example of change in diamond geometry for different wear mechanisms.

Diamond polishing is characterised by an increase in the flat area of diamond wear (A_d), in contrast, diamond fracturing maintains or reduces the flat area of diamond wear, and diamond removal leaves a pit on the cutting face.

Figure 5.3 and Figure 5.4 illustrate the percentage of each type of diamond wear with respect to the number of exposed diamonds. The remaining percentage represents diamonds that were not in contact with the rock. When drilling

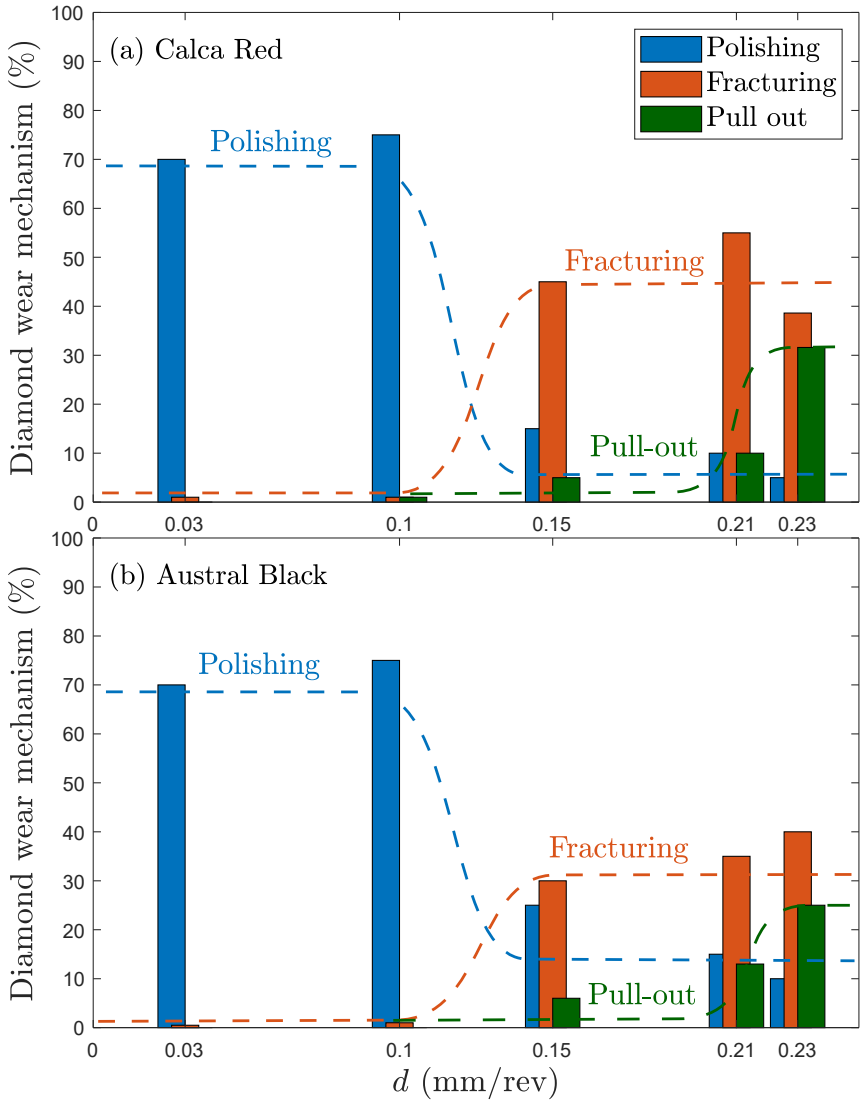

Figure 5.3: The effect of depth of cut on the percentage of diamond undergoing polishing, fracturing, and pull-out (part 1).

through Calca Red granite at a depth of cut of 0.03 mm/rev, 70% of exposed diamonds undergo polishing wear with almost no fracturing or pulling out, indicating a polishing dominant wear regime. At a depth of cut of 0.1 mm/rev, the percentage of diamonds that undergo polishing wear increases by 10% due

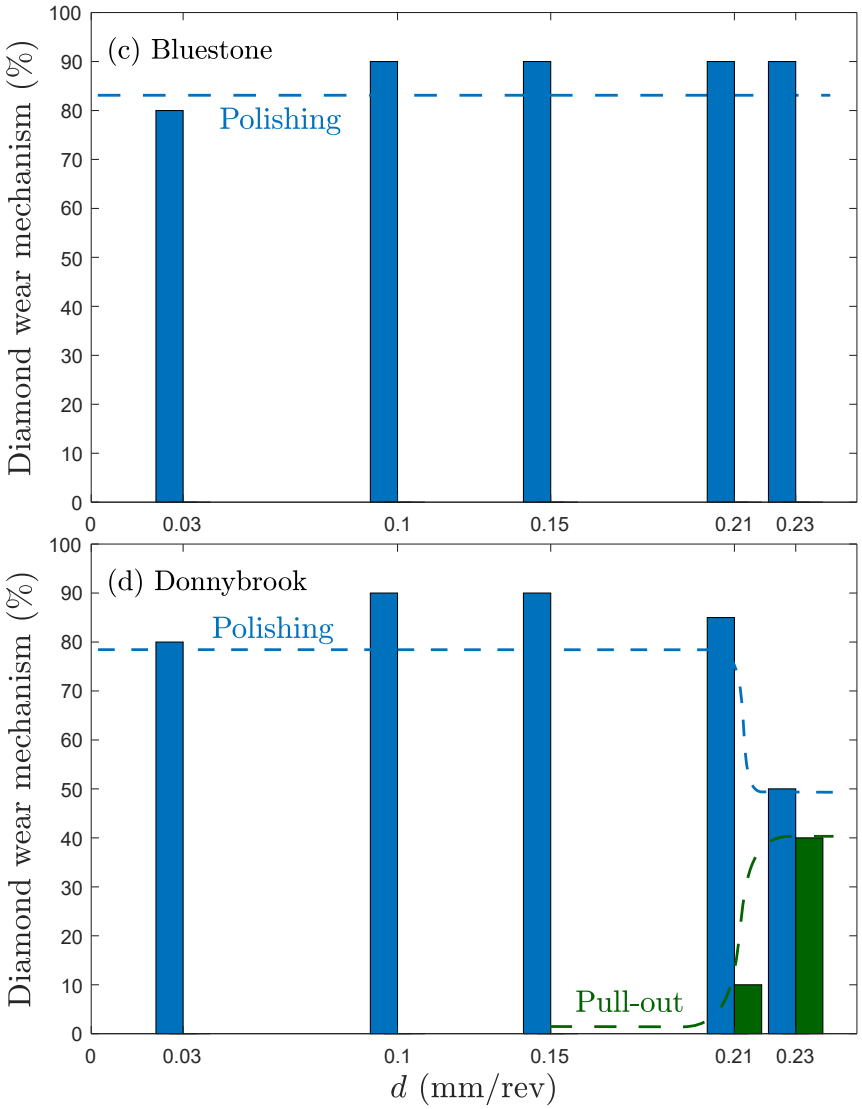

Figure 5.4: The effect of depth of cut on the percentage of diamond undergoing polishing, fracturing, and pull-out (part 2).

to more diamonds coming into contact with the rock. When the depth of cut increases to 0.15 mm/rev, diamond fracturing becomes dominant, with 45% of diamonds undergoing fracturing wear, and the percentage of diamond polishing decreases dramatically to only 15%. Thus, the depth of cut at the onset of the fracturing dominant regime is identified as 0.15 mm/rev for Calca Red granite. As the depth of cut continues to increase, the percentage of fractured diamonds increases. However, once the depth of cut exceeds 0.21 mm/rev (d_{**}) the per-

centage of diamond pulling out increases to 30% and a much higher wear rate is observed, indicating a pull-out dominant wear regime.

A similar result is obtained when drilling Austral Black granite, in which diamond fracturing becomes dominant at the depth of cut of 0.15 mm/rev. However, the percentage of diamond fracture at d_f and diamond pulled out in regime III is lower than it is in Calca Red granite, which is 30% and 25%, respectively. In contrast, diamond fracturing and pull-out were not observed when drilling Bluestone granite. Diamonds only undergo polishing wear across all depths of cut. Similarly, no diamond fracturing was observed when drilling Donnybrook sandstone, but the percentage of diamond pulled out is the highest among all four rocks when drilling at 0.23 mm/rev depth of cut. Given that the average grain size of Bluestone is 10 times smaller than the other three rocks and contains almost no hard mineral (less than 2% quartz content), it can be concluded that the depth of cut at the onset of the dominant wear regime is a function of rock properties.

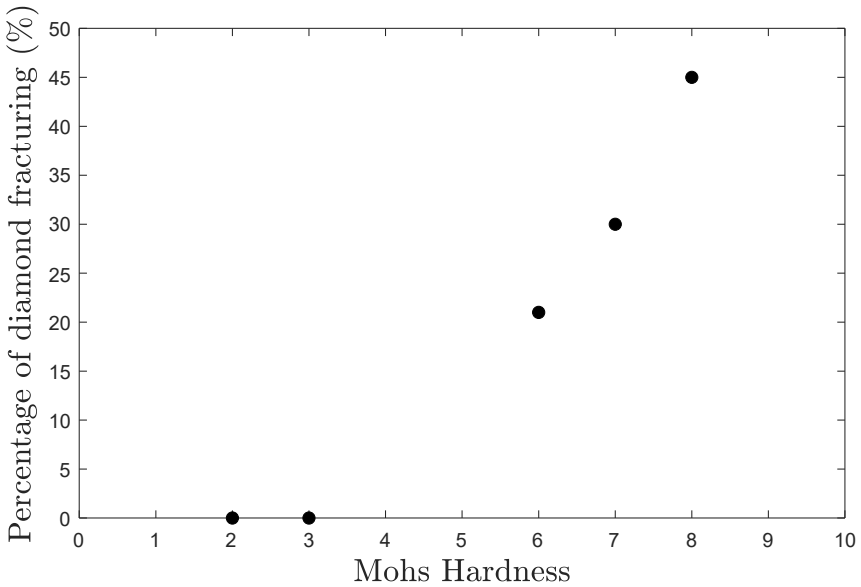

Figure 5.5: The relationship between the percentage of diamond fracturing at 0.15 mm/rev depth of cut and Mohs hardness.

Figure 5.5 shows that there is no diamond fracturing when drilling rocks with a Mohs hardness less than 4, and the percentage of diamonds that undergo

fracturing wear at d_f increases when the Mohs hardness of the rock increases from 7 to 8. This suggests that the rock may need to have a Mohs hardness greater than a critical value to fracture diamonds. However, more tests are needed on rocks with Mohs hardness between 3 and 7 to fully understand this relationship.

5.2.1 The effect of bit size on the depth of cut (d_f) at the onset of fracturing dominant regime

The test was repeated with an NQ-size bit and a single segment on Calca Red granite. Figure 5.6 shows that diamond fracturing becomes dominant at 0.02 mm/rev depth of cut for the segment and 0.18 mm/rev for the NQ-size bit. Combining the result obtained using the TT56-size bit, it was found that the depth of cut at the onset of the fracturing regime (d_f) is proportional to the number of diamonds on the same perimeter, after scaling, $d_f/n \approx 0.0025$ mm/rev for all bit sizes.

5.3 Polishing dominant wear regime, $d < d_f$

The variation of nominal lengths in the polishing dominant regime is studied by drilling at a depth of cut smaller than the depth of cut (d_f) at the onset of fracturing dominant regime.

5.3.1 Wear response

Figure 5.7 shows the wear response of the TT56-size bit drilling in Calca Red granite at 0.03 mm/rev depth of cut. It can be seen that both the scaled weight and the scaled torque increase linearly with cutting distance as a result of the development of wear flat lengths, but the scaled torque increases sharply and reaches the sensor's limit forcing the test to stop.

After removing the bit from the borehole, a stuck core was observed which caused a sharp increase in torque, and one of the segments on the bit was broken

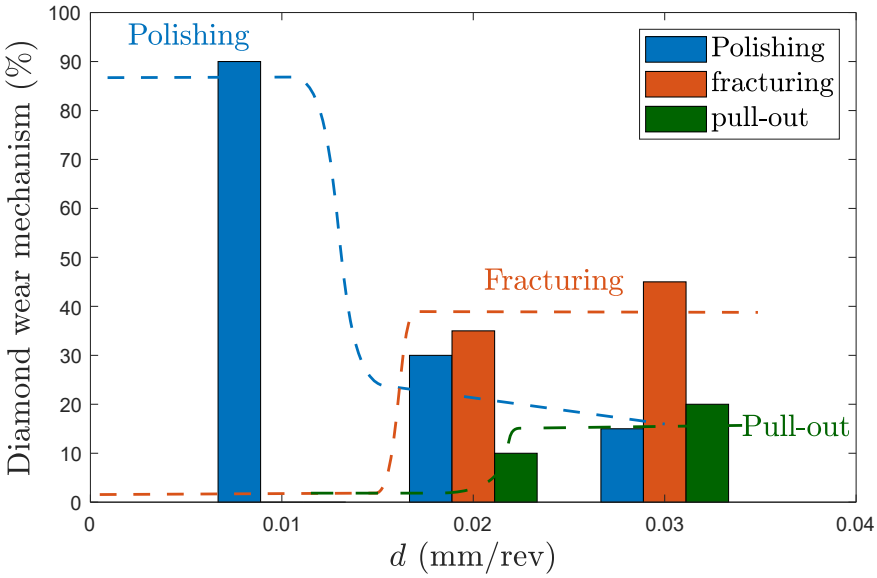

(a) ID segment

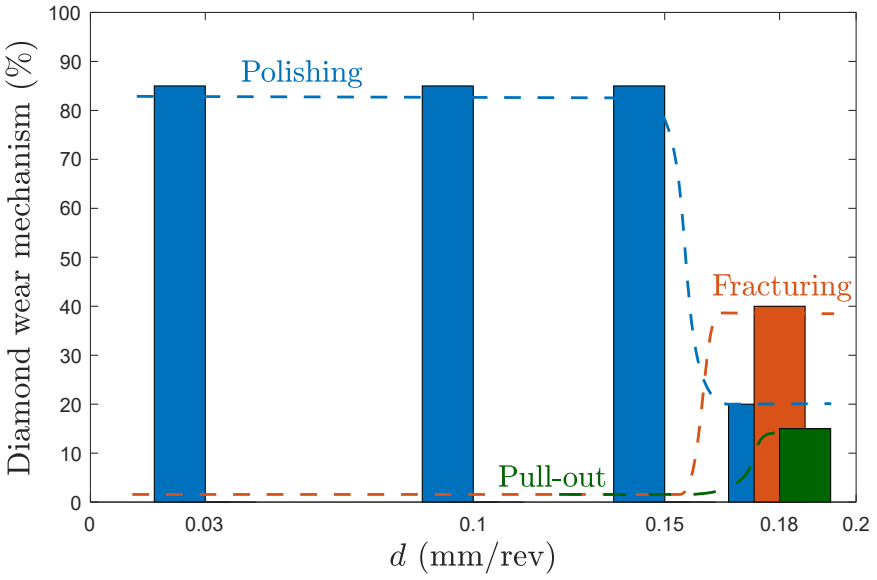

(b) NQ-size bit

Figure 5.6: The effect of bit size on the depth of cut at the onset of the fracturing regime (d_f).

due to this high force, see Figure 5.8. Thus, significant diamond polishing reduces drilling efficiency and can lead to serious consequences that require replacement of the bit.

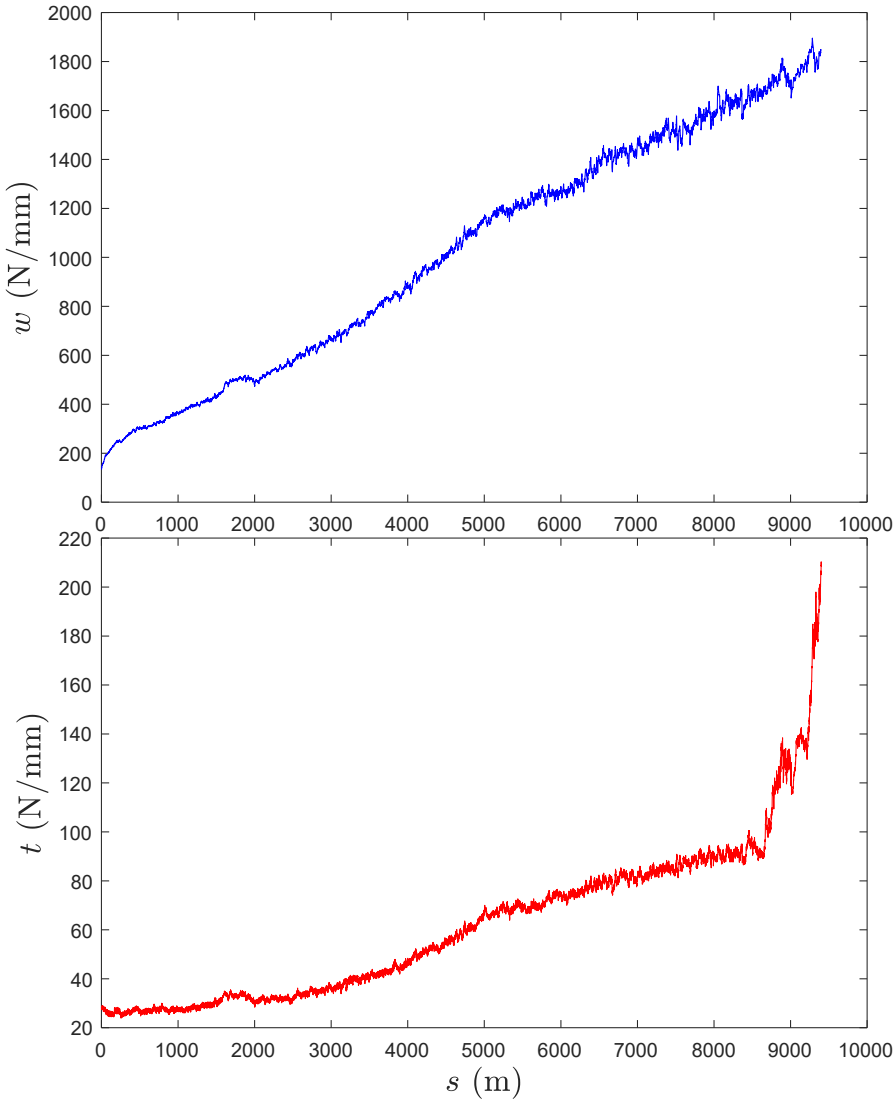

Figure 5.7: Wear response of a TT56-size bit in drilling Calca Red granite at 0.03 mm/rev depth of cut.

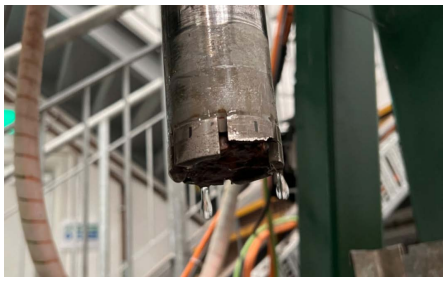

Figure 5.8: Broken bit and a stuck core at the end of a polishing test with TT56 ID bit.

5.3.2 Analysis of a single diamond geometry and bit topology

The bit cutting face was scanned using the Alicona microscope at intervals of 3 km linear cutting distance experienced by the bit.The diamond wear flat length (L_d) and diamond protrusion ($\bar{p}$) are calculated from the diamond wear flat area and diamond protrusion of all the diamonds on the bit face.

Figure 5.9 illustrates the changes in the diamond wear flat area (A_d) and the matrix wear flat area ($A_{\bar{m}}$) at the tail of a single diamond with cutting distance. It can be seen that the diamond wear flat area (A_d) increases from 0.029 mm^2

(a) $s = 0$ m (b) $s = 5$ km (c) $s = 9$ km

Figure 5.9: Evolution of diamond wear flat area (A_d) and matrix wear flat area ($A_{\bar{m}}$) at the tail of a single diamond in cutting Calca Red granite in the polishing dominant regime.

to 0.15 mm^2 and the matrix wear flat area at the tail ($A_{\bar{m}}$) increases from 0.006 mm^2 to 0.036 mm^2. The variation of diamond protrusion (p) is obtained from the cross-sectional image, see Figure 5.10. The matrix wear flat area at the crater ($A_{\hat{m}}$) remains unchanged, indicating that the three-body contact is not activated. The diamond height loss due to wear results in a decrease in diamond protrusion from 0.1 mm to 0.06 mm.

Repeating the same measurement for all diamonds on the bit, the variation of nominal lengths is illustrated in Figure 5.11. The diamond wear flat length (L_d) increases linearly with the cutting distance (S) from 0.3 to 3.5 mm, and the diamond protrusion ($\bar{p}$) decreases from 0.142 to 0.13 mm. The amount of decreases in the diamond protrusion was found to be of the same order of magnitude as the height loss (δH).

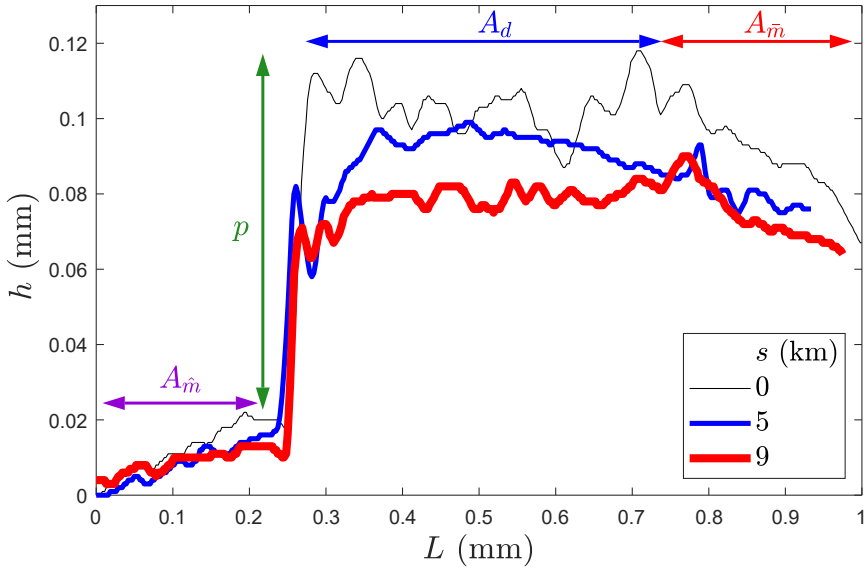

Figure 5.10: Evolution of protrusion (p) of a single diamond with cutting distance.

Therefore, we can conclude that, although the wear rate of the bit is insignificant due to no diamond fracturing or pull-out and minimal matrix wear, significant diamond polishing leads to an increase in both diamond wear flat and matrix wear flat, which in turn, results in higher forces. Excessive polishing also reduces the diamond protrusion. Based on the relationships between bit wear state and drilling responses developed in Chapter 4, the depth of cut (d_*) at the onset of regime I increases with the diamond wear flat length (L_d), and the depth of cut (d_{**}) at the onset of regime III decreases with the diamond protrusion. Consequently, the optimum drilling regime (regime II) is shortened, leading to a noticeable decrease in drilling performance.

5.3.3 Effect of rock properties on polishing rate ($\dot{L}_d$)

The tests was repeated on the other two types of granite (Austral Black and Bluestone) to investigate the effect of the Mohs hardness of the rock on the variation of diamond wear flat length ($\dot{L}_d$). Figure 5.12 shows the scaled weight and diamond wear flat length (L_d) increase linearly with the cutting distance,

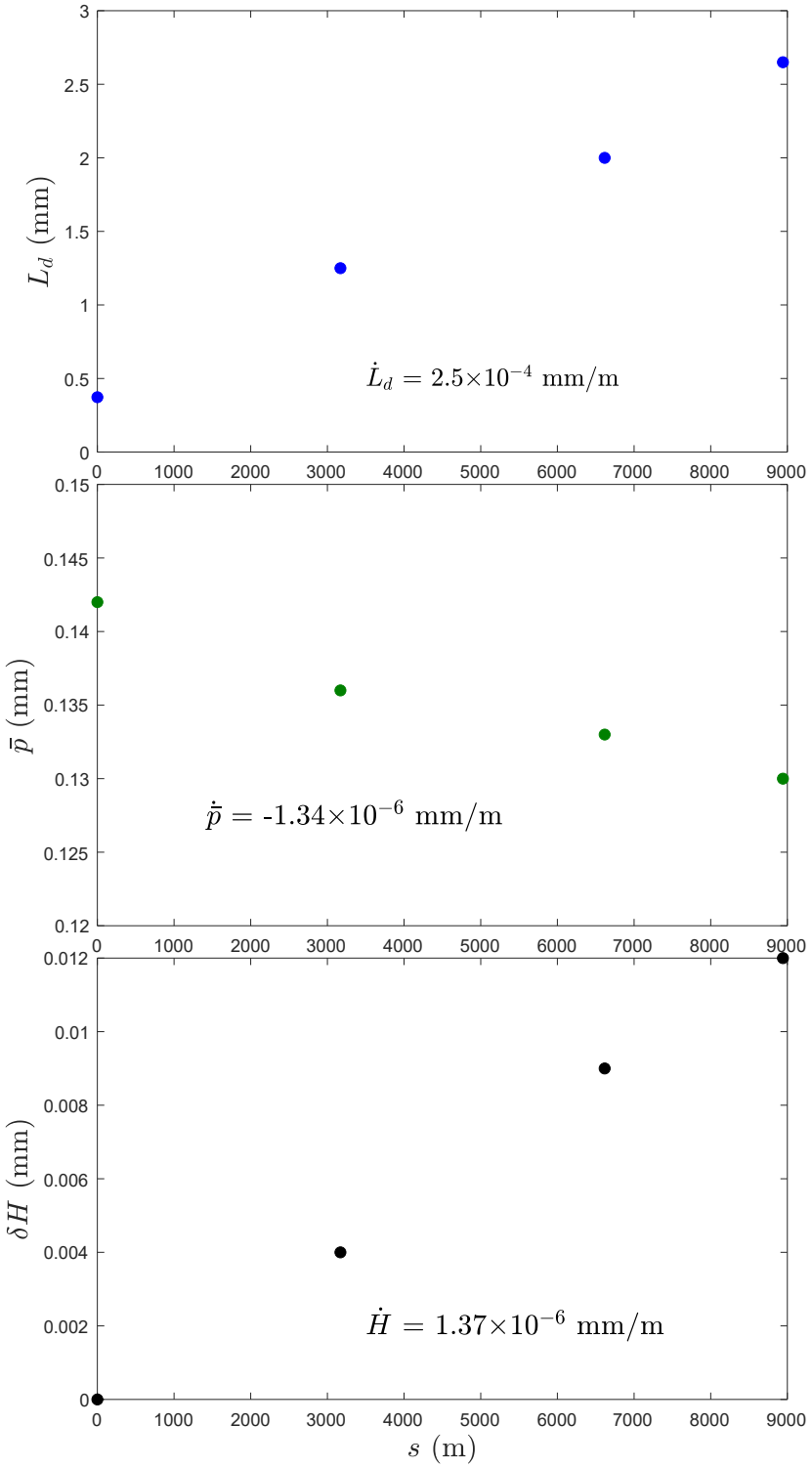

Figure 5.11: Variation of nominal lengths in drilling Calca Red granite at 0.03 mm/rev depth of cut.

but the rate of increase is controlled by the Mohs hardness. Using a linear fit on the variation in diamond wear flat length, we determine the polishing rate ($\dot{L}_d$) and plot it against the rock Mohs hardness on a semi-logarithmic scale. Figure 5.13 illustrates a linear relationship between these two variables.

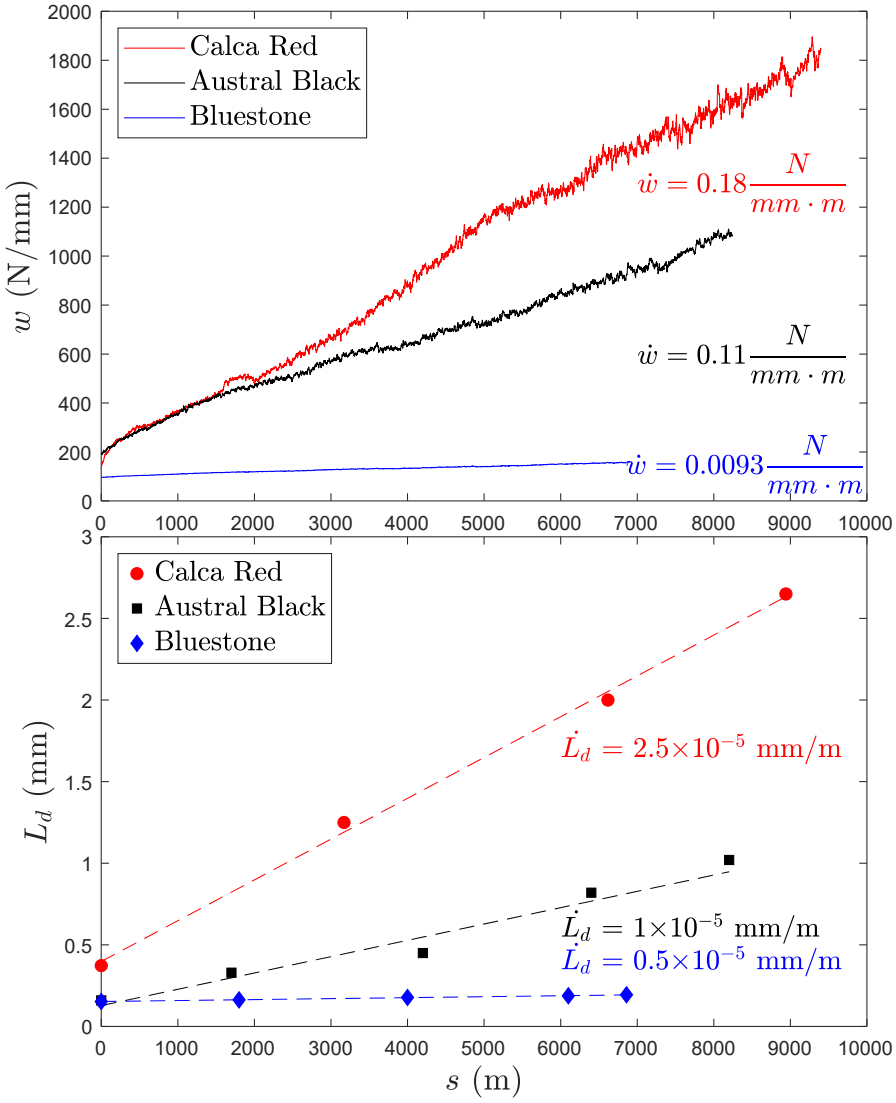

Figure 5.12: The effect of rock on the wear response and the variation of diamond wear flat length ($\dot{L}_d$). Tests were conducted using an TT56-size bit at 0.03 mm/rev depth of cut.

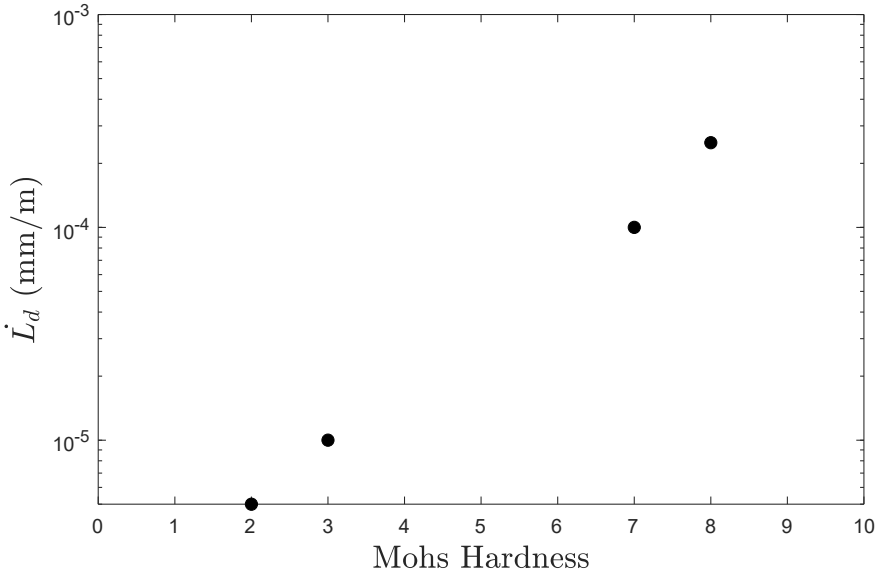

Figure 5.13: The relationship between the variation of diamond wear flat length ($\dot{L}_d$) and rock Mohs hardness.

5.4 Diamond fracturing dominant regime and pull-out dominant regime, $d_f \leq d$

The change in bit wear state (nominal lengths) and wear rate in both the diamond fracturing dominant regime and pull-out dominant regime are studied by conducting drilling tests at depths of cut equal to or higher than d_f and at depths of cut higher than d_{**}. Calca Red granite was drilled using a TT56-size bit at three different depths of cut: 0.15 mm/rev (d_f), 0.21 mm/rev (d_{**}), and 0.23 mm/rev (regime III).

5.4.1 Wear response

Figure 5.14 shows the wear responses at three depths of cut. It can be seen that the scaled forces remain relatively constant when drilling at d_f and d_{**}. Given that half of the diamonds undergo fracturing wear, it is likely that the wear flats are balanced in the diamond fracturing dominant regime. Scaled forces initially remain stable when drilling at 0.23 mm/rev but suddenly increase sharply, even-

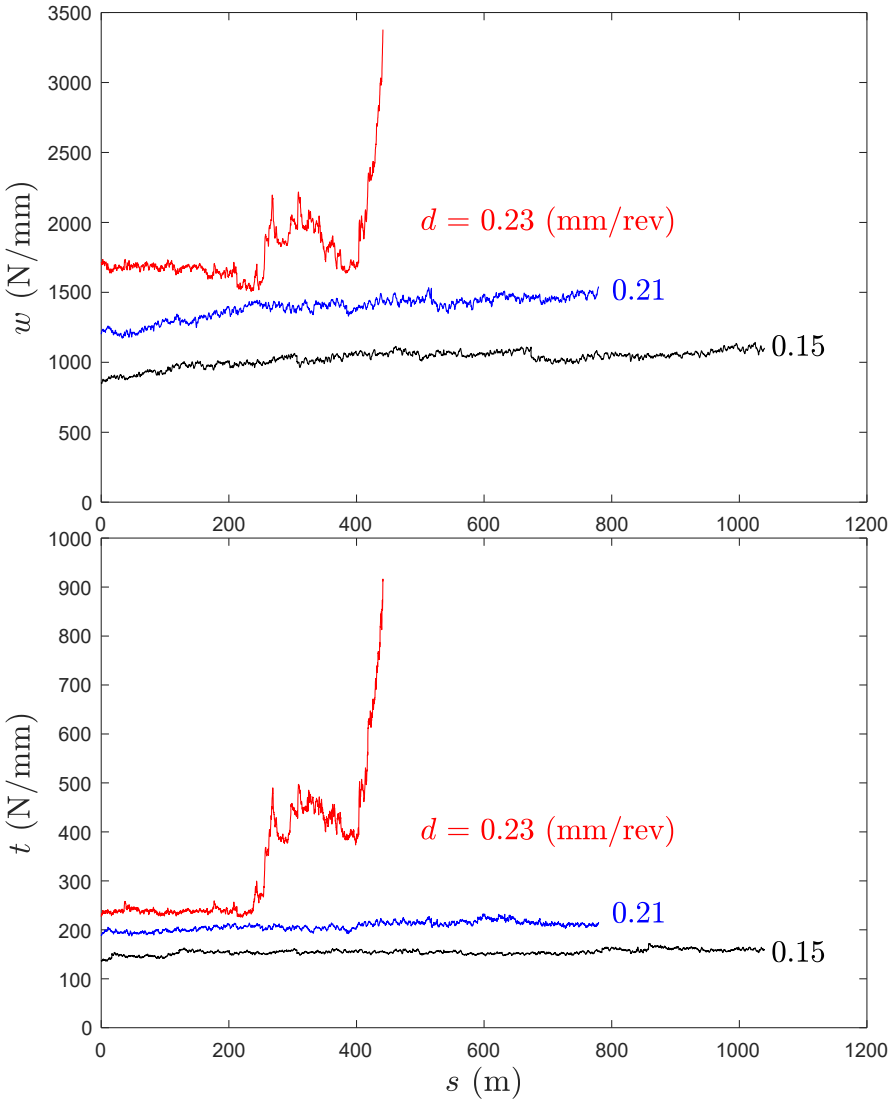

Figure 5.14: Wear responses of a TT56-size ID bit in drilling Calca Red granite at three different depths of cut: 0.15, 0.21 and 0.23 mm/rev

tually exceeding the sensor's limit forcing the test to stop. Unlike the gradual increase in force associated with diamond polishing, this abrupt increase may be due to an increase in matrix frictional contact at the crater.

5.4.2 Variation of nominal lengths and wear rate

Figure 5.15 illustrates how nominal lengths vary with cutting distance at different depths of cut. It can be observed that the diamond wear flat length (L_d) fluctuates

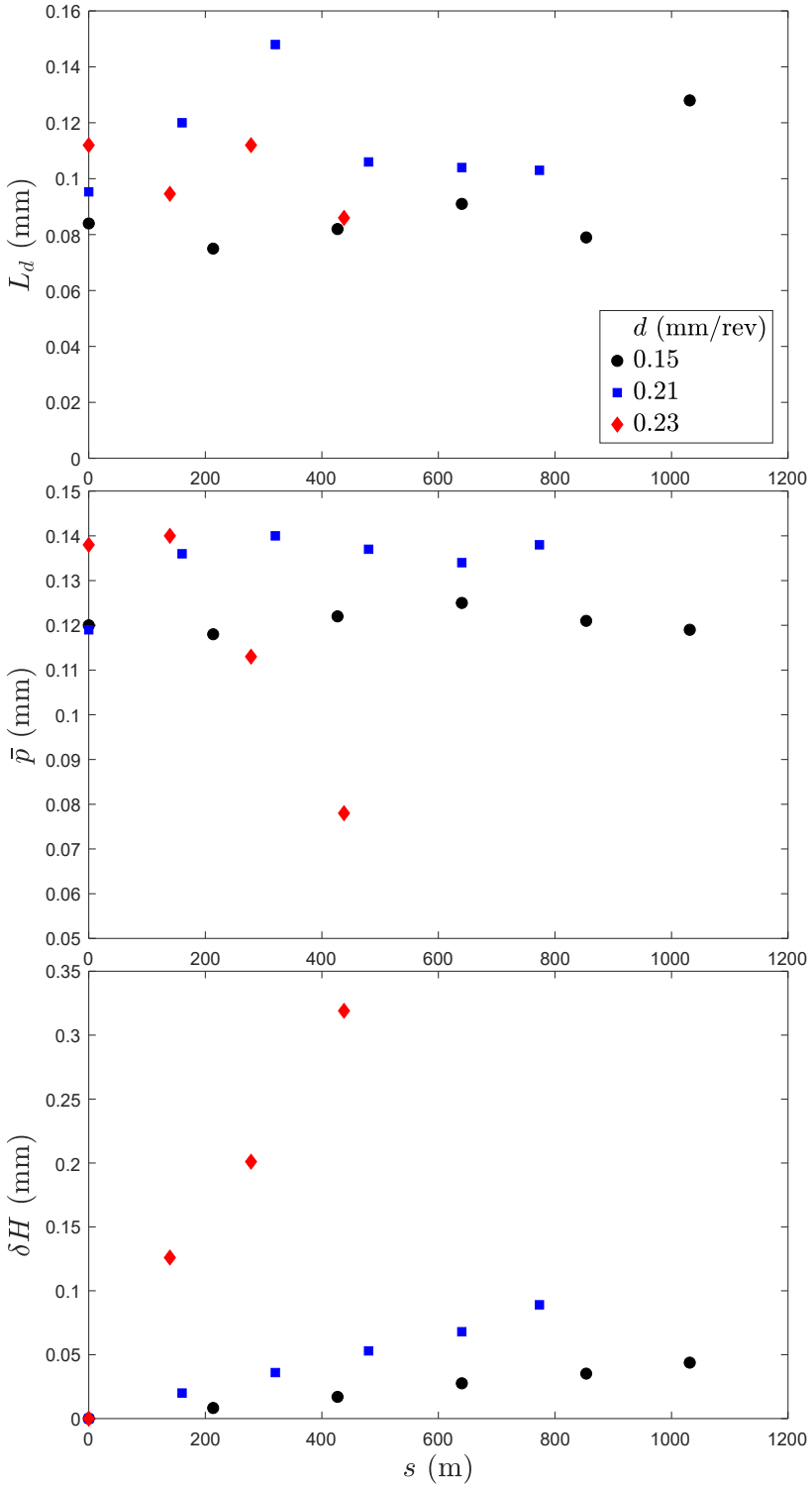

Figure 5.15: Variation of nominal lengths in drilling Calca Red granite with a TT56-size bit at three depths of cut: 0.15, 0.21, and 0.23 mm/rev.

around a mean value of 0.1 mm across all three depths of cut. This means that the wear flat areas are balanced by either fracturing or pull-out when $d_f \leq d$. Consequently, the forces remain relatively constant.

The diamond protrusion ($\bar{p}$) shows a same trend, remaining relatively stable at depths of cut of 0.15 mm/rev and 0.21 mm/rev depth of cut. This stability suggests that temporary three-body erosion compensates for the decrease in diamond height caused by fracturing. However, at a depth of cut of 0.23 mm/rev, the diamond protrusion decreases sharply after cutting for 200 metres. The decline in diamond exposure is due to the significant diamond pull-out resulting from the continuous three-body erosion that occurs at the crater and the poor distribution of the next layer of diamonds. As a result, the diamond protrusion cannot be maintained, leading to high forces towards the end of the test. The wear rate (height loss) of the bit increases with the depth of cut, particularly when d exceeds d_{**}. An increment of 0.02 mm/rev in the depth of cut results in a sevenfold increase in wear rate.

5.5 Bit life or wear rate

Based on the height loss measurement, it was found that the wear rate of the bit increases with the depth of cut for Calca Red granite, see Figure 5.16. The tests were repeated on Austral Black granite, Bluestone granite, and Donnybrook sandstone. The wear rate of the bit while drilling Austral Black granite follows the same exponential trend, but with a slightly lower wear rate. This reduction is attributed to a lower percentage of diamonds that experience fracturing and pull out at the same depth of cut. Compared to these two rocks, the bit wear rate while drilling Bluestone granite is minimal, primarily because there is no diamond fracturing or pull-out. This indicates that drilling beyond the depth of cut (d_{**}) at the onset of regime III in Bluestone will not significant impact the bit life. For Donnybrook sandstone, the bit wear rate at depths of cut below d_{**} is insignificant, but it increases dramatically when exceeding d_{**} due to three-body

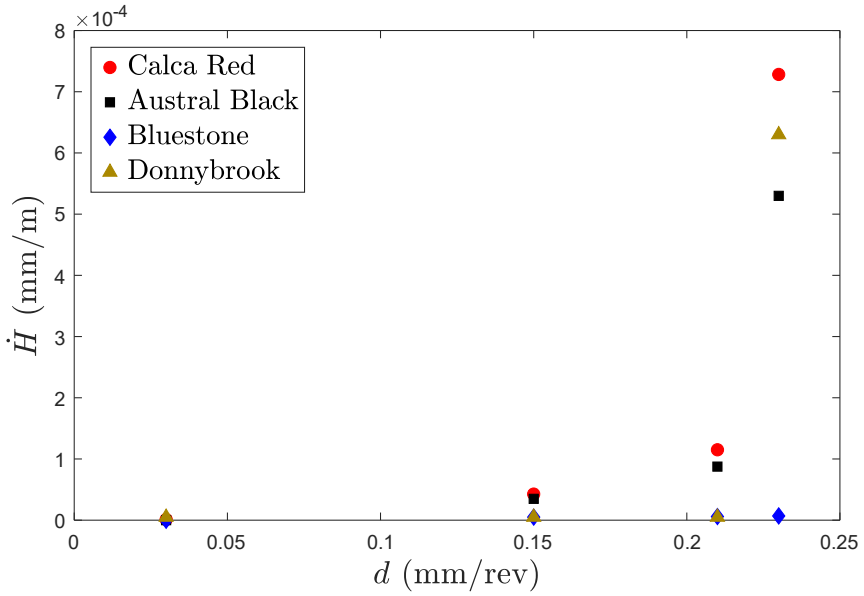

Figure 5.16: Effect of rock on the relationship between bit wear rate and depth of cut. Tests were carried out using a TT56-size bit.

contact and a substantial amount of diamond pull-out.

5.6 Effect of fluid viscosity

In Chapter 4, it has been found that, for a given bit wear state, the depth of cut (d_{**}) at the onset of regime III decreases with increasing fluid viscosity. For example, Figure 5.17 illustrates that the depth of cut (d_{**}) at the onset of regime III decreases from 0.21 mm/rev to 0.09 mm/rev when the marsh funnel viscosity of the fluid increases from 26 s to 45 s. With $d_f = 0.15$ mm/rev for Austral Black granite, this indicates that $d_{**} < d_f$ when $\eta = 45$ s. Consequently, as the depth of cut increases, the response transitions from polishing dominant regime directly to the pull-out dominant regime, potentially leading to a higher wear rate. To further investigate the effect of fluid viscosity on bit wear, drilling (wear) experiments were conducted at depth of cut of 0.15 mm/rev (d_f) across these three fluid viscosity, examining variations in wear mechanisms and wear rates.

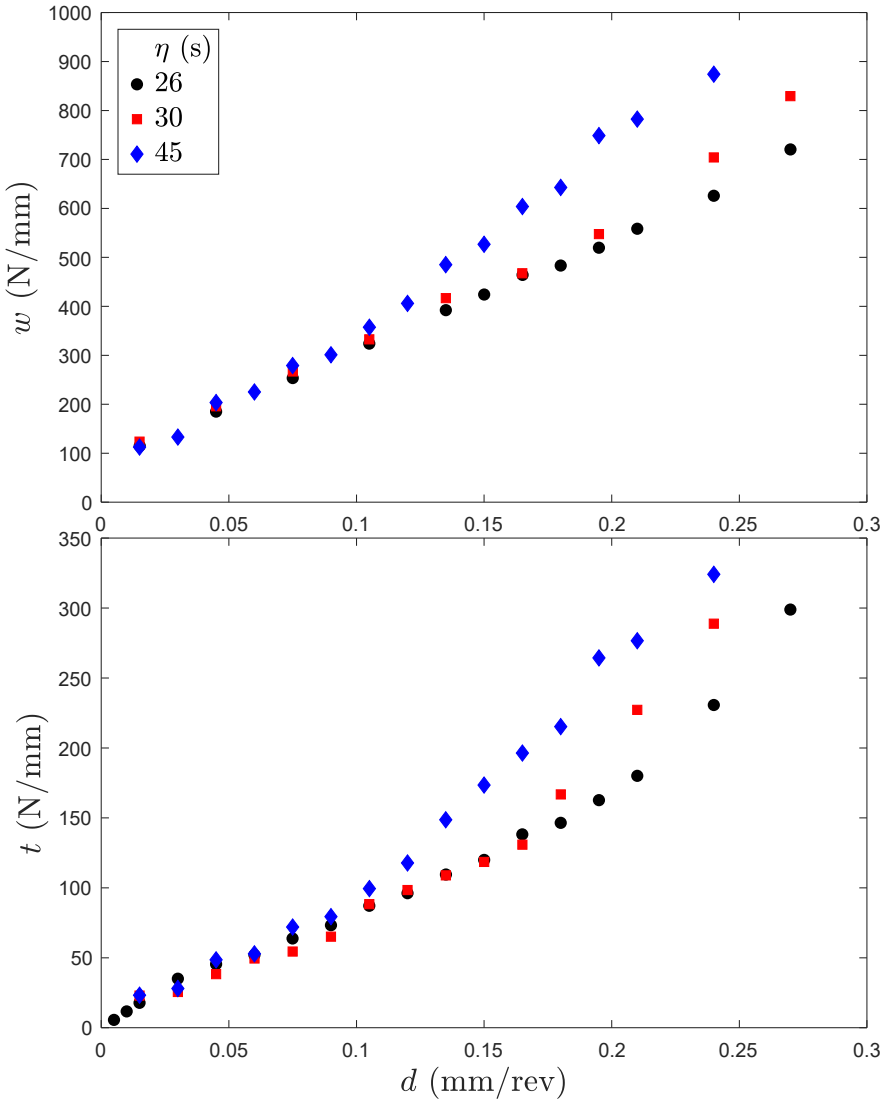

Figure 5.17: The effect of fluid viscosity on the stationary drilling responses. Drilling tests were conducted using a TT56-size bit in Austral Black granite.

Figure 5.18 shows that both the scaled weight and torque stabilise around 420 N/mm and 130 N/mm, respectively, when drilling with water ($\eta = 26$ s) and low viscosity drilling fluid ($\eta = 30$ s). When the fluid viscosity increases to 45 s, the forces remain relatively constant, but the scaled weight increases to 650 N/mm and the scaled torque increases to 160 N/mm. This increase in scaled forces is attributed to three-body contact caused by the higher viscosity, which forces the drilling response to transition into regime III.

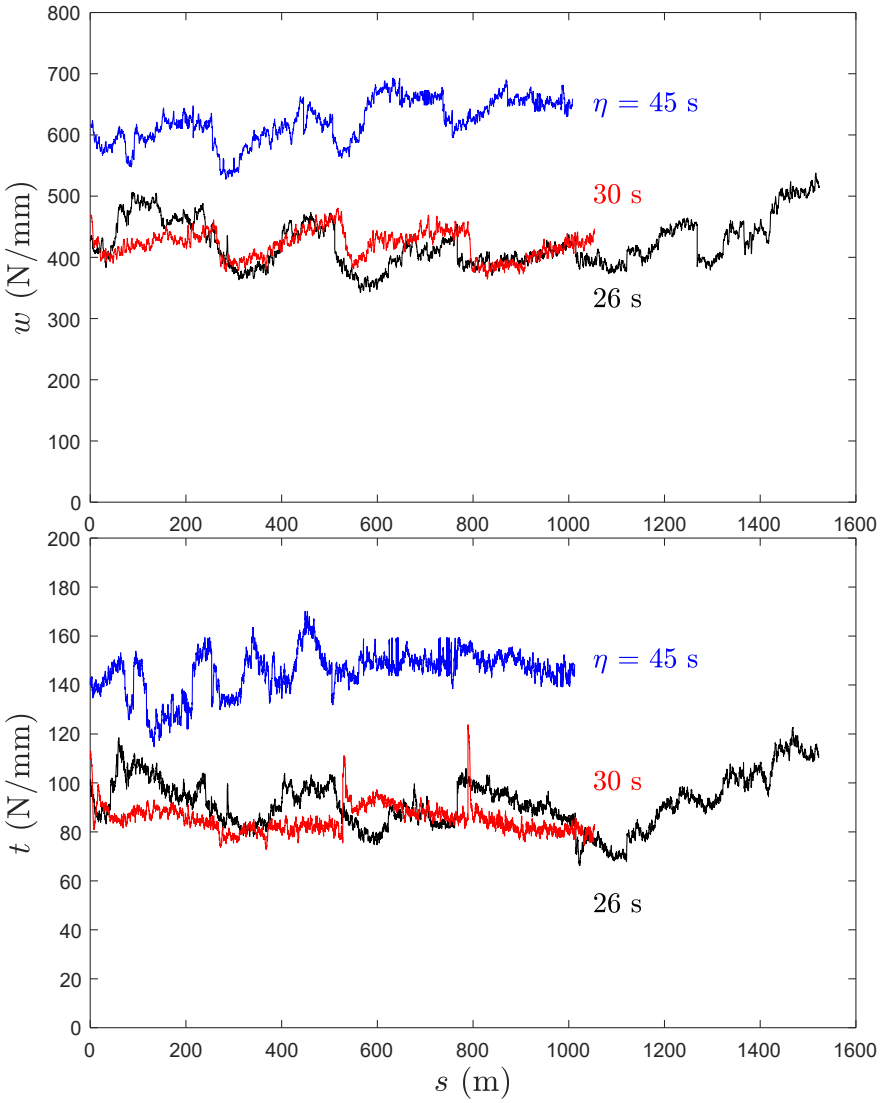

Figure 5.18: Effect of fluid viscosity on the wear responses. Drilling tests were conducted on Austral Black granite at 0.15 mm/rev depth of cut.

The bit topology was inspected during the tests to investigate potential change in wear mechanisms. Figure 5.19 shows that the percentage of diamonds experiencing fracturing wear remains unchanged when the fluid viscosity increases from 26 s to 30 s, which means that the depth of cut (d_f) at the onset of the fracturing dominant regime is not affected by the fluid viscosity. However, as the viscosity increases to 45 s, there is a noticeable increase in the percentage of diamonds experiencing pull-out wear, accompanied by a decrease in fracturing wear. This

shift indicates a transition from fracturing dominant to pull-out dominant. In

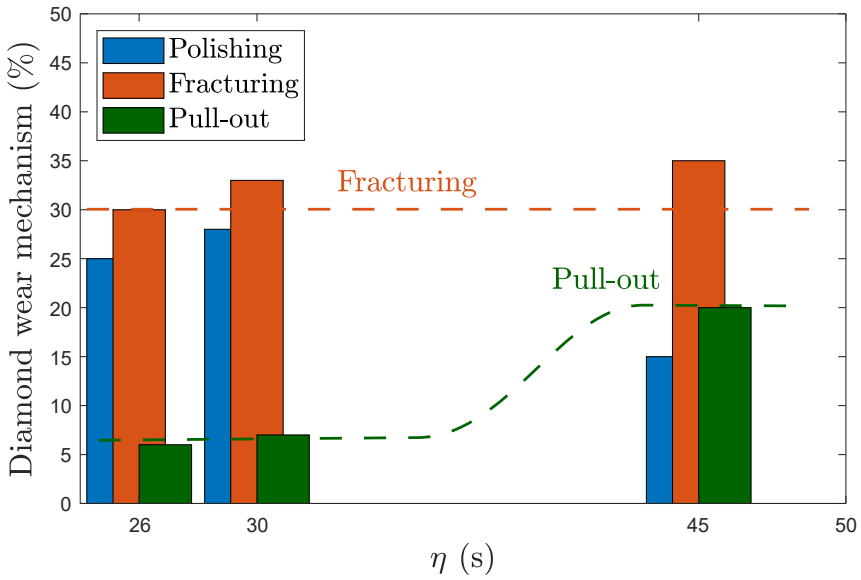

Figure 5.19: Effect of fluid viscosity on the percentage of different wear mechanisms.

terms of wear rate, the height loss remains consistent for fluid viscosity of 26 s and 30 s. However, height loss increases threefold when viscosity reaches 45 s, as illustrated in Figure 5.20. Therefore, the fluid viscosity needs to be carefully monitored during drilling and taken into account when selecting operating parameters.

5.7 Summary

In this chapter, the conceptual model of wear is captured through drilling and scanning experiments. The model identifies three dominant regimes: polishing, fracturing, and pull-out. Four different types of rock were tested at five different depths of cut covering a wide range of rock properties across all three regimes.

In the polishing dominant regime, more than 90 % of active diamonds undergo polishing wear, leading to an increase in both diamond wear flat length (L_d) and matrix wear flat length (L_m). The diamond protrusion decreases due to loss of

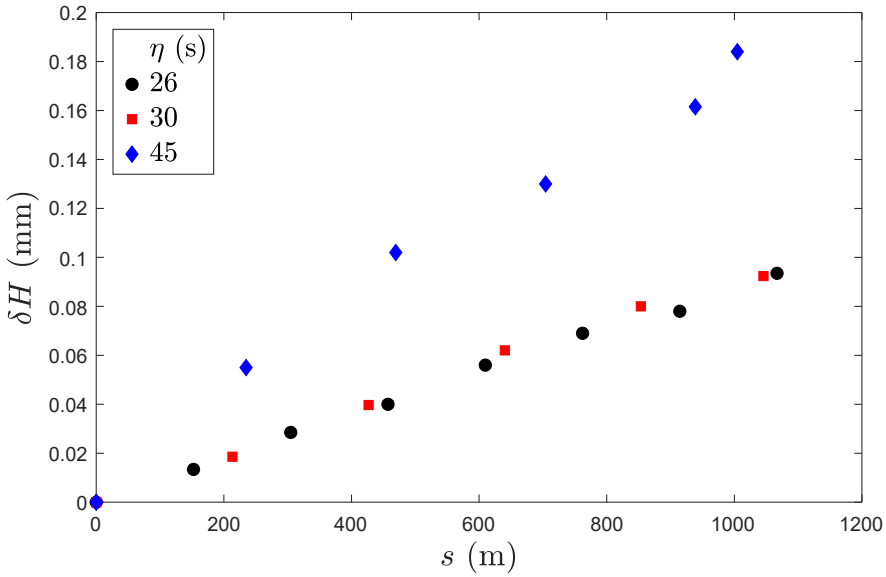

Figure 5.20: Effect of fluid viscosity on the bit wear rate.

material, with the reduction close to the height loss of the bit. In terms of drilling response, the depth of cut (d_*) at the onset of regime I increases, while the depth of cut (d_{**}) at the onset of regime III decreases with the extent of polishing. This results in a noticeable decline in drilling performance.

When the depth of cut equals to or exceeds the depth of cut (d_f) at the onset of fracturing dominant regime, more than 40% of diamonds experience fracturing wear. This results in balanced wear flat lengths (L_d and L_m). Diamond breakage leads to sudden decreases in diamond height, consequently reducing the diamond protrusion ($\bar{p}$). However, this reduction triggers a temporary three-body contact at the crater, eroding the matrix. Overall, the diamond protrusion remains relatively constant. This temporary three-body erosion weakens the diamond retention ability, eventually causing diamond loss. Hence, the wear rate ($\dot{H}$) is higher than during drilling in the polishing dominant regime.

When the depth of cut exceeds the depth of cut (d_{**}) at the onset of regime III, the temporary three-body contact observed in the fracturing dominant regime becomes permanent and continuously erodes the matrix. This results in more than 30% diamond loss and a significantly higher wear rate. For example, in

drilling Calca Red granite, a 10% increase in the depth of cut leads to a sixfold increase in height loss.

The Mohs hardness of the rock plays an important role in diamond wear mechanisms. The polishing rate ($\dot{L}_d$) in the polishing dominant regime increases with Mohs hardness, and the rock needs to have sufficient Mohs hardness to induce diamond fracturing in the fracture dominant regime. It was found that, when drilling Bluestone (Mohs hardness = 3), diamonds do not fracture regardless of depth of cut.

The fluid properties does not affect the diamond wear mechanism and specifically do not change d_f. However, an increase in fluid viscosity causes the depth of cut (d_{**}) at the onset of regime III to decrease, leading to diamond pull-out at a shallower depth of cut. When the viscosity is high enough such that $d_{**} < d_f$, an increase in depth of cut immediately transitions the response from the polishing dominant regime into the pull-out dominant regime, resulting in excessive bit wear.

The wear model can serve as a valuable tool to identify the optimum depth of cut based on rock properties. For rock with Mohs hardness greater than 6, it is recommended to drill at a depth of cut in between d_f and d_{**} to avoid excessive polishing or wear. For rock with low Mohs hardness but high quartz content, drill at d_{**} is advised to avoid excessive matrix erosion and diamond pull-out. However, if the quartz content is at the minimum, drilling at the highest possible speed is beneficial, as diamond does not fracture and matrix wear remains minimal.

Chapter 6

Conclusion

6.1 Contributions to experimental workflow

- **A novel method to quantify wear state of ID bits**

  The optical microscope, Alicona, provides 3D images of bit face with resolution up to 2 micrometer. I systematically measure the diamond protrusion (p) and the diamond wear flat area (A_d) of all diamonds on the bit face to compute the diamond protrusion ($\bar{p}$) and the accumulative diamond wear flat area ($\bar{A}_d$) that is later scaled by the width of the segment to arrive the diamond wear flat length (L_d) of the equivalent blade. Quantifying the bit wear state has always been challenging due to the number of diamonds (often more than 1000) and their complex geometry. We reduce this complexity to two measurable quantities.

- **Experimental protocol and procedures**

  I developed an experimental workflow that enables me to track the evolution of both bit wear state and drilling response (a relationship between forces and depth of cut at a given wear state) and to measure the wear rate.

  An ID bit with a given wear state is scanned followed by a drilling (step) test to capture the response at this wear state. The bit is then put back

for scan to confirm the bit wear is minimized during the test. As a result, I obtained a drilling response with a known bit wear state. Then, I use the bit to drill a rock at a given depth of cut for a period of time to wear the bit - the wear state changes. After the test, the cycle repeats to capture the new drilling response at the new wear state and measure the wear rate.

All drilling experiments are performed using state-of-the-art cutting and drilling rigs under kinematic control. This setup enables precise control over the linear and rotary movements of the bit, allowing to explore the range of very shallow depth of cut (less than 5 microns per revolution) with high accuracy. The weight on bit and torque on bit are recorded with a precision of about 0.1% across the entire range.

- **Transient regime and a minimisation function to derive model parameters**

  The drilling response model is characterized by three linear regimes. However, results show a transient regime between regime I and II, this non-linearity is caused by the geometry of the diamond wear flat. To fully understand and model this transient regime requires precise measurement of the diamond wear flat, which is beyond the scope of this research.

  To minimize the effect of the transient regime on the results and to provide a systematic method for deriving model parameters, we introduce a linear transient regime between regime I and II with a slope of α_t and two critical depths of cut: one at the onset of the transient regime (d_{*-}) and one at the end (d_{*+}). Using the minimization function 'fmincon', I fit the data with the new model and define the intersection of the extended regime I and II as the depth of cut (d_*) at the onset of regime II.

6.2 Contributions to drilling response model

- **Extensive and comprehensive experimental results**

An extensive and comprehensive set of cutting, drilling and scanning experiments have been carried out on three different types of granite and one type of sandstone using ID tools with three different sizes at various wear states. To the best of our knowledge, the scope of the experimental program is quite unique due to (i) the extensive volume of experimental results, including over cumulatively 100 meters depth drilled and more than 300 scanning tests performed. (ii) An in-depth parametric analysis and tailor-designed experimental protocol to isolate the effect of bit wear state, rock properties, and drilling fluid properties on the both drilling and wear responses. (iii) A novel method for quantifying the wear state and the wear rate of the bits.

- **Quantitative relationship between bit wear state and drilling response**

  An extensive set of experiments was conducted to identify how the bit wear state, rock properties and drilling fluid properties affect the model parameters associated with frictional contacts.

  - The depth of cut (d_*) at the onset of regime I, the coefficient (κ_d) representing the variation of the diamond frictional contact length, and the conformal diamond frictional contact length ($\hat{\ell}_d$) increases linearly with the diamond frictional contact length (L_d). The coefficient ($\kappa_{\bar{m}}$) representing the variation of matrix frictional contact length at the tail increases linearly with matrix wear flat length ($L_{\bar{m}}$) at the tail. All relationships are not functions of bit size, which validates the scale length of the equivalent blade. In addition, it was found that the matrix wear flat ($L_{\bar{m}}$) at the tail is proportional to the diamond wear flat length (L_d) due to the protection offered by the diamond. Thus, when the bit is sharp, both wear flat lengths are at the minimum and the slope of regime II in the $w - d$ space and the $t - d$ space are close

to $\zeta\varepsilon$ and ε, respectively.

- I identified that three-body contact takes place at the crater (in front of diamond) and yields to higher slope in regime III which is often referred to as cleaning issue. The experimental results show that the depth of cut (d_{**}) at the onset of regime III is proportional to the average diamond protrusion ($\bar{p}$) of the bit.
- The rock properties do not affect the model parameters associated with frictional contact but change the contact stress between the diamond and the rock (σ_d) and the matrix and rock (σ_m). Furthermore, it was found that the diamond/rock contact stress correlates well with rock strength by a factor of 7.
- The third body in the three-body contact at the crater is a mixture of cuttings and fluid. Increasing fluid viscosity causes the accumulation of cuttings building up at the crater as a result the average diamond protrusion ($\bar{p}$) decreases and therefore the depth of cut (d_{**}) at the onset of regime III decreases.

This model successfully differentiates parameters controlled by rock and bit wear state, which are often mixed up in the literature. For researchers using specific energy, an increase in specific energy only indicates that more energy is required to remove rock, without revealing whether the increase is due to variations in rock properties or bit wear. However, our model provides clarity: if the depths of cut (d_*) at the onset of regime II increases, it definitively indicates diamond polishing and an increase in the diamond wear flat length (L_d). Conversely, if the depth of cut (d_{**}) at the onset of regime III decreases, it signifies a reduction in diamond protrusion. Additionally, our model allows us to estimate the extent of the increase in the diamond wear flat length or the decrease in diamond protrusion.

6.3 Contribution to bit wear

- **Model of bit wear**

  I established a conceptual model of wear consisting of three dominant wear regimes: polishing, fracturing and pull out. Each regime is characterised by different wear mechanisms and wear rates governed by the depth of cut.

  - In the polishing dominant regime ($d < d_f$), all diamonds experience polishing wear. This results in a continuous increase in both the diamond wear flat length (L_d) and the matrix wear flat length ($L_{\bar{m}}$) at the tail, along with a decrease in the average diamond protrusion. The wear rate of the bit is at the minimum.
  - In the fracturing dominant regime ($d_f \leq d \leq d_{**}$), the percentage of diamonds experiencing fracturing wear increases sharply at the expenses of diamond polishing. The diamond wear flat length and the average diamond protrusion remain relatively constant, but the wear rate increases by three to four times.
  - In the pull-out dominant regime ($d_{**} < d$), more than 30% diamonds are removed, causing excessive wear.

  In the industry, there is confusion between the rock being abrasive and erosive. Our research shows that two distinct wear mechanisms occur in different locations on the bit: two-body abrasion (diamond wear flat and comet tail) and three-body erosion (crater, in front of diamonds). For example, a rock like sandstone, with a high quartz content but relatively low hardness, can be erosive to the matrix, but not necessarily abrasive to the bit. When the depth of cut is below d_{**}, there is no three-body contact, allowing the bit to last significantly longer without wear. However, if three-body contact occurs ($d > d_{**}$), the cuttings produced from larger quartz particles in the rock mixed with drilling fluid erode the matrix, causing a substantial increase in the wear rate (more than tenfold).

To avoid confusion between rocks that are abrasive and erosive, our model quantitatively relates operating conditions (depth of cut), wear mechanisms (polishing, fracturing, three-body erosion), and rock properties (Mohs hardness and quartz content). This approach allows for a clear distinction between the effects of rock hardness and mineral composition on bit wear, providing a more accurate understanding of how different rocks impact drilling performance.

6.4 Practical implications

- The quantitative relationships between bit wear state and drilling response can be leveraged to infer bit wear state from forces in the field. When the rock properties are unknown, the following steps should be taken:
  - Sharpen the bit to minimise the wear flat areas of the bit.
  - Quickly ramp the depth of cut to obtain a drilling response across all three regimes to determine the model parameters (three slopes, two critical depths of cut, and an intercept). An intercept of regime II (w_o or t_o) to 0, means that the diamond wear flat length (L_d) is minimal. Our observation suggests that the matrix wear flat length at the tail $L_{\bar{m}}$ is proportional to L_d and approaches 0 when L_d is minimal. Therefore, we can assume $L_{\bar{m}} = 0$. With this assumption, $\mu_m \sigma_{\bar{m}} \kappa_{\bar{m}} = 0$ and the slope of regime II - $\beta_{\mathbf{II}} = \varepsilon$.
  - Using the relationship between intrinsic specific energy (ε) and rock strength established by Chan (2022), we can estimate rock strength.
  - With known rock strength, estimate the diamond/rock contact stress (σ_d) using the established relationship between rock strength and diamond/rock contact stress. This estimation is essential to accurately determine the parameters related to the diamond frictional contact, including κ_d and $\hat{\ell}_d$.

  - We can then track the bit wear state by constructing the drilling response to derive d_*, d_{**},κ_d, and $\hat{\ell}_d$. Using the relationships between bit wear state and drilling response, we can infer the diamond wear flat length (L_d) and the average diamond protrusion ($\bar{p}$).

  One limitation of this approach is ensuring that the bit is sharpened to its optimal state. In addition, the rock properties can vary by every metre, requiring a repeat of the entire process if significant changes in the rock type occur. Moreover, in the field, the compliance of the drill string affects the transmission of force and the depth of cut. This method relies on precise measurements of the forces and depth of cut at the bit, which can be challenging.

- The wear model can be used to identify the optimum depth of cut. For rock with a Mohs hardness greater than 6, it is recommended to drill in the fracturing dominant regime (between d_f and d_{**}) to avoid excessive polishing or bit wear. When drilling a rock with a Mohs hardness below 4, the optimum depth of cut depends on the quartz content. If the quartz content is at the minimum, use the highest depth of cut otherwise drill at d_{**} to maximise the bit life, and d_{**} can be estimated from the drilling response.

6.5 Limitations and future works

- We were unable to accurately measure the matrix wear flat area ($\bar{A}_m$) and therefore to calculate the matrix wear flat length (L_m) and derive the matrix/rock frictional contact length (σ_m). As a result, the magnitude of model parameters associated with the matrix/rock frictional contact ($\kappa_{\bar{m}}$ and $\kappa_{\hat{m}}$) are not obtained. In addition, the relationship between $\kappa_{\hat{m}}$ and L_m is not clear due to the limited data in regime III. This study of drilling response and bit wear state was conducted using a single type of rock. Repeating

the tests on different rock types would provide a broader understanding of the relationship between drilling performance and bit wear under varying rock properties.

- Although we have studied three types of granite and one type of sandstone, more tests are needed on more rock. Diamonds were found to not fracture in drilling rock at d_f with Mohs hardness below 4 but do fracture when the Mohs hardness exceeds 7. There is no result for rocks with a Mohs hardness between 4 and 7. Therefore, it is not clear what the minimum Mohs hardness is leading to fracture diamonds. On top of it, the grain sizes of two rocks with high Mohs hardness are six times larger than the depth of cut, so we suspect diamond fracturing is induced by diamond cutting through a large grain. It is of interest to investigate whether diamonds will fracture at d_f when drilling a rock with a high Mohs hardness but a small grain size.

- In terms of operating parameters, we have only looked at how the depth of cut governs the wear mechanism and the wear rate of ID bits. However, Michaels (2021) found that both the depth of cut and the rotation speed govern the wear mechanism and the wear rate of PDC bits, and Mostofi (2014) showed that the flow rate controls the three-body contact between bit, matrix and cuttings and possibly affects the wear rate in the pull out dominant regime. It would be of interest to investigate the effect of rotation speed and flow rate on drilling and wear responses.

  Bit properties, particularly matrix hardness, also play a crucial role in controlling bit wear and have not been thoroughly studied yet.

Appendices

Appendix A

Nomenclatures

Below table lists the symbols that are frequently used throughout this the thesis. Symbols that appear only once are not included in the table for simplicity.

$\mathcal{A} =$	cross-sectional area of the bit face, mm^2
$A =$	wear flat area, mm^2
$A_d =$	diamond wear flat area, mm^2
$A_m =$	matrix wear flat area, $A_{\bar{m}} + A_{\hat{m}}$, mm^2
$A_{\bar{m}} =$	matrix wear flat area at the tail, mm^2
$A_{\hat{m}} =$	matrix wear flat area at the crater, mm^2
$\bar{A}_d =$	cumulative diamond wear flat area of the bit, $\sum_{i=1}^{n} A_{d_i}$, mm^2
$\bar{A}_{\bar{m}} =$	cumulative matrix wear flat area at the tail of the bit, $\sum_{i=1}^{n} A_{\bar{m}_i}$, mm^2
$\bar{A}_{\hat{m}} =$	cumulative matrix wear flat area at the crater of the bit, $\sum_{i=1}^{n} A_{\hat{m}_i}$, mm^2
$d =$	depth of cut of the bit, $2\pi V/\Omega$, mm/rev
$d_d =$	depth of cut per diamond on the bit face, mm/rev
$d_f =$	depth of cut at the onset of fracturing dominant regime, mm/rev
$d_* =$	depth of cut at the onset of regime II, mm/rev
$d_{**} =$	depth of cut at the onset of regime III, mm/rev
$F =$	force, N
$F_n =$	normal force, N

F_s= tangential force, N

H= height of the impregnated section of the bit, mm

$\dot{H}$= bit wear rate, $\frac{\delta H}{\delta S}$,mm

h= diamond height, mm

$\dot{h}$= diamond wear rate, $\frac{\delta h}{\delta S}$,mm

L = noimnal wear flat length, mm

L_d = nominal diamond wear flat length of the equivalent blade, $\bar{A}_d/(r_o - r_i)$, mm

L_m = nominal matrix wear flat length of the equivalent blade, $L_{\bar{m}} + L_{\hat{m}}$, mm

$L_{\bar{m}}$ = nominal matrix wear flat length at the tail of the equivalent blade, $\frac{\bar{A}_{\bar{m}}}{r_o - r_i}$, mm

$L_{\hat{m}}$ = nominal matrix wear flat length at the crater of the equivalent blade, $\frac{\bar{A}_{\hat{m}}}{r_o - r_i}$, mm

ℓ = effective contact length, mm

ℓ_d = effective diamond frictional contact length, mm

$\hat{\ell}_d$ = conformal effective contact length, mm

$\ell_{\bar{m}}$ = effective matrix frictional contact length at the tail, mm

$\ell_{\hat{m}}$ = effective matrix frictional contact length at the crater, mm

n= number of diamonds on the bit tracing the same groove

Q= flow rate, L/min

p= diamond protrusion, mm

$\bar{p}$= diamond protrusion of the equivalent blade, $\bar{p} = \frac{\sum_{i=1}^{n} p_i}{n}$, mm

q= uniaxial compressive strength of the rock, MPa

r= mean radius of the bit, $(r_o - r_i)/2$, mm

r_o= outer diameter of the bit, mm

r_i= inner diameter of the bit, mm

s= bit linear cutting distance, m

T= torque on bit, Nm

t = scaled torque on bit, $\frac{2T}{r_o^2 - r_i^2}$, N/mm

t_o= intercept of regime II in $t - d$ space, N/mm

V= penetration rate, mm/s

v= linear speed, Ωr,mm/s

$\mathcal{V}$= volume of rock removed by bit, mm^3

W = weight on bit, N

w = scaled weight on bit, $\frac{W}{r_o - r_i}$, N/mm

w_o= intercept of regime II in $w - d$ space, N/mm

α= slope of a cutting regime in $w - d$ space, N/mm

β= slope of a cutting regime in $t - d$ space, N/mm

η= Marsh funnel viscosity of the drilling fluid, s

ζ= inclination of the cutting face acting on the cutting face

ε= intrinsic specific energy, MPa

Ω= angular velocity, rad/s

μ= friction coefficient between two contact surfaces

σ= contact stress, MPa

κ_d = coefficient representing variation of diamond frictional contact length

$\kappa_{\bar{m}}$ = coefficient representing variation of matrix frictional contact length at tail

$\kappa_{\hat{m}}$ = coefficient representing variation of matrix frictional contact length at crater

I= regime I

II= regime II

III regime III

Appendix B

Model parameters derived from drilling responses

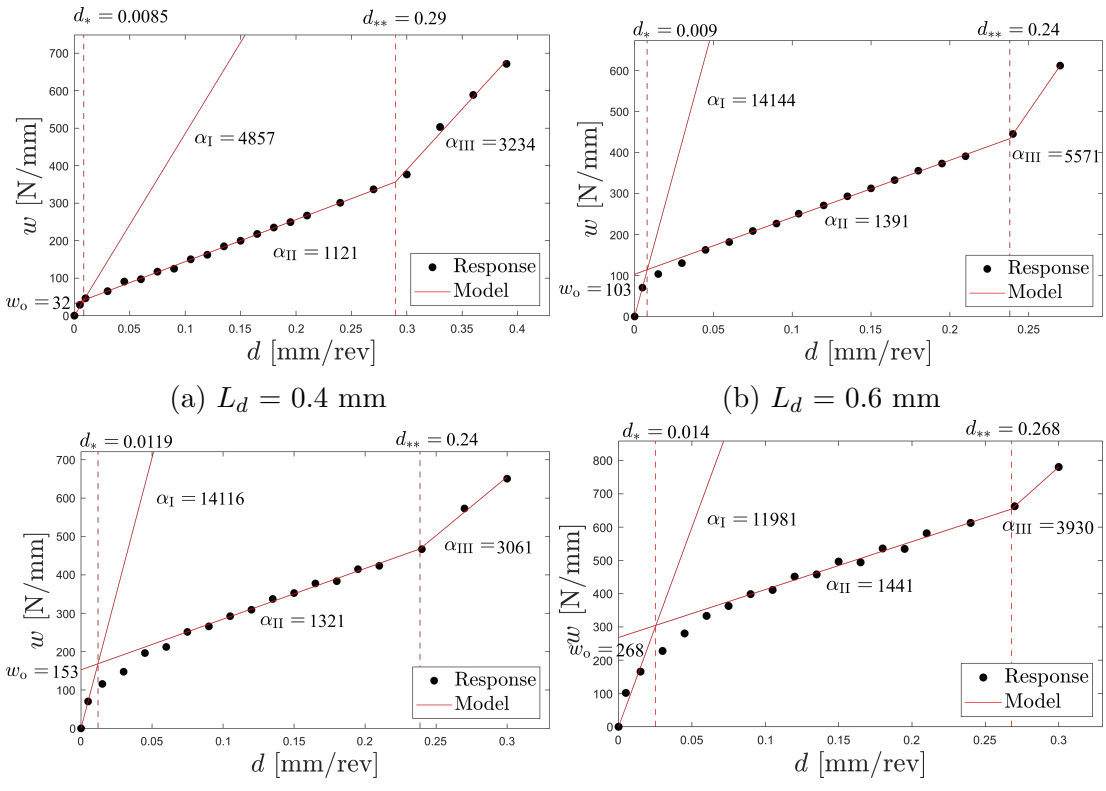

(a) $L_d = 0.4$ mm (b) $L_d = 0.6$ mm

(c) $L_d = 0.9$ mm (d) $L_d = 1.3$ mm

Figure B.1: Drilling response of an NQ-size bit used for driving model parameters listed in Table 4.1 (part 1).

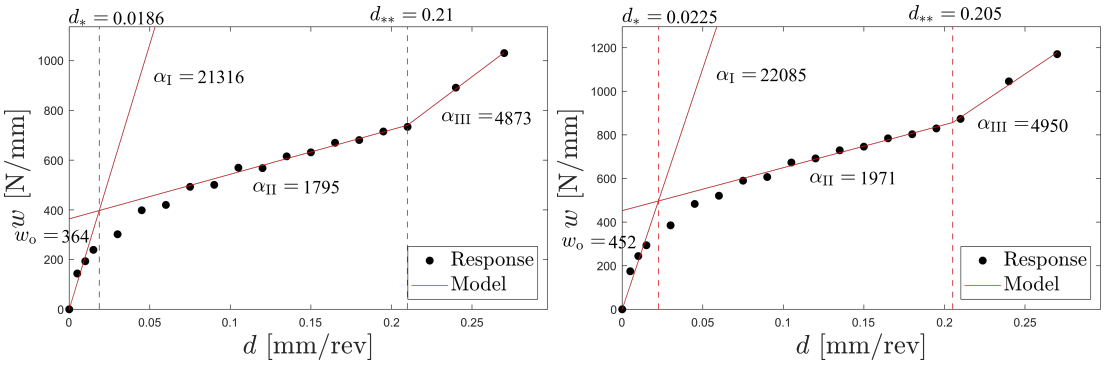

(a) $L_d = 1.7$ mm

(b) $L_d = 2.2$ mm

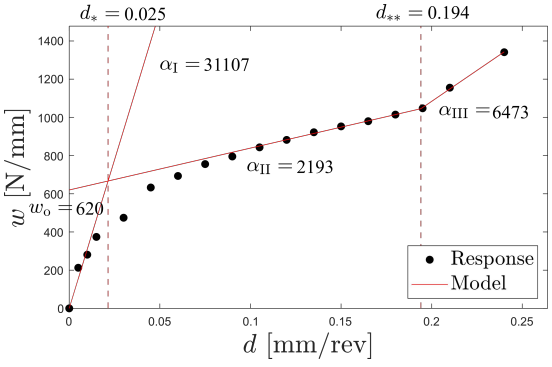

(c) $L_d = 2.8$ mm

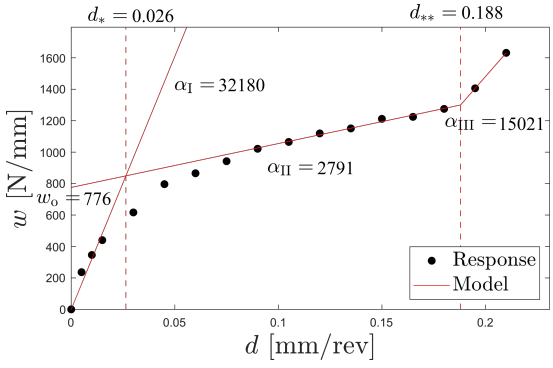

(d) $L_d = 3.9$ mm

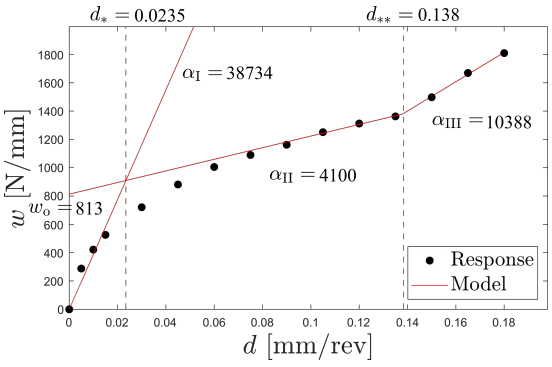

(e) $L_d = 5$ mm

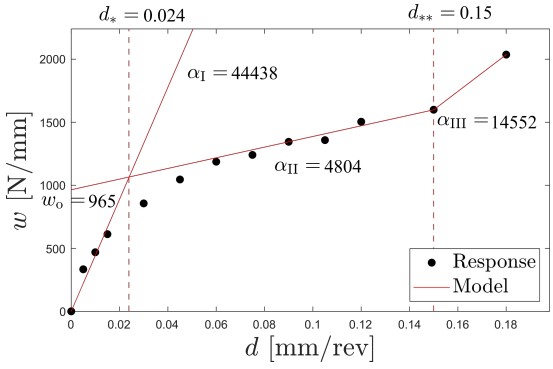

(f) $L_d = 6$ mm

Figure B.2: Drilling response of an NQ-size bit used for driving model parameters listed in Table 4.1 (part 2).

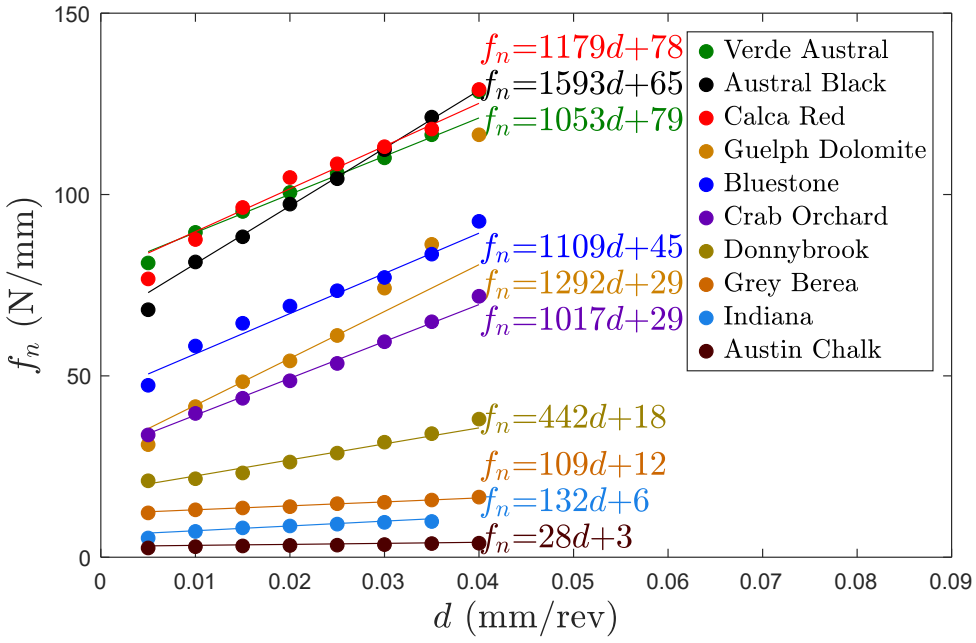

(a) L_d = 0.3 mm

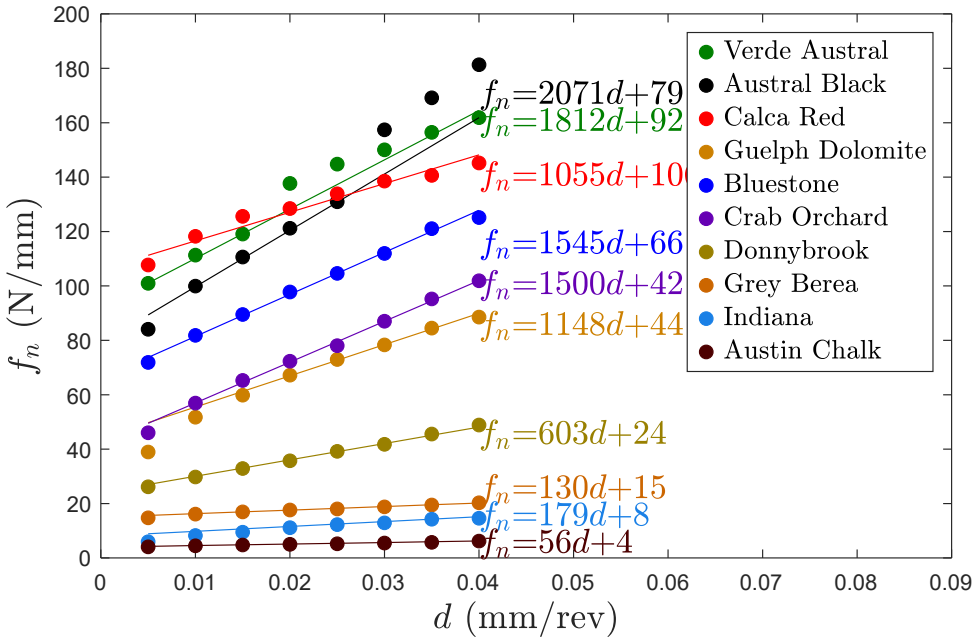

(b) L_d = 0.4 mm

Figure B.3: Cutting response of an ID segment used for driving model parameters listed in Table 3.1.

Bibliography

D Miller and A Ball. Rock drilling with impregnated diamond microbits—an experimental study. In *International Journal of Rock Mechanics and Mining Sciences Geomechanics Abstracts*, volume 27, pages 363–371. Elsevier, 1990. ISBN 0148-9062.

Boonsom Siribumrungsukha. *Investigations into diamond drilling and rock drillability: microscale and fullscale impregnated bits*. PhD thesis, University of Melbourne, 1980.

Masood Mostofi, LFP Franca, and T Richard. Drilling response of impregnated diamond bits: an experimental investigation. In *47th US Rock Mechanics/Geomechanics Symposium*. American Rock Mechanics Association, 2013. ISBN 0989484408.

Masood Mostofi and L Franca. The wear mechanisms of impregnated diamond bits. In *48th US rock mechanics/geomechanics symposium*. American Rock Mechanics Association, 2014. ISBN 0989484416.

Duncan Miller and Anthony Ball. The wear of diamonds in impregnated diamond bit drilling. *Wear*, 141(2):311–320, 1991. ISSN 0043-1648.

Masood Mostofi. *Drilling response of impregnated diamond bits: modelling and experimental investigations*. Thesis, Curtin University, 2014.

A Quacquarelli, G Mollon, T Commeau, and N Fillot. A dual numerical-

experimental approach for modeling wear of diamond impregnated tools. *Wear*, 478:203763, 2021. ISSN 0043-1648.

Masood Mostofi, Thomas Richard, Luiz Franca, and Suchay Yalamanchi. Wear response of impregnated diamond bits. *Wear*, 410-411:34–42, 2018. ISSN 00431648. doi: 10.1016/j.wear.2018.04.010.

AA Selim, CW Schultz, and KC Strebig. The effect of additives on impregnated diamond bit performance. *Society of Petroleum Engineers Journal*, 9(04):425–433, 1969. ISSN 0197-7520.

Hing Hao Chan. *A Method to Derive Rock Strength from the Drilling Response of Impregnated Diamond Bit.* Thesis, Curtin University, 2022.

United Nations. Paris agreement. In *report of the conference of the parties to the United Nations framework convention on climate change (21st session, 2015: Paris). Retrived December*, volume 4, page 2. HeinOnline, 2015.

Camille Parmesan, Mike D. Morecroft, and Yongyut Trisurat. *Climate change 2022: Impacts, adaptation, and vulnerability.* Thesis, GIEC, 2022.

S Hapugoda and JR Manuel. Techniques used and problems encountered in normal and reverse circulation drilling at the mt roseby project, cloncurry, north west queensland. In *Proceedings XXV International Mineral Processing Congress*, 2010.

MV Sneddon and DR Hall. Polycrystalline diamond: manufacture, wear mechanisms, and implications for bit design. *Journal of Petroleum Technology*, 40 (12):1593–1601, 1988.

H Geoffroy and D Nguyen Minh. Study on interaction between rocks and worn pdc's cutter. *International Journal of Rock Mechanics and Mining Sciences*, 34(3-4):95–e1, 1997.

D. S. Rowley and F. C. Appl. Analysis of surface set diamond bit performance. *Society of Petroleum Engineers Journal*, 9(03):301–310, 1969.

JD Dwan. Production of diamond impregnated cutting tools. *Powder metallurgy*, 41(2):84–86, 1998.

B. Kieback and C. Sauer. Metallic binders for diamond tool production. In *Proceedings of the Workshop on Diamond Tools*, Verona, Italy, May 2000.

Emmanuel Detournay and Paul Defourny. A phenomenological model for the drilling action of drag bits. In *International journal of rock mechanics and mining sciences geomechanics abstracts*, volume 29, pages 13–23. Elsevier, 1992. ISBN 0148-9062.

JL Peterson. Diamond drilling model verified in field and laboratory tests. *Journal of Petroleum Technology*, 28(02):213–222, 1976. ISSN 0149-2136.

Boart Longyear. Global product catalogue. https://www.boartlongyear.com/wp-content/uploads/Bits-Catalog.pdf, 2009.

Atlas Copco Australia. Professional diamond driller's handbook. https://narzedziawiertnicze.pl/wp-content/uploads/2016/07/poradnik_wiercen_rdzeniowych.pdf, 2015.

Dimatiec Inc. Operating parameters: Rotational speed for diamond impregnated core bits. https://www.dimatec.com/wp-content/uploads/2019/06/TD104_R5.pdf, 2019.

DP Singh. The drillability of rocks. *Mineral Science and Engineering*, 5, 1973.

J Paone and D Madson. Drillability studies: diamond bits. *United States Department of the Interior, Bureau of Mines, Report of Investigations*, 6776, 1966.

G Bullen. Synthetic versus natural diamond in hard rock drilling. *Industrial Diamond Review*, 42(5):277–283, 1982. ISSN 0019-8145. IDR. Industrial Diamond Review; GBR.

TM Warren and A Sinor. Drag bit performance modeling. In *SPE Annual Technical Conference and Exhibition?*, pages SPE–15618–MS. SPE, 1986. ISBN 1555636071.

Luiz F. P. Franca. Drilling action of roller-cone bits: Modeling and experimental validation. *Journal of Energy Resources Technology*, 132(4):043101, December 2010. doi: 10.1115/1.4003168. URL https://doi.org/10.1115/1.4003168.

K Spink. Nature of diamond drilling process. *Industrial Diamond Review*, 32 (379):230–, 1972. ISSN 0019-8145.

GJ Bullen and MW Bailey. Sda100 in hard rock drilling. *Industrial Diamond Review*, (OCT):352–355, 1979. ISSN 0019-8145.

Antoniomaria Di Ilio and Antonio Togna. A theoretical wear model for diamond tools in stone cutting. *International Journal of Machine Tools and Manufacture*, 43(11):1171–1177, 2003. ISSN 0890-6955.

D.M. Busch and B.S. HILL. Concrete drilling with diamond impregnated bits. *Industrial Diamond Review*, 35(172-6), 1975.

S Malkin and NH Cook. The wear of grinding wheels: part 1—attritious wear. 1971. ISSN 0022-0817.

GJ Bullen. Hard rock drilling: some recent test results. *IDR. Industrial diamond review*, 44(504):270–275, 1984. ISSN 0019-8145.

JR Hird and JE Field. Diamond polishing. *Proceedings of the Royal Society of London. Series A: Mathematical, Physical and Engineering Sciences*, 460 (2052):3547–3568, 2004. ISSN 1364-5021.

KA Zacny and GA Cooper. Investigation of diamond-impregnated drill bit wear while drilling under earth and mars conditions. *Journal of Geophysical Research: Planets*, 109(E7), 2004. ISSN 0148-0227.

James Paone and William E Bruce. *Drillability studies: diamond drilling*, volume 6324. Bureau of Mines, 1963.

R Teale. The concept of specific energy in rock drilling. In *International journal of rock mechanics and mining sciences geomechanics abstracts*, volume 2, pages 57–73. Elsevier, 1965. ISBN 0148-9062.

J Moller and K Spink. Calibration of machines for specific energy experiments. *Industrial Diamond Review*, 33(394):348–352, 1973. ISSN 0019-8145.

WC Maurer. The state of rock mechanics knowledge in drilling. In *ARMA US Rock Mechanics/Geomechanics Symposium*, pages ARMA–66–0355. ARMA, 1966.

K Sasaki, N Yamakado, F Shiohara, and M Tobe. Investigations of diamond core bit boring. *Ind. Diamond Rev*, 22(259):178–186, 1962.

James Paone, William E Bruce, and Pauline R Virciglio. *Drillability studies: statistical regression analysis of diamond drilling*. US Department of the Interior, Bureau of Mines, 1966. ISBN 1066-5552.

A Ersoy and MD Waller. Prediction of drill-bit performance using multi-variable linear regression analysis. In *International Journal of Rock Mechanics and Mining Sciences and Geomechanics Abstracts*, volume 6, page 279A, 1995a.

Malgorzata B Ziaja and Stefan Miska. Mathematical model of the diamond-bit drilling process and its practical application. *Society of Petroleum Engineers Journal*, 22(06):911–922, 1982. ISSN 0197-7520.

KC Strebig, A Aly Selim, and Clifford W Schultz. *Effect of organic additives on impregnated diamond drilling*, volume 7494. US Department of Interior, Bureau of Mines, 1971.

RM Goktan and N Gunes Yılmaz. Diamond tool specific wear rate assessment in granite machining by means of knoop micro-hardness and process parameters. *Rock Mechanics and Rock Engineering*, 50:2327–2343, 2017. ISSN 0723-2632.

A Ersoy, S Buyuksagic, and U Atici. Wear characteristics of circular diamond saws in the cutting of different hard abrasive rocks. *Wear*, 258(9):1422–1436, 2005. ISSN 0043-1648.

A Ersoy and MD Waller. Textural characterisation of rocks. *Engineering geology*, 39(3-4):123–136, 1995b. ISSN 0013-7952.

C Fairhurst and WD Lacabanne. Hard rock drilling techniques. *Mine Quarry Eng*, 23:157–161, 1957.

Thomas Richard, Emmanuel Detournay, Andrew Drescher, Pascal Nicodeme, and Dominique Fourmaintraux. The scratch test as a means to measure strength of sedimentary rocks. In *SPE/ISRM rock mechanics in petroleum engineering*, pages SPE–47196. SPE, 1998.

LFP Franca, Masood Mostofi, and Thomas Richard. Interface laws for impregnated diamond tools for a given state of wear. *International Journal of Rock Mechanics and Mining Sciences*, 73:184–193, 2015. ISSN 1365-1609.

JeFoa Archard. Contact and rubbing of flat surfaces. *Journal of applied physics*, 24(8):981–988, 1953. ISSN 0021-8979.

Wojciech Kapłonek, Krzysztof Nadolny, and Grzegorz M Królczyk. The use of focus-variation microscopy for the assessment of active surfaces of a new generation of coated abrasive tools. *Meas. Sci. Rev*, 16(2):42–53, 2016.

Yassmin Seid Ahmed, Jose Mario Paiva, Danielle Covelli, and Stephen Clarence Veldhuis. Investigation of coated cutting tool performance during machining of super duplex stainless steels through 3d wear evaluations. *Coatings*, 7(8): 127, 2017. ISSN 2079-6412.

Ifechukwu H Michaels. *Experimental Study of Polycrystalline Diamond Compacts (PDCs) Wear Mechanisms.* Thesis, Curtin University, 2021.